# 異常な超伝導近接効果の数理構造

# Physics of flat-band zero-energy states at a dirty surface of a nodal topological superconductor

Satoshi Ikegaya

March 6, 2018

# Acknowledgments

First of all, I would like to express my sincere gratitude to my supervisor Associate Prof. Yasuhiro Asano for the continuous support of my Ph.D. study, for his motivation, immense knowledge, and patience. His guidance helped me in all the time. He is a mentor in my life and a person who I respect the most. I would like to thank Prof. Kousuke Yakubo and Dr. Hideaki Obuse for giving me useful advices on my research and my presentations.

I am grateful to Yukio Tanaka, Alexander A. Golubov, Yakov V. Fominov, and Shu Suzuki for useful discussions on the physics of unconventional superconductivity. I would like to thank Shingo Kobayashi, Masatoshi Sato, and Jay D. Sau for fruitful discussions on the topological phase of matter.

Lastly, I would like to express my appreciation for Akira and Ayako Ikegaya who are my parents. They gave me essential advice on life. Although their words were sometimes harsh, I felt their warmness and kindness behind such words. Without their cooperations, I could not finish this research and could not take my Ph.D. degree. I hope they live a long and healthy life.

# Contents

# Chapter 1

# General Introduction

In the past decade, topologically nontrivial superconductors have attracted enormous attention due to the existence of exotic bound states at their surfaces [1–3]. The early studies in this context focused mainly on the topological phase of a fully gapped superconductor listed in the tenfold topological classification [4]. The bulk-boundary correspondence suggests the equivalence between the number of the surface bound states and the absolute value of a topological invariant $\mathcal{Z}$ defined in the bulk states [5, 6]. A unique physical consequence of such a topological superconductor might be the zero-bias conductance quantization at $G_{\mathrm{NS}} = (2e^2/h)|\mathcal{Z}|$ in an normal-metal/superconductor (NS) junction [7, 8]. In experiments, however, it is not be easy to observe the conductance quantization clearly due to following reasons. The invariant $\mathcal{Z}$ is usually limited to small numbers in real fully gaped superconductors, whereas the number of the propagating channels $N_c$ is much larger than unity in two- or three-dimensional NS junctions. Therefore the electric current through normal propagating channels would smear the effects of the resonant transmission through the topological bound states.

Nowadays, it has been widely accepted that a topologically nontrivial phase is realized also in a superconductor whose gap function has nodes on the Fermi surface [9–11]. The most striking feature of such a nodal superconductor is the appearance of flat-band zero-energy states (ZESs) at its clean surface. It has been well established that the conductance of a NS junction consisting of such a nodal superconductor is quantized at $G_{\mathrm{NS}} = (2e^2/h)\mathcal{N}_{\mathrm{clean}}$ [12–15]. Here, $\mathcal{N}_{\mathrm{clean}}$ is the number of the surface bound states at the zero energy and is of the order of $N_c$. In addition to the zero-bias conductance quantization, the fractional Josephson effect [16–20], the paramagnetic response at a surface [21–26], and the anomalies in heat transport [27] are physical phenomena unique to a nodal superconductor hosting the flat-band ZESs at its surface. Since $\mathcal{N}_{\mathrm{clean}}$ is the same order as $N_c$, the effects of the surface bound states on the electromagnetic phenomena in a nodal superconductor can be more noticeable than those in a fully gapped topological superconductor. Therefore a nodal superconductor is a promising testing ground for physics of topologically nontrivial superconductivity.

The dimensional reduction is a useful theoretical tool for characterizing a nodal superconductor topologically. In a $d$-dimensional nodal superconductor, one can still find a fully gapped one-dimensional partial Brillouin zone by fixing $(d-1)$-dimensional momentum at a certain point (say $k$). In such a one-dimensional Brillouin zone, it is possible to define a winding number $w(k)$ [9, 11]. The nonzero winding number $w(k)$ suggests $|w(k)|$-fold degenerate ZESs at a surface for each $k$. Therefore, $\mathcal{N}_{\text{clean}} = \sum_k |w(k)|$ describes the number of the ZESs at a clean surface of a nodal superconductor. Actually the existence of degenerate surface ZESs has been suggested in time-reversal unconventional superconductors [12, 13, 28–30], noncentrosymmetric superconductors [31–35], semiconductor/superconductor heterostructures [36–38], helical $p$-wave superconductors with inplane magnetic fields [39, 40], superconductor/topological insulator heterostructures [41], and superconducting Weyl semimetals [42].

In a real superconductor, however, the potential disorder is inevitable in the vicinity of the surface or the junction interface. In the dimensional reduction, translational symmetry is necessary to define the winding number $w(k)$ in the one-dimensional Brillouin zone. However, such partial Brillouin zone itself is not well defined at all because the momentum $k$ is not a good quantum number under the potential disorder. Therefore, $\mathcal{N}_{\text{clean}}$ can be no longer used to predict the number of flat-band ZESs at a dirty surface [43]. In other words, the potential disorder may lift the high degeneracy in the surface ZESs and may wash out the characteristic transport properties. Such a situation requires a theoretical method that measures the stability of degenerate ZESs at a dirty surface of a nodal superconductor. We address such issue in this paper. On the basis of obtained results, we will indicate a way of observing the topologically nontrivial nature of a nodal superconductor in experiments.

By paying attention to chiral symmetry of a Bogoliubov-de Gennes Hamiltonian [44–46], we show that a mathematical index, $\mathcal{N}_{\text{ZES}}$, well characterizes the number of ZESs at the dirty surface of a nodal superconductor. The index $\mathcal{N}_{\text{ZES}}$ is an invariant defined in terms of the solutions of the differential equation. Simultaneously, the index is closely related to the one-dimensional winding number $w(k)$. In mathematics, such integer number is called Atiyah-Singer index. We will show that the index $\mathcal{N}_{\text{ZES}}$ describes well the bulk-boundary correspondence of a nodal superconductor with the dirty surface. We also discuss the zero-bias differential conductance $G_{\text{NS}}$ of a normal-metal/superconductor junction, where the superconductor is characterized by unconventional pairing symmetries such as $d_{xy}$-, $p_x$-, and $f$-wave. By using the lattice Green function technique, we numerically demonstrate that $G_{\text{NS}}$ is quantized at $(4e^2/h)|\mathcal{N}_{\text{ZES}}|$ in the limit of strong impurity scattering in the normal segment. The analysis in terms of chiral symmetry of the

Hamiltonian enables us to prove the existence of $|\mathcal{N}_{\mathrm{ZES}}|$-fold degenerate resonant states in the dirty normal segment and provide a microscopic understanding of the quantization in the conductance minimum. In addition to the NS junctions, we discuss the stability of the degenerate ZESs appearing in a $p_x$-wave superconductor/dirty normal metal/$p_x$-wave superconductor junction in two-dimension. As a consequence, we demonstrate that the the degenerate ZESs protected by chiral symmetry cause the fractional Josephson effect even in the presence of potential disorders. To our knowledge, $\mathcal{N}_{\mathrm{ZES}}$ becomes nonzero in several nodal superconductors characterized by spin-triplet pairing symmetries. However, it has been difficult to fabricate spin-triplet superconducting junctions using existing materials. Nevertheless, we also demonstrate that a superconducting thin-film with the Dresselhaus [110] spin-orbit coupling [37] shows the prefect conductance quantization due to the effective $p_x$-wave pairing symmetry. The results suggest a way of observing the drastic transport properties of a topological superconductor in experiments by combining existing materials.

This thesis is organized as follows. In chapter 2, we discuss the stability of the flat-band ZESs at a dirty surface of a nodal superconductor [47]. The index $\mathcal{N}_{\mathrm{ZES}}$ is defined in terms of the chiral eigenvalues of ZESs and is connected to the one-dimensional winding number $w(k)$ through the Atiyah-Singer index theorem. In chapter 3, we discuss the minimum value of the zero-bias differential conductance in a normal-metal/unconventional-superconductor junction [48]. We analytically prove the quantization of conductance minimum by taking the chiral property into account. In chapter 4, we discuss the chiral property of ZESs appearing in a $p_x$-wave superconductor/dirty normal metal/$p_x$-wave superconductor junction [49]. In chapter 5, we demonstrate the conductance quantization and the fractional Josephson effect of an artificial superconducting states with Dresselhaus spin-orbit coupling [50]. We summarize this thesis in Sec. 6.

# Chapter 2

# Stability of flat-band zero-energy states at a dirty surface of a nodal superconductor

## 2.1 Abstract

We discuss the stability of highly degenerate zero-energy states that appear at the surface of a nodal superconductor preserving time-reversal symmetry. The existence of such surface states is a direct consequence of the nontrivial topological numbers defined in the restricted Brillouin zones in the clean limit. In experiments, however, potential disorder is inevitable near the surface of a real superconductor, which may lift the high degeneracy at zero energy. We show that an index defined in terms of the chiral eigenvalues of the zero-energy states can be used to measure the degree of degeneracy at zero energy in the presence of potential disorder. We also discuss the relationship between the index and the topological numbers.

## 2.2 Introduction

The discovery of a topological insulator [51, 52] had an impact on researchers studying the physics of superconductivity. The gapped band structures in a superconductor can also be topologically nontrivial. The bulk-boundary correspondence, which is the interrelationship between the nontrivial topological invariant in superconducting states in the bulk and the number of gapless states at its surface, immediately ensures the existence of surface bound states. Recently such topologically nontrivial superconductors have attracted enormous attention due to the existence of exotic surface bound states, some of which are composed of Majorana particles [53, 54]. Using the ten-fold classification as a basis [4], the early studies in this context were devoted to fully gapped topological superconductors [55–70].

The ten-fold topological classification, however, covers only some real superconductors. A number of real unconventional superconductors display nodes in the superconducting gap. Nevertheless, such a nodal superconductor can often host highly degenerate surface bound states at zero energy (Fermi level). The sign change in the pair potential on the Fermi surface, which is possible only in the presence of nodes in the gap functions, is the source of a topologically nontrivial superconducting phase preserving time-reversal symmetry [12, 13]. When a three (two) dimensional nodal superconductor has the superconducting line (point) nodes, the surface bound states have flat-dispersion in terms of two (one) dimensional wave number parallel to the surface. A prescription called dimensional reduction enables us to topologically characterize such flat zero-energy states of a nodal superconductor. In a $d$-dimensional superconductor, it is possible to choose a one-dimensional Brillouin zone by fixing a ($d$-1)-dimensional wave number at a certain point (say $k$). When the energy spectrum in the one-dimensional Brillouin zone at $k$ are gapped, we can define the winding number $w(k)$ [9–11]. According to the bulk-boundary correspondence for each Brillouin zone, a nodal superconductor often hosts degenerate ZESs at its clean surface. Namely, $\sum_k |w(k)|$-fold degenerate ZESs are expected at a surface parallel to $k$. Actually the existence of degenerate surface ZESs has been suggested in time-reversal unconventional superconductors [12, 13, 28–30], noncentrosymmetric superconductors [31–35], semiconductor/superconductor heterostructures [36–38], helical $p$-wave superconductors with in-plane magnetic fields [39, 40] superconductor/topological insulator heterostructures [41], and superconducting Weyl semimetals [42]. It is widely accepted that flat ZESs cause various anomalies in low-energy transport such as the zero-bias anomaly in the conductance of a normal-metal/superconductor junction [12–15]. and the fractional Josephson effect in a superconductor/insulator/superconductor junction [16–20]. These phenomena are unique to topologically nontrivial superconductors.

In experiments, however, non-magnetic potential disorder is inevitable in the vicinity of the surface or junction interface of a superconductor. The one-dimensional Brillouin zone is not well defined with the disordered potential breaking the translational symmetry. Therefore, the winding number $w(k)$ can not describe the number of ZESs at the dirty surface [43]. In other words, the potential disorder may lift the high degeneracy in the surface ZESs and may wash out the characteristic transport properties. Such a situation requires a theoretical tool that mesures the stability of degenerate ZESs in the presence of potential disorders. This paper addresses this issue and will provide experimentalists with helpful information.

By paying attention to the chiral symmetry of a Bogoliubov-de Gennes (BdG) Hamiltonian [44–46], we show that a mathematical index, $\mathcal{N}_{\mathrm{ZES}}$, well characterizes the number of ZESs at a dirty surface. The index $\mathcal{N}_{\mathrm{ZES}}$ is an invariant defined in terms of the chirality of the surface ZESs and is closely related to the one-dimensional winding number $w(k)$. We conclude that the index $\mathcal{N}_{\mathrm{ZES}}$ calculated in a clean superconductor exactly predicts the degree of degeneracy in ZESs at the dirty surface of a nodal superconductor. Numerical simulations for several nodal superconductors ensure the validity of the conclusion.

The organization of this chapter is as follows. In Sec. (2.3), we discuss the one-dimensional winding number for a nodal superconductor preserving chiral symmetry. The index $\mathcal{N}_{\mathrm{ZES}}$ is defined in terms of the chiral eigenvalues of ZESs and is connected to the one-dimensional winding number through the index theorem in mathematics. In Sec. (2.4), we confirm the validity of our conclusion for several superconductors such as $p$-, $d$- and $f$-wave unconventional superconductors, and two noncentrosymmetric superconductors. Section (2.5) provides our conclusion.

## 2.3 Chiral symmetry and Index theorem

### 2.3.1 Winding number in a clean superconductor

We begin our discussion with a brief summary of the topological property of a nodal superconductor in the clean limit. The BdG Hamiltonian in momentum space is represented by,

$$\mathcal{H}_0(\boldsymbol{k}) = \begin{bmatrix} h(\boldsymbol{k}) & \Delta(\boldsymbol{k}) \\ -\Delta^*(-\boldsymbol{k}) & -h^*(-\boldsymbol{k}) \end{bmatrix}, \tag{2.1}$$

where $\xi(\boldsymbol{k})$ denotes the $M \times M$ Hamiltonian for an electron, $\Delta(\boldsymbol{k})$ is the $M \times M$ pair potential and where $M$ represents the number of degrees of freedom for an electron such as spin and band. The BdG Hamiltonian intrinsically preserves particle-hole symmetry

$$\mathcal{C}\,\mathcal{H}_0(\boldsymbol{k})\,\mathcal{C}^{-1} = -\mathcal{H}_0(-\boldsymbol{k}), \tag{2.2}$$

$$\mathcal{C} = \mathcal{U}_{\mathcal{C}}\,\mathcal{K}, \qquad \mathcal{U}_{\mathcal{C}} = \begin{bmatrix} 0 & I \\ I & 0 \end{bmatrix}, \tag{2.3}$$

where $I$ is the $M \times M$ unit matrix and $\mathcal{K}$ denotes the complex-conjugation operator. We assume that the BdG Hamiltonian preserves time-reversal or time-reversal-like symmetry as

$$\mathcal{T}_{\pm}\ \mathcal{H}_0(\boldsymbol{k})\ \mathcal{T}_{\pm}^{-1} = \mathcal{H}_0(-\boldsymbol{k}), \tag{2.4}$$

$$\mathcal{T}_{\pm} = \mathcal{U}_{\pm}\ \mathcal{K}, \qquad \mathcal{U}_{\pm} = \begin{bmatrix} u_{\pm} & 0 \\ 0 & u_{\pm}^* \end{bmatrix}, \tag{2.5}$$

where $u_{\pm}$ is an $M \times M$ unitary matrix satisfying $u_{\pm}u_{\pm}^* = \pm I$. Time-reversal symmetry is denoted with $u_- u_-^* = -I$, while time-reversal-like symmetry is denoted with $u_+ u_+^* = I$. By combining the particle-hole symmetry operator $\mathcal{C}$ and the time-reversal symmetry operator $\mathcal{T}_-$, we can define a operator

$$\mathcal{S} = -i\mathcal{U}_{\mathcal{C}}\ \mathcal{U}_- = \begin{bmatrix} 0 & -iu_-^* \\ -iu_- & 0 \end{bmatrix}, \tag{2.6}$$

where $\mathcal{S}$ is an unitary operator satisfying $\mathcal{S}^2 = +1$. The BdG Hamiltonian satisfies

$$\mathcal{S}\ \mathcal{H}_0(\boldsymbol{k})\ \mathcal{S}^{-1} = -\mathcal{H}_0(\boldsymbol{k}), \tag{2.7}$$

which represents chiral symmetry of the Hamiltonian. The chiral symmetry operator for a case of time-reversal-like symmetry is also defined in a similar way

$$\mathcal{S}\ \mathcal{H}_0(\boldsymbol{k})\ \mathcal{S}^{-1} = -\mathcal{H}_0(\boldsymbol{k}), \qquad \mathcal{S} = -\mathcal{U}_{\mathcal{C}}\ \mathcal{U}_+ = \begin{bmatrix} 0 & -u_+^* \\ -u_+ & 0 \end{bmatrix}, \tag{2.8}$$

where $\mathcal{S}$ is an unitary operator satisfying $\mathcal{S}^2 = +1$.

In a superconductor under consideration, the pair potential has nodes on the Fermi surface. Therefore, it is impossible to define a topological invariant by using the wave functions of whole Brillouin zone. In a three- (two-) dimension, we assume that the pair potential has line (point) nodes on the Fermi surface. The nodal point $\boldsymbol{k}_0$ satisfies $\det[\mathcal{H}_0(\boldsymbol{k}_0)] = 0$. Even in in presence of the nodes, it is still possible to define a one-dimensional partial BZ by fixing a $(d-1)$-dimensional momentum $\boldsymbol{k}_{\parallel}$ at a certain point. When the pair potential in such a partial Brillouin zone is fully gapped, one can define the one-dimensional winding number as

$$w(\boldsymbol{k}_{\parallel}) = \frac{i}{4\pi}\int dk_{\perp}\mathrm{Tr}[\mathcal{S}\ \mathcal{H}_0^{-1}(\boldsymbol{k})\ \partial_{k_{\perp}}\mathcal{H}_0(\boldsymbol{k})], \tag{2.9}$$

where $k_{\perp}$ is the momentum in the one-dimensional BZ. The winding number $w(\boldsymbol{k}_{\parallel})$ cannot be defined when the integral path along $k_{\perp}$ in Eq. (2.9) intersects the gap nodes $\boldsymbol{k}_0$. Therefore, we have to choose $\boldsymbol{k}_{\parallel}$ so that $k_{\perp}$ can be kept away from the nodal points.

When $w(\boldsymbol{k}_\parallel)$ is nonzero at $\boldsymbol{k}_\parallel$, according to the bulk-boundary correspondence, $|w(\boldsymbol{k}_\parallel)|$-fold degenerate ZESs are expected at a clean surface parallel to $\boldsymbol{k}_\parallel$. Thus, the total number of the ZESs at the clean surface is given by

$$\mathcal{N}_{\mathrm{clean}} = {\sum_{\boldsymbol{k}_\parallel}}' |w(\boldsymbol{k}_\parallel)|, \tag{2.10}$$

where ${\sum_{\boldsymbol{k}_\parallel}}'$ denotes a summation over $\boldsymbol{k}_\parallel$ excluding the nodal points. Such highly degenerate surface bound states are called flat-band ZES because the energy dispersion is independent of $\boldsymbol{k}_\parallel$. In what follows, we describe the degree of degeneracy in the ZESs at a dirty surface in the presence of potential disorder.

### 2.3.2 Zero-energy states at a dirty surface

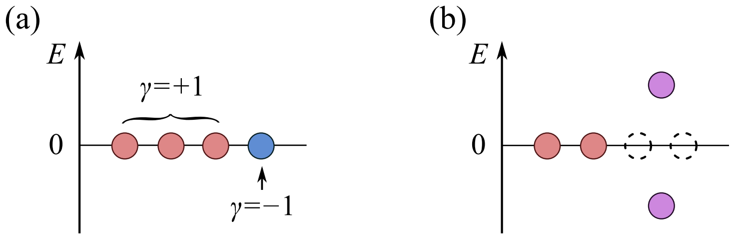


**Figure 2.1:** (Color online) (a) Four-fold degenerate zero-energy states (ZESs) in the absence of random potential. Three of them belong to the positive chiral eigenvalue, (i.e., $N_+ = 3$). One remaining ZES belongs to the negative chiral eigenvalue (i.e., $N_- = 1$). The four-fold degeneracy is protected by translational symmetry. (b)In the presence of random potential, a positive and a negative chiral ZES form a pair and departs from zero energy. However two positive chiral ZESs remain at zero energy. The index $\mathcal{N}_{\mathrm{ZES}} = N_+ - N_- = 2$ represents the number of ZESs remaining at zero energy in the presence of random potential.

We consider a semi-infinite nodal superconductor occupying $x_\perp \geq 0$. The potential disorder in the bulk region strongly suppresses unconventional superconductivity. Thus, we assume that the potential disorders exist only near the surface $x_\perp \ll \xi_{\mathrm{S}}$, where $\xi_{\mathrm{S}}$ represents the superconducting coherence length. The BdG Hamiltonian in real space $\mathcal{H}_0(\boldsymbol{r})$ is obtained by replacing the momentum $\boldsymbol{k}$ by $-i\nabla_{\boldsymbol{r}}$. The non-magnetic random impurity potential in the vicinity of the surface is represented by

$$\mathcal{H}_{\mathrm{imp}}(\boldsymbol{r}) = \begin{bmatrix} v(\boldsymbol{r})I & 0 \\ 0 & -v(\boldsymbol{r})I \end{bmatrix}, \tag{2.11}$$

where the random potential $v(\boldsymbol{r})$ finite only for $x_\perp \ll \xi_{\mathrm{S}}$. The total Hamiltonian is given by

$$\mathcal{H}(\boldsymbol{r}) = \mathcal{H}_0(\boldsymbol{r}) + \mathcal{H}_{\rm imp}(\boldsymbol{r}). \tag{2.12}$$

The momentum $\boldsymbol{k}_\parallel$ is no longer a good quantum number because the impurity potential breaks the translational symmetry. As a result, it is impossible to define the one-dimensional winding number $w(\boldsymbol{k}_\parallel)$ in the presence of the potential disorder. However, the Hamiltonian $\mathcal{H}(\boldsymbol{r})$ preserves the chiral symmetry of the Hamiltonian in Eqs. (2.7) or (2.8), which is the most important factor in the argument below. The central ingredient of our theory consists of the following two important properties of the eigenstates in the presence of chiral symmetry [9] [See also Appendix (A)].

(i) First, the zero-energy states of $\mathcal{H}$ are simultaneously the eigenstates of the chiral operator $\mathcal{S}$. Since $\mathcal{S}^2 = 1$, the eigenvalue of $\mathcal{S}$ is either $\gamma = +1$ or $\gamma = -1$. Namely, a ZES satisfying $\mathcal{H}(\boldsymbol{r})\varphi_\gamma(\boldsymbol{r}) = 0$ also satisfies $\mathcal{S}\varphi_\gamma(\boldsymbol{r}) = \gamma\varphi_\gamma(\boldsymbol{r})$. We refer to $\gamma$ as the chirality in the following.

(ii) Second, the nonzero energy states of $\mathcal{H}$ are described by the linear combination of the two states: one has $\gamma = +1$ and the other has $\gamma = -1$. Namely, a nonzero energy state is described as $\varphi_{E\neq 0}(\boldsymbol{r}) = c_+\chi_+(\boldsymbol{r}) + c_-\chi_-(\boldsymbol{r})$, where $\mathcal{S}\chi_\pm(\boldsymbol{r}) = \pm\chi_\pm(\boldsymbol{r})$. Moreover, the relation $|c_+| = |c_-|$ always holds [50].

Here we define two integer numbers, $N_+$ and $N_-$, in the clean limit. According to property (i), we can immediately conclude that each ZES at a clean surface belongs to either the positive or the negative chiral state. The integer $N_+$ ($N_-$) is the number of ZESs that have the positive (negative) chiral eigenvalue. [See also Fig. 3.3 (a)]. The total number of ZESs at a clean surface is represented by $N_+ + N_-$, which must be identical to $\mathcal{N}_{\rm clean}$ in Eq. (2.24).

The stability of the flat ZESs in the presence of impurities can be discussed by using property (ii). A ZES departs from zero energy only when it can form a pair with its chiral partner. When $N_+ > N_-$, for example, $N_-$ negative chiral ZESs can couple to $N_-$ positive chiral ZESs under potential disorder. As a result, they form nonzero energy states whose number is $2N_-$. However, $N_+ - N_-$ positive chiral states remain at zero energy even in the presence of impurities because their chiral partner is absent. The integer number defined by

$$\mathcal{N}_{\rm ZES} = N_+ - N_-, \tag{2.13}$$

represents the number of ZESs that remain at a dirty surface. When $N_+ < N_-$, the number of ZESs at a dirty surface is given by $N_- - N_+$. Therefore, in general, $|\mathcal{N}_{\rm ZES}|$ is the degree of degeneracy at zero energy in the presence of potential disorder. The essence of this argument is illustrated in Figs. 3.3 (a) and (b) with $N_+ = 3$ and $N_- = 1$. In Fig. 3.3 (a), we consider four ZESs at a clean surface. In Fig. 3.3 (b), we introduce the impurity potential at the surface. Although the index $\mathcal{N}_{\rm ZES}$ is defined in the presence of translational symmetry, it represents the degree of the degeneracy at zero energy in the absence of translational symmetry. This is the main conclusion of our paper.

### 2.3.3 Relation with topological number

At the end of this section, we discuss the topological aspect of $\mathcal{N}_{\rm ZES}$. As examined in Ref. [9], the index theorem relates to the winding number $w(\boldsymbol{k}_\parallel)$ and the number of ZESs on a clean surface as follows

$$w(\boldsymbol{k}_\parallel) = \pm \left[n_+(\boldsymbol{k}_\parallel) - n_-(\boldsymbol{k}_\parallel)\right], \tag{2.14}$$

where $n_+(\boldsymbol{k}_\parallel)$ $[n_-(\boldsymbol{k}_\parallel)]$ denotes the number of positive (negative) chiral zero-energy states at $\boldsymbol{k}_\parallel$. There are two possible choice for the sign on the right-hand side of Eq. (2.14). When we consider the surface of a semi-infinite superconductor occupying $x_\perp \leq 0$ ,we should choose the positive sign. On the other hands, we should choose the negative sign at the surface of a semi-infinite superconductor occupying $x_\perp \geq 0$ [9]. However, this sign has no physical meaning because the number of ZESs is always given by $|n_+(\boldsymbol{k}_\parallel) - n_-(\boldsymbol{k}_\parallel)|$. As discussed in the previous subsection, the index $\mathcal{N}_{\rm ZES}$ is represented by the difference between the total numbers of positive and negative chiral ZESs. Therefore, by taking Eq. (2.14) into account, we find an important relation

$$\mathcal{N}_{\rm ZES} = \sum_{\boldsymbol{k}_\parallel}{}' w(\boldsymbol{k}_\parallel) = \pm(N_+ - N_-), \tag{2.15}$$

as a result of the index theorem. More specifically, the index $\mathcal{N}_{\rm ZES}$ is a topological invariant defined in terms of the wave function in the superconducting states. Simultaneously it is an invariant defined in terms of the zero-energy solutions in a differential equation. The index theorem mathematically bridges the two different invariants. In physics, the index $\mathcal{N}_{\rm ZES}$ is an invariant that measures the degree of degeneracy of the ZESs staying at the dirty surface of a nodal superconductor. In the next section, we check the validity of our conclusion by performing numerical simulations on tight-binding model.

## 2.4 Numerical results

### 2.4.1 unconventional superconductors

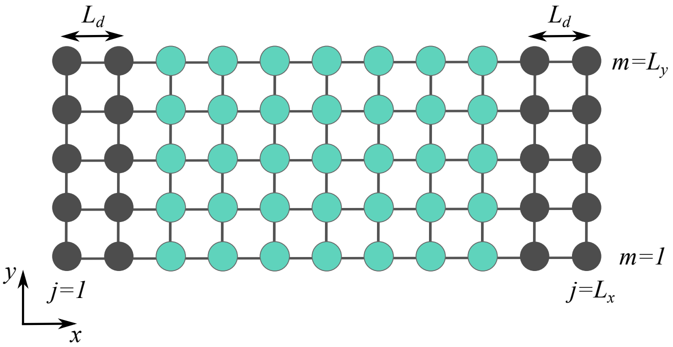


**Figure 2.2:** (Color online) Schematic picture of a superconductor on the tight-binding lattice.

We apply the general argument in Sec. (2.3) to the several time-reversal superconductors in two-dimension. The first example is the three types of unconventional superconductors characterized by $p_x$-, $d_{xy}$-, and $f$-wave pairing symmetry. We describe the present superconductors by the $2 \times 2$ BdG Hamiltonian,

$$\hat{H}_0(\boldsymbol{k}) = \begin{bmatrix} \xi(\boldsymbol{k}) & \Delta_\mu(\boldsymbol{k}) \\ \Delta_\mu(\boldsymbol{k}) & -\xi(\boldsymbol{k}) \end{bmatrix}, \tag{2.16}$$

$$\xi(\boldsymbol{k}) = \frac{\hbar^2 \boldsymbol{k}^2}{2m} - \mu_{\mathrm{F}}, \tag{2.17}$$

$$\Delta_{p_x}(\boldsymbol{k}) = \frac{\Delta_0}{k_{\mathrm{F}}} k_x, \quad \Delta_{d_{xy}}(\boldsymbol{k}) = \frac{\Delta_0}{k_{\mathrm{F}}^2} k_x k_y, \quad \Delta_f(\boldsymbol{k}) = \frac{\Delta_0}{k_{\mathrm{F}}^3} k_x (k_{\mathrm{F}}^2 - 2k_y^2), \tag{2.18}$$

where the subscript $\mu = p_x$, $d_{xy}$, $f$ labels the pairing symmetry, $m$ denotes the effective mass of an electron, $\mu_{\mathrm{F}}$ is the chemical potential, $\Delta_0$ is the amplitude of the pair potential at zero temperature, and $k_{\mathrm{F}} = \sqrt{2m\mu_{\mathrm{F}}}/\hbar$ represents the Fermi wave number. The Hamiltonian satisfies

$$\hat{S}\ \hat{H}_0(\boldsymbol{k})\ \hat{S}^{-1} = -\hat{H}_0(\boldsymbol{k}), \quad \hat{S} = \begin{bmatrix} 0 & -i \\ i & 0 \end{bmatrix}, \tag{2.19}$$

which represents chiral symmetry of the Hamiltonian.

The one-dimensional winding number in Eq. (2.9) can be further simplified to [9,11]

$$w_\mu(k_y) = \frac{1}{2}\sum_{\xi(\boldsymbol{k})=0} \mathrm{sgn}[\partial_{k_x}\xi(\boldsymbol{k})]\mathrm{sgn}[\Delta_\mu(\boldsymbol{k})] \tag{2.20}$$

where the summation is carried out for $k_x$ satisfying $\xi(\boldsymbol{k}) = 0$ with fixed $k_y$. From Eq. (2.20), the winding number for each pairing symmetry is calculated as

$$w_{p_x}(k_y) = \begin{cases} 1 & \text{for} \quad |k_y| < k_\mathrm{F} \\ 0 & \text{for} \quad |k_y| > k_\mathrm{F}, \end{cases} \tag{2.21}$$

$$w_{d_{xy}}(k_y) = \begin{cases} 1 & \text{for} \quad 0 < k_y < k_\mathrm{F} \\ -1 & \text{for} \quad 0 > k_y > -k_\mathrm{F} \\ 0 & \text{for} \quad |k_y| > k_\mathrm{F}, \end{cases} \tag{2.22}$$

$$w_{f}(k_y) = \begin{cases} 1 & \text{for} \quad |k_y| < k_f \\ -1 & \text{for} \quad k_f < |k_y| < k_\mathrm{F} \\ 0 & \text{for} \quad |k_y| > k_\mathrm{F}, \end{cases} \tag{2.23}$$

where $k_f = k_\mathrm{F}/\sqrt{2}$. The total number of topologically protected ZESs at the clean surface is calculated as

$$\mathcal{N}_\mathrm{clean} = {\sum_{k_y}}' |w_\mu(k_y)|, \tag{2.24}$$

according to the bulk-boundary correspondence. The number of ZESs at the dirty surface, on the other hand, is evaluated by the index $\mathcal{N}_\mathrm{ZES}$. By substituting Eq. (2.21) - (2.23) into Eq. (2.15), we obtain the index $N_\mathrm{ZES}$ for each pairing symmetry as

$$|\mathcal{N}_\mathrm{ZES}| = \begin{cases} \sum_{|k_y|<k_\mathrm{F}} = \mathcal{N}_\mathrm{clean} & \text{for } p_x\text{-wave} \\ 0 & \text{for } d_{xy}\text{-wave} \\ \sum_{|k_y|<k_f} - \sum_{k_f<|k_y|<k_\mathrm{F}} \neq 0 & \text{for } f\text{-wave.} \end{cases} \tag{2.25}$$

To check the validity of Eq. (2.25), we numerically calculate the eigen energy of an isolating unconventional superconductor on the two-dimensional tight-binding model as shown in Fig. 2.2. A lattice site is indicated by a vector $\boldsymbol{r} = j\ a_0\boldsymbol{x} + m\ a_0\boldsymbol{y}$, where $a_0$ denotes the lattice constant and $\boldsymbol{x}$ ($\boldsymbol{y}$) is a unit vector in the $x$ ($y$) direction. The number of the lattice site in the $x$ and $y$ direction are denoted by $L_x/a_0$ and $L_y/a_0$, respectively. In the $y$ direction, the periodic boundary condition is applied. In the $x$ direction, we apply the hard-wall boundary condition. The wave functions of zero-energy surface states decay exponentially into the bulk. Therefore, when the system length $L_x$

is much longer than the decay length of the zero-energy states $\xi_{\rm S}$, we can ignore the couplings between the zero energy states at the left surface (i.e. $j = 1$) and the right surface (i.e. $j = L_x$), As a consequence, we obtain $2 \times \mathcal{N}_{\rm clean}$ ($2 \times \mathcal{N}_{\rm ZES}$) zero-energy states in the clean (dirty) superconductor, where the factor 2 is derived from the contribution from two different surfaces in the $x$ direction. In the following numerical simulations, we only consider the enough long system which enables us to ignore the couplings between the zero energy states at the different surfaces. We introduce the non-magnetic impurity potential by adding the random on-site potentials $v(\boldsymbol{r})$ in the outermost $L_d/a_0$ layers in the $x$-direction as shown in Fig. 2.2. The amplitude of $v(\boldsymbol{r})$ is given randomly in the range of $-W/2 \leq v(\boldsymbol{r}) \leq W/2$. We numerically diagonalize the BdG Hamiltonian on the tight-binding model which is shown in Appendix (B.1). We fix several parameters as $\mu_{\rm F} = 1.5t$, $\Delta_0 = 1.0t$, $L_x = 60a_0$ and $L_y = 18a_0$ where $t$ denotes the nearest-neighbor hopping integral. The number of the zero-energy states at a clean surface is evaluated from $\mathcal{N}_{\rm clean}$ in Eq. (2.24). This parameter choice leads to $\mathcal{N}_{\rm clean} = 7$ for a $p_x$- and a $f$-wave superconductor, and $\mathcal{N}_{\rm clean} = 6$ for a $d_{xy}$-wave superconductor. The number of the zero-energy states at a dirty surface is evaluated from the index $\mathcal{N}_{\rm ZES}$ in Eq. (2.25). In the present parameters choice, we obtain $\mathcal{N}_{\rm ZES} = 7$, 0, and 3 for $p_x$-, $d_{xy}$-, and $f$-wave pairing symmetry, respectively. In Figs. 2.3(a) - 2.3(c), we show the numerical results of energy eigenvalues, where the eigen energy is labeled by an integer $n$. The open symbols and the filled symbols respectively denote the energy eigenvalues in a superconductor with clean surfaces and those with dirty surfaces. We chose $W = 3.0t$ and $L_d = 5a_0$ to realize the dirty surfaces. As shown in the open symbols of Figs. 2.3(a) - 2.3(c), we find $2 \times \mathcal{N}_{\rm clean} = 14$ zero energy states at the clean surfaces of $p_x$-wave and $f$-wave superconductor and $2 \times \mathcal{N}_{\rm clean} = 12$ zero energy states at the clean surfaces of $d_{xy}$-wave superconductor. Therefore, our parameter choice satisfies the condition $L_x \gg \xi_{\rm S}$ for all the zero-energy states. As shown in filled symbols of Fig. 2.3(c), for instance, eight ZESs of the $f$-wave superconductor leaves away from the zero energy by introducing the impurity potentials. Even though, we find that six ZESs still keep staying at zero energy. Since $2 \times |\mathcal{N}_{\rm ZES}| = 6$ under the present parameter choice, the argument in Sec. 2.3 predicts the number of ZESs at a dirty surface exactly. Figures 2.3(a) and 2.3(b) show the perfect agreement between our theory and numerical results. For a $p_x$-wave superconductor, $2 \times |\mathcal{N}_{\rm ZES}| = 14$ states remain at zero energy. In a $d_{xy}$-wave case, the ZESs are absent at the dirty surfaces.

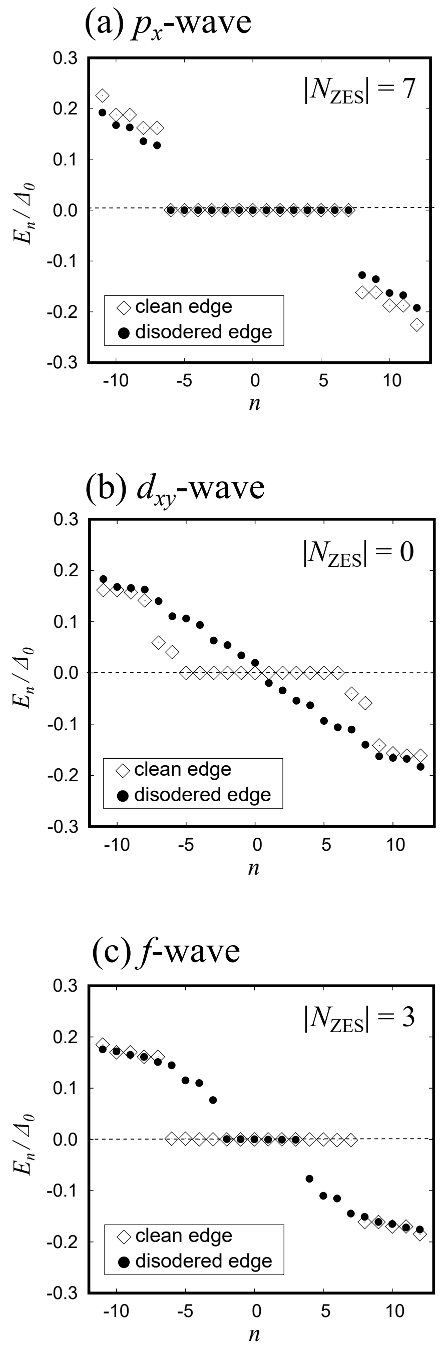


**Figure 2.3:** Energy eigenvalues of (a) $p_x$- , (b)$d_{xy}$-, and (c) $f$-wave superconductor are plotted. In numerical simulation, eigenvalues are calculated in decreasing order labeled by $n$ in the horizontal axis. In the clean limit, as shown with the open symbols, we find $2 \times \mathcal{N}_{\mathrm{clean}} = 14$ zero-energy states (ZESs) for $p_x$- and $f$-wave cases. For a $d_{xy}$-symmetry, the two states at a gap nodal point $k_y = 0$ are leave from zero energy due to the finite size effect. Thus the number of ZESs becomes $2 \times \mathcal{N}_{\mathrm{clean}} = 12$. In the presence of potential disorder at two surfaces, as shown with the filled symbols, the number of the ZESs is identical to $2 \times |\mathcal{N}_{\mathrm{ZES}}|$ which is 14 in (a), 0 in (b), and 6 in (c).

### 2.4.2 Noncentrosymmetric superconductor I

Secondly, we apply the argument in Sec. (2.3) to the noncentrosymmetric superconductors (NCSs) in two-dimension. The BdG Hamiltonian for a NCS is given by

$$\check{H}(\boldsymbol{k}) = \begin{bmatrix} \hat{h}(\boldsymbol{k}) & \hat{\Delta}(\boldsymbol{k}) \\ -\hat{\Delta}^*(-\boldsymbol{k}) & -\hat{h}^*(-\boldsymbol{k}) \end{bmatrix}, \tag{2.26}$$

$$\hat{h}(\boldsymbol{k}) = \xi(\boldsymbol{k})\hat{\sigma}_0 + \boldsymbol{g}(\boldsymbol{k}) \cdot \hat{\boldsymbol{\sigma}}, \tag{2.27}$$

$$\hat{\Delta}(\boldsymbol{k}) = i[\psi(\boldsymbol{k}) + \boldsymbol{d}(\boldsymbol{k}) \cdot \hat{\boldsymbol{\sigma}}]\hat{\sigma}_y, \tag{2.28}$$

where $\hat{\boldsymbol{\sigma}} = (\hat{\sigma}_x, \hat{\sigma}_y, \hat{\sigma}_z)$ and $\hat{\sigma}_0$ denote Pauli matrices in spin space and the $2 \times 2$ unit matrix, respectively. The absence of inversion symmetry leads the spin-orbit coupling (SOC) potential denoted by $\boldsymbol{g}(\boldsymbol{k}) = -\boldsymbol{g}(-\boldsymbol{k})$. Furthermore, the pair potential becomes the admixture of the even-parity spin-singlet component $\psi(\boldsymbol{k}) = \psi(-\boldsymbol{k})$ and the odd-parity spin-triplet pair component $\boldsymbol{d}(\boldsymbol{k}) = -\boldsymbol{d}(-\boldsymbol{k})$ because parity is no longer a good quantum index [71, 72]. The spin-triplet pairing vector $\boldsymbol{d}(\boldsymbol{k})$ is set to be parallel to the polarization vector of the SOC $\boldsymbol{g}(\boldsymbol{k})$ [71]. The BdG Hamiltonian satisfies

$$\check{S}\ \check{H}_0(\boldsymbol{k})\ \check{S}^{-1} = -\check{H}_0(\boldsymbol{k}), \quad \check{S} = \begin{bmatrix} 0 & \hat{\sigma}_y \\ \hat{\sigma}_y & 0 \end{bmatrix}, \tag{2.29}$$

which represents the chiral symmetry of the Hamiltonian.

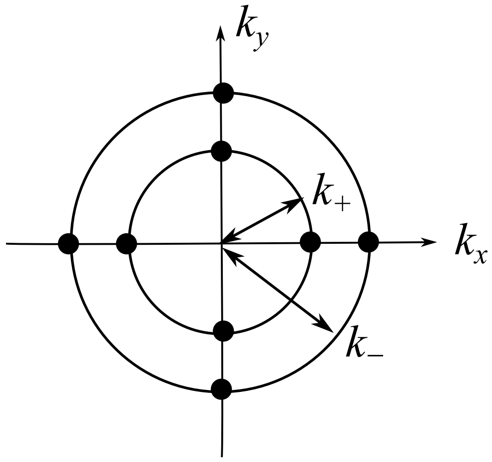


**Figure 2.4:** Two Fermi surfaces under the Rashba SOC are illustrated. The eight nodal points are indicated by the black dots.

A superconductor with $(d_{xy} + p)$-wave pairing symmetry is an example of NCS which host the flat ZES at its clean surface [31, 32, 43, 73]. Under the Rashba type SOC $\boldsymbol{g}_{\mathrm{r}}(\boldsymbol{k}) =$

$\alpha(k_y\boldsymbol{x} - k_x\boldsymbol{y})$ with $\alpha$ being the coupling amplitude, the normal state Fermi surface splits into the two circles as illustrated in Fig. 2.4, where the two wave numbers

$$k_{\pm} = \mp\frac{m\alpha}{\hbar^2} + \sqrt{k_{\mathrm{F}}^2 + \left(\frac{m\alpha}{\hbar^2}\right)^2}, \tag{2.30}$$

characterize the two Fermi surfaces. The pair potential of the $(d_{xy}+p)$-wave superconductor is given as

$$\psi(\boldsymbol{k}) = \Delta_s f(\boldsymbol{k}), \quad \boldsymbol{d}(\boldsymbol{k}) = \Delta_t f(\boldsymbol{k})\frac{\boldsymbol{g}_{\mathrm{r}}(\boldsymbol{k})}{\alpha k}, \tag{2.31}$$

with $f(\boldsymbol{k}) = (k_x k_y/k^2)$ and $k = \sqrt{k_x^2 + k_y^2}$. In this pair potential, there are eight nodal points which are located at $(\pm k_{\pm}, 0)$ and $(0, \pm k_{\pm})$ as illustrated in Fig. 2.4.

By applying a unitary transformation shown in Appendix (C), it is possible to deform the BdG Hamiltonian of the $(d_{xy}+p)$-wave superconductor as

$$\check{H}_0'(\boldsymbol{k}) = \begin{bmatrix} \hat{H}_+(\boldsymbol{k}) & 0 \\ 0 & \hat{H}_-(\boldsymbol{k}) \end{bmatrix}, \tag{2.32}$$

$$\hat{H}_{\pm}(\boldsymbol{k}) = \begin{bmatrix} \xi_{\pm}(\boldsymbol{k}) & -\Delta_{\pm}(\boldsymbol{k}) \\ -\Delta_{\pm}(\boldsymbol{k}) & -\xi_{\pm}(\boldsymbol{k}) \end{bmatrix}, \tag{2.33}$$

$$\xi_{\pm}(\boldsymbol{k}) = \xi(\boldsymbol{k}) \pm |\boldsymbol{g}_{\mathrm{r}}(\boldsymbol{k})|, \qquad \Delta_{\pm}(\boldsymbol{k}) = f(\boldsymbol{k})\left[\Delta_t \pm \Delta_s\right]. \tag{2.34}$$

The chiral symmetry in this new basis is represented as

$$\hat{S}_{\pm}\, \hat{H}_{\pm}(\boldsymbol{k})\, \hat{S}_{\pm}^{-1} = -\hat{H}_{\pm}(\boldsymbol{k}), \quad \hat{S}_{\pm} = \mp\hat{\sigma}_y. \tag{2.35}$$

By using Eqs. (2.33) and (2.35), the relevant winding number can be calculated as [9, 11]

$$w(k_y) = w_+(k_y) - w_-(k_y), \tag{2.36}$$

$$w_{\pm}(k_y) = \frac{1}{2}\sum_{\xi_{\pm}(\boldsymbol{k})=0} \mathrm{sgn}[\partial_{k_x}\xi_{\pm}(\boldsymbol{k})]\mathrm{sgn}[\Delta_{\pm}(\boldsymbol{k})], \tag{2.37}$$

where the summation is carried out for $k_x$ that satisfies $\xi_{\pm}(\boldsymbol{k}) = 0$ with fixed $k_y$. From Eq. (2.36), we obtain

$$w(k_y) = \begin{cases} 2\mathrm{sgn}(k_y) & \text{for} \quad |k_y| < k_+ \\ \mathrm{sgn}(k_y) & \text{for} \quad k_+ < |k_y| < k_- \\ 0 & \text{for} \quad |k_y| > k_-, \end{cases} \tag{2.38}$$

for $\Delta_s > \Delta_t$, and

$$w(k_y) = \begin{cases} 0 & \text{for} \quad |k_y| < k_+ \\ -\mathrm{sgn}(k_y) & \text{for} \quad k_+ < |k_y| < k_- \\ 0 & \text{for} \quad |k_y| > k_-, \end{cases} \tag{2.39}$$

for $\Delta_t > \Delta_s$. The index $\mathcal{N}_{\mathrm{ZES}}$ is calculated from Eq. (2.15). Since the winding number satisfies $w(k_y) = -w(-k_y)$, we immediately find $\mathcal{N}_{\mathrm{ZES}} = 0$ for both $\Delta_s > \Delta_t$ and $\Delta_t > \Delta_s$.

The figure 2.5 shows the eigenvalues of the BdG Hamiltonian for a $(d_{xy} + p)$-wave superconductor. The expression of the Hamiltonian on the tight-binding model is given in Appendix (B.2). We chose parameters as $\mu_{\mathrm{F}} = 2.0t$, $\alpha = 0.1t$, $\Delta_s = 0.8t$, $\Delta_t = 0.2t$, $L_x = 50a_0$, $L_y = 10a_0$ and $L_d = 5a_0$. The open and the filled symbols denote the energy eigenvalues of a superconductor with the clean surface ($W = 0$) and the dirty surfaces ($W = 3.0$t), respectively. The present parameter choice leads $\mathcal{N}_{\mathrm{clean}} = 8$. As shown with the open symbol, we indeed find the $2 \times \mathcal{N}_{\mathrm{clean}} = 16$ zero-energy states at the clean surface. The random potential at the surfaces completely lifts the degeneracy at zero energy as shown with the filled symbols. The numerical results agree with the argument in Sec. (2.3). Since $\mathcal{N}_{\mathrm{ZES}} = 0$, the flat ZES in a $(d_{xy} + p)$-wave superconductor is fragile under the potential disorder. At finte energies, the eigenvalues for dirty surfaces are always doubly degenerate, which corresponds to the Kramers doublets protected by time-reversal symmetry.

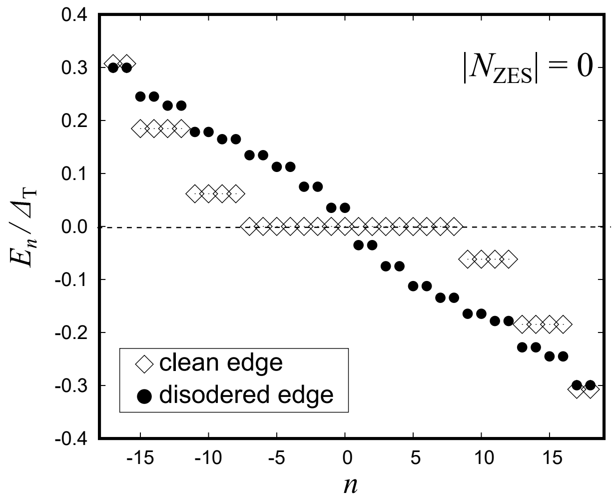


**Figure 2.5:** Energy eigenvalues of a $(d_{xy} + p)$-wave superconductor are plotted in the same manner as in Fig. 2.3. A energy is normalized by $\Delta_{\mathrm{T}} = \Delta_s + \Delta_t$. In the clean limit, there are 16 zero-energy states as shown with the open symbols. In the presence of random potential at the two surfaces, on the other hand, the ZESs are absent as shown with the filled symbols in agreement with $\mathcal{N}_{\mathrm{ZES}} = 0$.

### 2.4.3 Noncentrosymmetric superconductor II

In a zincblende semiconductor quantum well confined in the [110] crystal direction, the Dresselhaus [110] type spin-orbit coupling described by $\boldsymbol{g}_{\rm d}(\boldsymbol{k}) = \beta k_x \boldsymbol{z}$ becomes dominant. The Hamiltonian for the normal states is given by

$$\hat{h}_{\rm P}(\boldsymbol{k}) = \xi(\boldsymbol{k})\hat{\sigma}_0 + \beta k_x \hat{\sigma}_z. \tag{2.40}$$

The electronic states described by Eq. (2.40) have been well studied in spintronics because they show an unusual spin property called persistent spin helix [74–77]. As shown in Appendix (D), the persistent spin-helix states can be also obtained in the thin film growing along the [001] crystal direction [74,75]. In what follows, we discuss the flat ZESs appearing at a surface of a proximity-induced superconducting Dresselhaus[110] thin film described by

$$\check{H}_0(\boldsymbol{k}) = \begin{bmatrix} \hat{h}_{\rm P}(\boldsymbol{k}) & \hat{\Delta}_{\rm P}(\boldsymbol{k}) \\ -\hat{\Delta}^*_{\rm P}(-\boldsymbol{k}) & -\hat{h}^*_{\rm P}(-\boldsymbol{k}) \end{bmatrix}, \tag{2.41}$$

$$\hat{\Delta}_{\rm P} = i\left[\Delta_s + \Delta_t \frac{k_x}{k_{\rm F}}\hat{\sigma}_z\right]\hat{\sigma}_y, \tag{2.42}$$

where we assume the $s$-wave pairing symmetry for the spin-singlet component. The Dresselhaus[110] SOC potential shifts the Fermi surfaces in the $k_x$ direction as illustrated in Fig. 2.6. The center of the Fermi surfaces are located at $(\pm Q, 0)$ with $Q = m\beta/\hbar^2$. The superconducting gap has four nodes on the Fermi surface when the condition

$$\frac{\beta k_{\rm F}}{\mu_{\rm F}} > \frac{\Delta_s^2 - \Delta_t^2}{\Delta_s \Delta_t} \tag{2.43}$$

is satisfied. The four nodal points are located at

$$(\pm r_{st} k_{\rm F}, \pm k_{\rm Q}), \qquad k_{\rm Q} = k_{\rm F}\sqrt{1 - r_{st}^2 + r_{st}(\beta k_{\rm F}/\mu_{\rm F})}, \tag{2.44}$$

as indicated by filled circle in Fig. 2.6, where $r_{st} = (\Delta_s/\Delta_t)$. The BdG Hamiltonian preserves both time-reversal and time-reversal-like symmetry as

$$\check{T}_\pm\, \check{H}_0(\boldsymbol{k})\, \check{T}_\pm^{-1} = \check{H}_0(-\boldsymbol{k}), \tag{2.45}$$

$$\check{T}_+ = \begin{bmatrix} i\hat{\sigma}_x & 0 \\ 0 & -i\hat{\sigma}_x \end{bmatrix}\mathcal{K}, \quad \check{T}_- = \begin{bmatrix} i\hat{\sigma}_y & 0 \\ 0 & i\hat{\sigma}_y \end{bmatrix}\mathcal{K}, \tag{2.46}$$

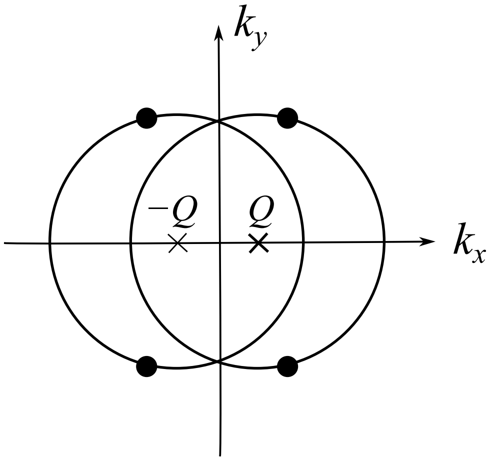


**Figure 2.6:** Fermi surfaces under the Dresselhaus[110] SOC are illustrated. The eight nodal points are indicated by the black dots. Strictly speaking, the positions of the nodal points depend on the parameters as shown in Eq. (2.44).

where $\check{T}_{\pm}^2 = \pm 1$. Therefore we obtain two different chiral symmetry operators as

$$\check{S}_{\pm}\ \check{H}_0(\boldsymbol{k})\ \check{S}_{\pm}^{-1} = -\check{H}_0(\boldsymbol{k}), \tag{2.47}$$

$$\check{S}_{+} = \begin{bmatrix} 0 & -i\hat{\sigma}_x \\ i\hat{\sigma}_x & 0 \end{bmatrix}, \quad \check{S}_{-} = \begin{bmatrix} 0 & \hat{\sigma}_y \\ \hat{\sigma}_y & 0 \end{bmatrix}. \tag{2.48}$$

By applying the unitary transformation as

$$\check{H}'(\boldsymbol{k}) = \check{U}_0^{\dagger} H_0(\boldsymbol{k}) \check{U}_0, \quad \check{U}_0 = \begin{bmatrix} 1 & 0 & 0 & 0 \\ 0 & 0 & 1 & 0 \\ 0 & 0 & 0 & 1 \\ 0 & 1 & 0 & 0 \end{bmatrix}, \tag{2.49}$$

the BdG hamiltonian is block-diagonalized into the two $2\times 2$ sectors as $\check{H}' = \mathrm{diag}(\hat{H}_1, \hat{H}_2)$,

$$\hat{H}_j(\boldsymbol{k}) = \begin{bmatrix} \xi_j(\boldsymbol{k}) & -\Delta_j(\boldsymbol{k}) \\ -\Delta_j(\boldsymbol{k}) & -\xi_j(\boldsymbol{k}) \end{bmatrix}, \tag{2.50}$$

for $j = 1 - 2$ with

$$\xi_{1(2)}(\boldsymbol{k}) = \xi(\boldsymbol{k}) + (-)\beta k_x, \tag{2.51}$$

$$\Delta_{1(2)}(\boldsymbol{k}) = \left[\Delta_t \frac{k_x}{k_{\mathrm{F}}} + (-)\Delta_s\right]. \tag{2.52}$$

The chiral symmetry of each block component is represented as

$$\hat{S}_{\pm,j}\ \hat{H}_j(\boldsymbol{k})\ \hat{S}_{\pm,j}^{-1} = -\hat{H}_j(\boldsymbol{k}), \tag{2.53}$$

for $j = 1 - 2$, where

$$\hat{S}_{+,1} = \hat{\sigma}_y, \quad \hat{S}_{+,2} = \hat{\sigma}_y, \tag{2.54}$$

is originated from time-reversal like symmetry, and

$$\hat{S}_{-,1} = \hat{\sigma}_y, \quad \hat{S}_{-,2} = -\hat{\sigma}_y. \tag{2.55}$$

is originated from time-reversal symmetry. The definition of the winding number depends on the form of the chiral symmetry operator. From the chiral symmetry operator originated from the time-reversal symmetry in Eq. (2.55), the winding number is given by

$$w(k_y) = w_1(k_y) - w_2(k_y), \tag{2.56}$$

with

$$w_j(k_y) = \frac{1}{2} \sum_{\xi_j(\boldsymbol{k})=0} \mathrm{sgn}[\partial_{k_x}\xi_j(\boldsymbol{k})]\mathrm{sgn}[\Delta_j(\boldsymbol{k})], \tag{2.57}$$

for $j = 1 - 2$, where the summation is carried out for $k_x$ satisfying $\xi_j(\boldsymbol{k}) = 0$ at a fixed $k_y$. The winding number in each sector is calculated to be

$$w_1(k_y) = w_2(k_y) = \left\{ \begin{array}{ll} 1 & \text{for} \quad |k_y| < k_{\mathrm{Q}} \\ 0 & \text{for} \quad |k_y| > k_{\mathrm{Q}}. \end{array} \right. , \tag{2.58}$$

Although the winding number in each sector $w_{1(2)}(k_y)$ is nontrivial, the relation $w(k_y) = 0$ always holds. As a consequence, we find $\mathcal{N}_{\mathrm{ZES}} = 0$. The results suggest the degeneracy at zero energy would be fragile under the potential disorder. However, the winding number originated from time-reversal-like symmetry can be nontrivial because the winding number defined with Eq. (2.54) is given as

$$w(k_y) = w_1(k_y) + w_2(k_y). \tag{2.59}$$

As a result, we obtain

$$w(k_y) = \begin{cases} 2 & \text{for} \quad |k_y| < k_{\mathrm{Q}} \\ 0 & \text{for} \quad |k_y| > k_{\mathrm{Q}}. \end{cases}, \tag{2.60}$$

$$\mathcal{N}_{\mathrm{clean}} = \mathcal{N}_{\mathrm{ZES}} = 2 \sum_{|k_y|<k_{\mathrm{Q}}} . \tag{2.61}$$

In Fig. 2.7, we show the energy eigenvalues of the NCS with the Dresselhaus[110] SOC on the tight-binding model. The BdG Hamiltonian used in the numerical simulation is show in Appendix (B.3). We chose parameters as $\mu_{\mathrm{F}} = 1.0t$, $\beta = 0.1t$, $\Delta_s = 0.1t$, $\Delta_t = 0.9t$, $L_x = 50a_0$, and $L_y = 10a_0$. This parameter choice leads $|\mathcal{N}_{\mathrm{ZES}}| = \mathcal{N}_{\mathrm{clean}} = 6$. The results for a superconductor with clean surface show $2 \times \mathcal{N}_{\mathrm{clean}} = 12$ ZES as shown with the open symbols. Although we introduce random impurity potential at its surfaces, the flat ZESs remain unchanged as shown with the filled symbols in agreement with the relation $|\mathcal{N}_{\mathrm{ZES}}| = \mathcal{N}_{\mathrm{clean}}$. This suggests the validity of our conclusion in Sec. (2.3). The degeneracy at zero energy is protected by chiral symmetry originated from the time-reversal-like symmetry.

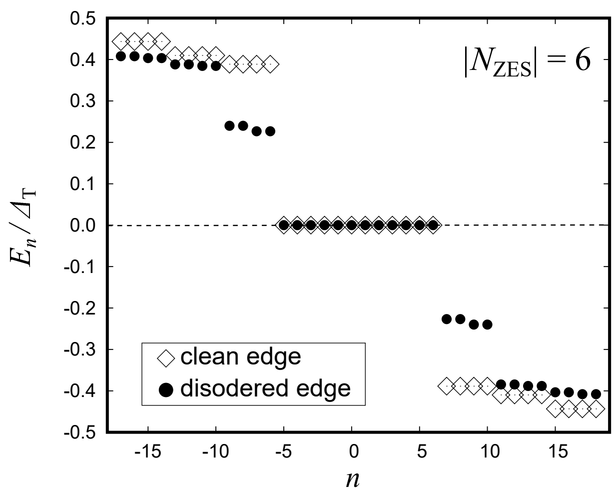


**Figure 2.7:** Energy eigenvalues of a NCS with Dresselhaus[110] SOC are plotted in the same manner as Fig. 2.3. The results are normalized by $\Delta_{\mathrm{T}} = \Delta_s + \Delta_t$. The number of ZESs is 12 in the clean case as shown with the open symbols. All of the ZESs keep staying at zero energy even in the presence of random potential at the two surfaces as predicted by the index $2 \times |\mathcal{N}_{\mathrm{ZES}}| = 12$.

## 2.5 Conclusion

We have discussed the effects of the random impurity potential on the degenerate zero-energy states appearing at the surface of a nodal superconductor preserving chiral symmetry. A method called dimensional reduction enables us to topologically characterize nodal superconductors in the presence of translational symmetry. The number of zero-energy bound states at a clean surface, $\mathcal{N}_{\text{clean}}$, is calculated by using a winding number defined in a one-dimensional Brillouin zone and is usually much larger than unity proportional to the surface width. By focusing on the chiral symmetry of the Bogoliubov-de Gennes Hamiltonian, we show that an index, $\mathcal{N}_{\text{ZES}}$, characterizes the number of zero-energy states at a dirty surface. We confirmed our conclusion with numerical simulations on the tight-binding model. The index $\mathcal{N}_{\text{ZES}}$ is defined by the chiral eigenvalues of zero-energy states. Simultaneously, $\mathcal{N}_{\text{ZES}}$ is calculated from the winding number in a one-dimensional Brillouin zone. The index theorem explains the coincidence of two $\mathcal{N}_{\text{ZES}}$ calculated in the two different ways. We conclude that $\mathcal{N}_{\text{ZES}}$ measures degree of the degeneracy of zero-energy states at a dirty superconductor surface [47]. In experiments, potential disorder is inevitable in the vicinity of the surface. Therefore, our conclusion sends a useful message to experimentalists in this field as regards choosing a target material.

# Chapter 3

# Quantization of conductance minimum and index theorem

## 3.1 Abstract

We discuss the minimum value of the zero-bias differential conductance in a normal-metal/unconventional-superconductor junction. We demonstrate that the zero-bias conductance is quantized at $(4e^2/h)|\mathcal{N}_{\rm ZES}|$ in the limit of strong impurity scatterings in the normal metal. The integer $\mathcal{N}_{\rm ZES}$ represents the number of perfect transmission channels through the junction. An analysis of the chiral symmetry of the Hamiltonian enables us to understand the relationship between the quantization of conductance minimum and the Atiyah-Singer index $\mathcal{N}_{\rm ZES}$.

## 3.2 Introduction

The quantization of an observable value in physics is closely related some of the time to an invariant in mathematics. A good example may be the quantized Hall conductivity in condensed matter physics [78]. Although the quantization of the Hall conductivity itself occurs for physical reasons, the quantized value is proportional to a Chern invariant in a two-dimensional manifold [79]. Another example is the number of gapless states at the surface of a topologically nontrivial material characterized by a topological invariant $Z$ [5, 52]. The integer $Z$ depends on the spatial dimensionality and the symmetry class of the Hamiltonian [4]. The conductance in a junction consisting of such a topologically nontrivial superconductor is quantized at $(2e^2/h)Z$ with $Z = 1$ for a one-dimensional class D superconductor [8, 80, 81]. A similar phenomenon has been discussed as regards superconductors in class BDI with $Z$ being an integer number [81, 82]. The Atiyah-Singer theorem relates a topological invariant to an invariant defined in terms of solutions of a differential equation. The index theorem provides the mathematical background to the quantum anomaly in particle physics. In condensed matter physics, the index theorem describes the number of gapless modes at a boundary between two chiral superfluids. When a quantized physical value is described by a mathematical invariant, the quantization should be robust under various perturbations preserving the invariant. In this paper, we show a relationship between the minimum value of the conductance in a superconducting junction and the Atiyah-Singer index.

In this chapter, we discuss the zero-bias differential conductance $G_{\rm NS}$ in a two-dimensional normal-metal/unconventional-superconductor (NS) junction, where the normal segment consists non-magnetic impurities. The superconductor is characterized by unconventional nodal pairing symmetries such as $d_{xy}$-, $p_x$- and $f$-wave pairing symmetry. On the basis of the lattice Green function techniques, we find that the $G_{\rm NS}$ decreases to the quantized value of $(4e^2/h)|\mathcal{N}_{\rm ZES}|$ with decreasing the normal conductance $G_{\rm N}$. Here, the integer number $\mathcal{N}_{\rm ZES}$ denotes the Atiyah-Singer index that relates the topological property of an unconventional superconductor with the number of zero-energy states at its dirty surface [47]. In the NS junction, the index $\mathcal{N}_{\rm ZES}$ represents the number of perfect transmission channels in a disordered normal segment. The analysis in terms of chiral symmetry of the Hamiltonian enables us to explain the robustness of $|\mathcal{N}_{\rm ZES}|$-fold degenerate resonant states in the dirty NS junction and provide the microscopic understanding of the minimal conductance quantization. To confirm the theoretical prediction by experiments, temperature $T$ must be low so that the thermal coherent length $\xi_T = \sqrt{\hbar D/2\pi k_{\rm B}T}$ is much longer than the length of the the dirty normal segment, where $D$ represents the diffusion constant in the normal segment.

## 3.3 Preliminary

At first, we briefly review the topological property of a nodal unconventional superconductor. Let us consider the three types of unconventional superconductors with $p_x$-wave, $d_{xy}$-wave, and $f$-wave pairing symmetry. We describe the present superconductor by the $2\times 2$ Bogoliubov-de Gennes Hamiltonian (BdG) in momentum space as

$$\hat{H}_0(\boldsymbol{k}) = \left[\begin{array}{cc} \xi(\boldsymbol{k}) & \Delta(\boldsymbol{k}) \\ \Delta(\boldsymbol{k}) & -\xi(\boldsymbol{k}) \end{array}\right], \quad \Delta(\boldsymbol{k}) = \left\{\begin{array}{cl} \Delta_0 k_x k_y/k_{\rm F}^2 & \text{for } d_{xy}\text{-wave}, \\ \Delta_0 k_x/k_{\rm F} & \text{for } p_x\text{-wave}, \\ \Delta_0 k_x(k_{\rm F}^2 - 2k_y^2)/k_{\rm F}^3 & \text{for } f\text{-wave}, \end{array}\right. \tag{3.1}$$

where $\xi(\boldsymbol{k}) = (\hbar^2\boldsymbol{k}^2/2m) - \mu_{\mathrm{F}}$, $m$ denotes the effective mass of an electron, $\mu_{\mathrm{F}}$ is the chemical potential, $\Delta_0$ is the amplitude of the pair potential at zero temperature, and $k_{\mathrm{F}} = \sqrt{2m\mu_{\mathrm{F}}}/\hbar$ represents the Fermi wave number. The Hamiltonian satisfies

$$\left\{\hat{S}, \hat{H}_0(\boldsymbol{k})\right\} = 0, \quad \hat{S} = \hat{\tau}_2, \tag{3.2}$$

which represents chiral symmetry of the Hamiltonian. Pauli matrices in Nambu space is denoted by $\tau_i$ for $i$ = 1-3. Since the pair potentials in Eq. (3.1) have nodes on the Fermi surface, it is impossible to topologically characterize such the superconductors in terms of wave functions of the whole Brillouin zone. Alternatively, we define a winding number in a restricted one-dimensional Brillouin zone as

$$w(\boldsymbol{k}_{\parallel}) = \frac{i}{4\pi}\int dk_{\perp}\mathrm{Tr}[\hat{S}\hat{H}_0{}^{-1}(\boldsymbol{k})\partial_{k_{\perp}}\hat{H}_0(\boldsymbol{k})], \tag{3.3}$$

where $\boldsymbol{k}_{\parallel}$ ($k_{\perp}$) is momenta parallel (perpendicular) to the surface we consider. The winding number $w(\boldsymbol{k}_{\parallel})$ is ill-defined when the integration path along $k_{\perp}$ intersects the nodal points. Therefore, we have to choose $\boldsymbol{k}_{\parallel}$ so that $k_{\perp}$ can keep away from the nodal points. The winding number $w(\boldsymbol{k}_{\parallel})$ can be nonzero in the finite region of $\boldsymbol{k}_{\parallel}$. In what follows, we consider the surface perpendicular to the $x$ direction. Namely, we chose $k_{\perp} = k_x$ and $\boldsymbol{k}_{\parallel} = k_y$, respectively. According to the bulk-boundary correspondence, the total number of topologically protected zero-energy Andreev bound states (ABSs) at the clean surface is calculated by

$$\mathcal{N}_{\mathrm{clean}} = {\sum_{k_y}}' |w(k_y)|, \tag{3.4}$$

where ${\sum_{k_y}}'$ denotes a summation over $k_y$ excluding the nodal points.

Next, we discuss the degree of degeneracy in the ABSs at the dirty surface of an unconventional superconductor. The random impurity potentials in the bulk region strongly suppress the unconventional superconducting pair potential. Thus, we assume the potential disorder exists only near the surface. The BdG Hamiltonian in real space $\hat{H}_0(\boldsymbol{r})$ is obtained by replacing the momentum $\boldsymbol{k}$ by $-i\nabla_{\boldsymbol{r}}$ in Eq. (3.1). The non-magnetic random impurity potential in the vicinity of the surface is represented by $\hat{H}_{\mathrm{imp}}(\boldsymbol{r}) = v(\boldsymbol{r})\hat{\tau}_3$, where the random potential v $(\boldsymbol{r})$ disappears rapidly with the increases of distance from the surface. The total Hamiltonian is given by $\hat{H}(\boldsymbol{r}) = \hat{H}_0(\boldsymbol{r}) + \hat{H}_{\mathrm{imp}}(\boldsymbol{r})$. In the presence of potential disorders, the winding number $w(\boldsymbol{k}_{\parallel})$ is not well defined because the momentum $\boldsymbol{k}_{\parallel}$ is no longer a good quantum number in the absence of translational symmetry. This implies that $w(\boldsymbol{k}_{\parallel})$ cannot predict straightforwardly the number of the ZESs at a dirty surface. Nevertheless, it is possible to characterize the flat-band ZESs at the dirty surface by an alternative index [47]

$$\mathcal{N}_{\mathrm{ZES}} = \sum_{\boldsymbol{k}_\parallel}{}' w(\boldsymbol{k}_\parallel). \tag{3.5}$$

The absolute value of the index $\mathcal{N}_{\mathrm{ZES}}$ coincides with the number of the ZESs at the dirty surface as long as chiral symmetry is preserved. In the following, we discuss the differential conductance of a diffusive normal-metal/unconventional-superconductor junction.

## 3.4 Conductance minimum

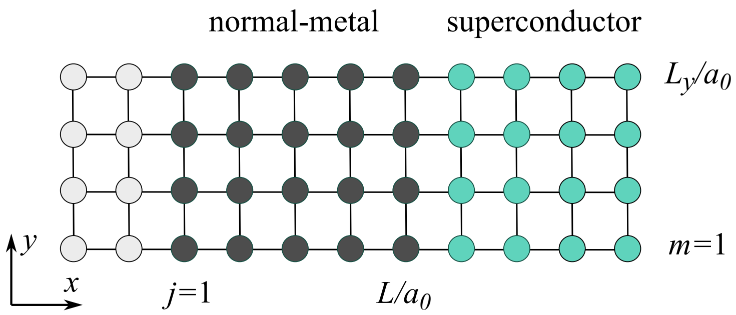


**Figure 3.1:** (Color online) Schematic image of a NS junction on the tight-binding model.

Let us consider an NS junction on the tight-binding model with the lattice constance $a_0$ as shown in Fig. 5.1. A lattice site is indicated by a vector $\boldsymbol{r} = j\ \boldsymbol{x} + m\ \boldsymbol{y}$, where $\boldsymbol{x}$ ($\boldsymbol{y}$) is vector in the $x$ ($y$) direction with $|\boldsymbol{x}| = |\boldsymbol{y}| = a_0$. The present junction consists of three segments: an ideal lead wire ($-\infty \leq j \leq 0$), a normal-metal ($0 < j \leq L/a_0$) and a superconductor ($L/a_0 < j \leq \infty$). In the $y$-direction, the number of the lattice site is $L_y/a_0$ and the periodic boundary condition is applied. In the superconducting segment, we consider the three types of pairing symmetries such as $d_{xy}$-wave, $p_x$-wave, and $f$-wave pairing symmetry. The Hamiltonian reads,

$$H_{\mathrm{NS}} = H_{\mathrm{kin}} + H_\alpha + H_{\mathrm{imp}}. \tag{3.6}$$

The first term in Eq. (3.6) represents the kinetic energy of electrons

$$\begin{aligned} H_{\mathrm{kin}} = & -t \sum_{m=1}^{L_y/a_0} \sum_{j=-\infty}^{\infty} \left[\psi^\dagger_{\boldsymbol{r}+\boldsymbol{x}}\psi_{\boldsymbol{r}} + \boldsymbol{r}^\dagger\psi_{\boldsymbol{r}+\boldsymbol{x}}\right] - t \sum_{m=1}^{L_y/a_0} \sum_{j=-\infty}^{\infty} \left[\psi^\dagger_{\boldsymbol{r}+\boldsymbol{y}}\psi_{\boldsymbol{r}} + \psi^\dagger_{\boldsymbol{r}}\psi_{\boldsymbol{r}+\boldsymbol{y}}\right] \\ & + \sum_{m=1}^{L_y/a_0} \sum_{j=-\infty}^{\infty} (4t-\mu)\psi^\dagger_{\boldsymbol{r}}\psi_{\boldsymbol{r}}, \end{aligned} \tag{3.7}$$

where $\psi_{\boldsymbol{r}}$ ($\psi^\dagger_{\boldsymbol{r}}$) is the annihilation (creation) operator of an electron at $\boldsymbol{r}$, $t$ is the hopping integral, $\mu$ is the chemical potential. The second term $H_\alpha$ ($\alpha = d_{xy},\ p_x,\ f$) denotes the pair potential in the superconducting segment

$$\begin{aligned} H_{d_{xy}} = & \frac{\Delta}{4} \sum_{m=1}^{L_y/a_0} \sum_{j=L/a_0+1}^{\infty} \\ & \left[\psi^\dagger_{\boldsymbol{r}+\boldsymbol{x}+\boldsymbol{y}}\psi^\dagger_{\boldsymbol{r}} + \psi^\dagger_{\boldsymbol{r}}\psi^\dagger_{\boldsymbol{r}+\boldsymbol{x}+\boldsymbol{y}} - \psi^\dagger_{\boldsymbol{r}+\boldsymbol{x}-\boldsymbol{y}}\psi^\dagger_{\boldsymbol{r}} - \psi^\dagger_{\boldsymbol{r}}\psi^\dagger_{\boldsymbol{r}+\boldsymbol{x}-\boldsymbol{y}}\right] + \mathrm{H.c.}, \end{aligned} \tag{3.8}$$

$$H_{p_x} = i\frac{\Delta}{2} \sum_{m=1}^{L_y/a_0} \sum_{j=L/a_0+1}^{\infty} \left[\psi^\dagger_{\boldsymbol{r}+\boldsymbol{x}}\psi^\dagger_{\boldsymbol{r}} - \psi^\dagger_{\boldsymbol{r}}\psi^\dagger_{\boldsymbol{r}+\boldsymbol{x}}\right] + \mathrm{H.c.} \tag{3.9}$$

$$\begin{aligned} H_f = & i\frac{\Delta}{4} \sum_{m=1}^{L_y/a_0} \sum_{j=L/a_0+1}^{\infty} \\ & \left[\psi^\dagger_{\boldsymbol{r}+\boldsymbol{x}+2\boldsymbol{y}}\psi^\dagger_{\boldsymbol{r}} - \psi^\dagger_{\boldsymbol{r}}\psi^\dagger_{\boldsymbol{r}+\boldsymbol{x}+2\boldsymbol{y}} + \psi^\dagger_{\boldsymbol{r}+\boldsymbol{x}-2\boldsymbol{y}}\psi^\dagger_{\boldsymbol{r}} - \psi^\dagger_{\boldsymbol{r}}\psi^\dagger_{\boldsymbol{r}+\boldsymbol{x}-2\boldsymbol{y}}\right] + \mathrm{H.c.}, \end{aligned} \tag{3.10}$$

where $\Delta$ is the amplitude of the pair potential. We also introduce the disordered potential in the normal segment

$$H_{\mathrm{imp}} = \sum_{m=1}^{L_y/a_0} \sum_{j=1}^{L/a_0} v(\boldsymbol{r})\psi^\dagger_{\boldsymbol{r}}\psi_{\boldsymbol{r}}, \tag{3.11}$$

where $V(\boldsymbol{r})$ is given randomly in range of the $-W/2 \leq v(\boldsymbol{r}) \leq W/2$. We calculate the zero-bias differential conductance $G_{\mathrm{NS}}$ of the NS junctions based on the Blonder-Tinkham-Klapwijk formula [83]

$$G_{\mathrm{NS}} = \frac{2e^2}{h} \sum_{\zeta,\eta} \left[\delta_{\zeta,\eta} - \left|r^{ee}_{\zeta,\eta}\right|^2 + \left|r^{he}_{\zeta,\eta}\right|^2\right], \tag{3.12}$$

where $r^{ee}_{\zeta,\eta}$ and $r^{he}_{\zeta,\eta}$ denote the normal and Andreev reflection coefficients at the zero energy, respectively. The index $\zeta$ and $\eta$ label the outgoing channel and the incoming one, respectively. These reflection coefficients are numerically calculated by using the lattice Green's function technique [84, 85, 88].

In Fig. 3.2, we plot the zero-bias conductance $G_{\mathrm{NS}}$ versus the normal conductance $G_{\mathrm{N}}$, where $G_{\mathrm{N}}$ is calculated by setting $\Delta = 0$. The parameters are chosen as $\mu/t = 1.0$, $\Delta/t = 0.01$, $L/a_0 = 30$, and $W/a_0 = 25$, respectively. With this parameter choice, the number of propagating channels $N_{\mathrm{C}}$ become nine, and the index $\mathcal{N}_{\mathrm{ZES}}$ becomes $\mathcal{N}_{\mathrm{ZES}} = 0$, 9, and 5 for $d_{xy}$-, $p_x$-, and $f$-wave pairing symmetry, respectively. As shown in Fig. 3.2, the ZBC of $d_{xy}$-wave NS junction goes to zero in the dirty limit ($G_{\mathrm{N}} \approx 0$) [7, 87, 87, 88]. In the $p_x$-wave case, on the other hand, the ZBC is quantized at $(4e^2/h) \times 9$ irrespective of $G_{\mathrm{N}}$ [14, 15]. For the $f$-wave symmetry, the ZBC decreases to the quantized value of $(4e^2/h) \times 5$ by decreasing $G_{\mathrm{N}}$. By summarizing these numerical results, we can describe the $G_{\mathrm{NS}}$ in the dirty limit as

$$\lim_{G_{\mathrm{N}} \to 0} G_{\mathrm{NS}} = \frac{4e^2}{h} |\mathcal{N}_{\mathrm{ZES}}|. \tag{3.13}$$

The index $\mathcal{N}_{\mathrm{ZES}}$ is originally proposed as the topological index denoting the number of ZESs at the dirty surface of an isolating unconventional superconductor. In the NS junction, on the other hand, the quantization of conductance minimum in Eq. (3.13) suggests the existence of $|\mathcal{N}|_{\mathrm{ZES}}$ resonant transmission channels in the dirty normal segment. In the following section, we analytically prove the robustness of $|\mathcal{N}_{\mathrm{ZES}}|$-fold degenerate resonant states in the diffusive NS junction and provide the microscopic understanding of the minimal conductance quantization.

## 3.5 Chirality analysis

In this section, we describe the NS junction in continuous space for simplicity. The Bogolibov-de Gennes (BdG) Hamiltonian is represented by

$$\hat{H}_{\mathrm{NS}}(\boldsymbol{r}) = \begin{bmatrix} \xi(\boldsymbol{r}) + v(\boldsymbol{r})\Theta(-x) & \Delta_\alpha(\boldsymbol{r})\Theta(x) \\ \Delta_\alpha(\boldsymbol{r})\Theta(x) & -\xi(\boldsymbol{r}) - v(\boldsymbol{r})\Theta(-x) \end{bmatrix}, \tag{3.14}$$

$$\xi(\boldsymbol{r}) = -\hbar^2 \boldsymbol{\nabla}^2/(2m) - \mu, \tag{3.15}$$

$$\Delta_{d_{xy}}(\boldsymbol{r}) = -\Delta\partial_x\partial_y/k_{\mathrm{F}}^2, \quad \Delta_{p_x}(\boldsymbol{r}) = -i\Delta\partial_x/k_{\mathrm{F}}, \quad \Delta_f(\boldsymbol{r}) = -i\Delta\partial_x(k_{\mathrm{F}}^2 - 2\partial_y^2)/k_{\mathrm{F}}^3, \tag{3.16}$$

where $m$ is the effective of an electron, $k_{\mathrm{F}} = \sqrt{2m\mu_{\mathrm{F}}}/\hbar$ is the Fermi wave number, and $\Theta(x)$ denotes the step function. The NS interface is located at $x = 0$. The Hamiltonian

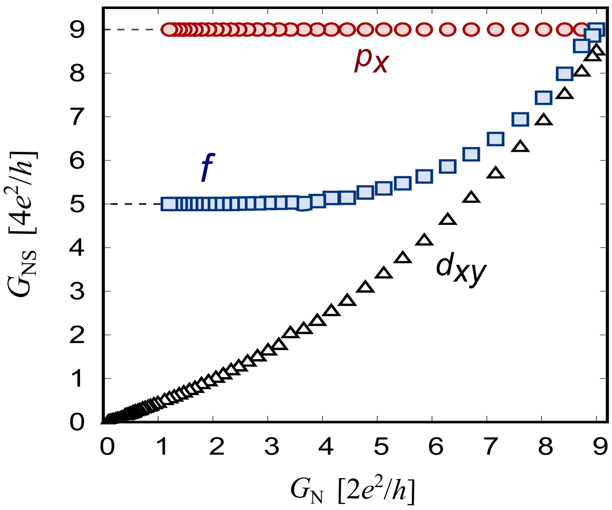


**Figure 3.2:** (Color online) Zero-bias conductance $G_{\rm NS}$ as a function of the normal conductance $G_{\rm N}$ is plotted. The number of the samples for the ensemble average is $10^3$.

satisfies

$$\left\{\hat{S}, \hat{H}_{\rm NS}(\boldsymbol{r})\right\} = 0, \tag{3.17}$$

which represents chiral symmetry of the Hamiltonian. Here we summarize the two important features of eigenstates of $\hat{H}_{\rm NS}(\boldsymbol{r})$ preserving chiral symmetry [9].

(i) First, the zero-energy states of $\hat{H}_{\rm NS}(\boldsymbol{r})$ are simultaneously the eigenstates of the chiral operator $\hat{S}$. Since $\hat{S}^2 = 1$, the eigenvalue of $\hat{S}$ is either $\gamma = +1$ or $\gamma = -1$. Namely, a zero-energy states satisfying $\hat{H}_{\rm NS}(\boldsymbol{r})\varphi_\gamma(\boldsymbol{r}) = 0$ also satisfies $\hat{S}\varphi_\gamma(\boldsymbol{r}) = \gamma\varphi_\gamma(\boldsymbol{r})$. We refer to $\gamma$ as the chirality in the following.

(ii) Second, the nonzero energy states of $\hat{H}_{\rm NS}(\boldsymbol{r})$ are described by the linear combination of the two states: one has $\gamma = +1$ and the other has $\gamma = -1$. Namely, a nonzero energy state is described as $\varphi_{E\neq 0}(\boldsymbol{r}) = c_+\chi_+(\boldsymbol{r}) + c_-\chi_-(\boldsymbol{r})$, where $\hat{S}\chi_\pm(\boldsymbol{r}) = \pm\chi_\pm(\boldsymbol{r})$. Moreover, the relation $|c_+| = |c_-|$ always holds [50].

Below, we examine the stability of degenerate zero-energy states in the diffusive NS junction by taking these features into account.

We first analyze the chiral property of the zero-energy Andreev bound states (ABSs) appearing at the surface of the semi-infinite superconductor occupying $x \geq 0$. To do this, we remove the normal segment ($x < 0$) and apply the hard-wall boundary condition at $x = 0$. By solving the Bogoliubov-de Gennes equation, we obtain the wave function for

**Table 3.1:** The key integer numbers are summarized, where $P = L_y k_\mathrm{F}/\pi$ and $[\cdots]_\mathrm{G}$ is the Gauss symbol giving the integer part of the argument.

| | $N_+$ | $N_-$ | $N_\mathrm{ZES}$ |
|---|---|---|---|
| $d_{xy}$ | $[P/2]_\mathrm{G}$ | $[P/2]_\mathrm{G}$ | $0$ |
| $p_x$ | $N_\mathrm{C}$ | $0$ | $N_\mathrm{C}$ |
| $f$ | $\left[P/\sqrt{2}\right]_\mathrm{G}$ | $\left[P(1-1/\sqrt{2})\right]_\mathrm{G}$ | $\left[P(\sqrt{2}-1)\right]_\mathrm{G}$ |

the ABSs as

$$\varphi_{\mathrm{S},q}(\boldsymbol{r}) = \begin{bmatrix} 1 \\ -is(q) \end{bmatrix} X_q(x) Y_q(y), \tag{3.18}$$

$$s(q) = A_\alpha(q)/|A_\alpha(q)|, \tag{3.19}$$

$$X_q(x) = \sin[p_q x] e^{-x/\xi_q}, \quad Y_q(y) = e^{iqy}/\sqrt{L_y}, \tag{3.20}$$

$$p_q^2 = k_q^2 - \xi_q^{-2}, \quad k_q^2 = k_\mathrm{F}^2 - q^2, \quad \xi_q = \hbar^2 k_\mathrm{F}/m|A_\alpha(q)|, \tag{3.21}$$

$$A_{d_{xy}}(q) = \Delta(q/k_\mathrm{F}), \quad A_{p_x}(q) = \Delta, \quad A_f(q) = \Delta[1 - 2(q/k_\mathrm{F})^2] \tag{3.22}$$

where $q < k_\mathrm{F}$ indicates the propagating channel. The total number of propagating channel is represented by $N_\mathrm{C} = [(L_y k_\mathrm{F}/\pi)]_\mathrm{G}$, where $[\cdots]_\mathrm{G}$ is the Gauss symbol giving the integer part of the argument. As suggested by the chiral property (i), the wave function $\varphi_{\mathrm{S},q}(\boldsymbol{r})$ become the eigenstate of $\hat{S}$ belonging to its eigenvalue $\gamma = s(q)$. Here, we define two integer numbers $N_+$ and $N_-$ in the clean limit, where $N_+$ ($N_-$) represents the number of ABSs with positive (negative) chiral eigenvalue. We count $N_\pm$ for each pairing symmetry as listed in Table 3.1. For the $d_{xy}$-wave pairing symmetry, we obtain $N_+ = N_- = [(L_y k_\mathrm{F}/\pi)/2]_\mathrm{G}$ because the ABSs for $q > 0$ ($q < 0$) belong to $\gamma = +1$ ($-1$). For the $p_x$-wave pairing symmetry, we find $N_+ = N_\mathrm{C}$ and $N_- = 0$ because $\gamma = +1$ for all the propagating channels. For the $f$-wave pairing symmetry, we find $N_+ = \left[(L_y k_\mathrm{F}/\pi)/\sqrt{2}\right]_\mathrm{G}$ and $N_- = \left[(L_y k_\mathrm{F}/\pi)(1 - 1/\sqrt{2})\right]_\mathrm{G}$. The index $\mathcal{N}_\mathrm{ZES}$ is related with the chiral eigenvalue of the ABSs as $|\mathcal{N}_\mathrm{ZES}| = |N_+ - N_-|$ [47]. As a result, we obtain

$$|\mathcal{N}_\mathrm{ZES}| = \begin{cases} 0 & \text{for } d_{xy}\text{-wave}, \\ N_\mathrm{C} & \text{for } p_x\text{-wave}, \\ \left[(L_y k_\mathrm{F}/\pi)(\sqrt{2}-1)\right]_\mathrm{G} & \text{for } f\text{-wave}. \end{cases} \tag{3.23}$$

Next, we attach the clean normal segment to the left side of the superconductor ($x < 0$). In the absence of potential disorders ( i.e., $v(\boldsymbol{r}) = 0$), the wave function in the normal segment at $E = 0$ is described by

$$\varphi_{\mathrm{N},q}(\boldsymbol{r}) = \left( \begin{bmatrix} 1 \\ r_q^{he} \end{bmatrix} e^{ik_q x} + \begin{bmatrix} r_q^{ee} \\ 0 \end{bmatrix} e^{-ik_q x} \right) Y_q(y), \tag{3.24}$$

where the normal and Andreev reflection coefficients for the channel $q$ are represented by $r_q^{ee}$ and $r_q^{he}$, respectively. From the boundary condition at the NS interface ($x = 0$), the reflection coefficients are calculated to be

$$r_q^{ee} = 0, \quad r_q^{he} = is(q). \tag{3.25}$$

By substituting Eq. (3.25) into Eq. (3.24), we find that $\varphi_{\mathrm{N},q}(\boldsymbol{r})$ belongs to the same chirality of $\varphi_{\mathrm{S},q}(\boldsymbol{r})$ as $\hat{S}\varphi_{\mathrm{N},q}(\boldsymbol{r}) = s(q)\varphi_{\mathrm{N},q}(\boldsymbol{r})$. Namely, the Andreev reflection copies the chirality of the ABSs to the wave functions in the normal segment.

Finally, we introduce the disordered potential $v(\boldsymbol{r})$ in the normal segment. In the presence of potential disorders breaking translational symmetry, the channel index $q$ is no longer a good quantum number. Thus, the high degree of degeneracy in the ZESs of the clean NS junction seems to be fragile against potential disorders. Nevertheless, the chiral properties enable us to explain the minimal conductance quantization in Eq. (3.13). The essence of the argument below is also illustrated in Fig. 3.3. With the $d$-wave symmetry, the index $\mathcal{N}_{\mathrm{ZES}} = 0$ because the relation $N_+ = N_-$ always holds [See also Fig. 3.3(a) with $N_+ = N_- = 2$]. The potential disorder completely eliminate the degeneracy at zero energy because two ZESs with $\gamma = +1$ and $\gamma = -1$ couple to one-by-one and form two nonzero-energy states according to the chiral property (ii) [See also Fig. 3.3(b)]. This explains the absence of the proximity effect in a $d_{xy}$-wave NS junction [7, 87, 87, 88]. In the $p_x$-wave case, on the other hand, all ZESs possess the positive chirality $\gamma = +1$ [See also Fig. 3.3(c) with $N_+ = 4$]. Therefore, the relation $|\mathcal{N}_{\mathrm{ZES}}| = N_{\mathrm{C}}$ always holds. According to the property (ii), such the pure chiral states cannot form nonzero-energy states because they need negative chiral ZESs to construct nonzero-energy states [See also Fig. 3.3(d)]. According to the property (i), the ZESs in the dirty NS junction must be the eigenstates of $\hat{S}$. We emphasize that the wave function for the normal segment in Eq. (3.24) can be the eigenstates of $\hat{S}$ only when $|r^{ee}| = 0$ and $|r^{he}| = |\gamma| = 1$ is satisfied. Therefore, the $N_{\mathrm{C}}$-fold degenerate ZESs in the dirty normal metal form the $N_{\mathrm{C}}$ perfect transmission channels there. This fact explains the anomalous proximity effect of a $p_x$-wave superconductor [14, 15, 19, 20]. In the $f$-wave case, the ZESs belonging to $\gamma = +1$ and $\gamma = -1$ coexist at the clean NS junction, where the relation $N_+ > N_-$ holds [See also Fig. 3.3(e) with $N_+ = 3$ and $N_- = 1$]. By introducing potential disorder, $N_-$ negative chiral ZESs can couple to $N_-$ positive chiral ZESs. As a result, they form the nonzero

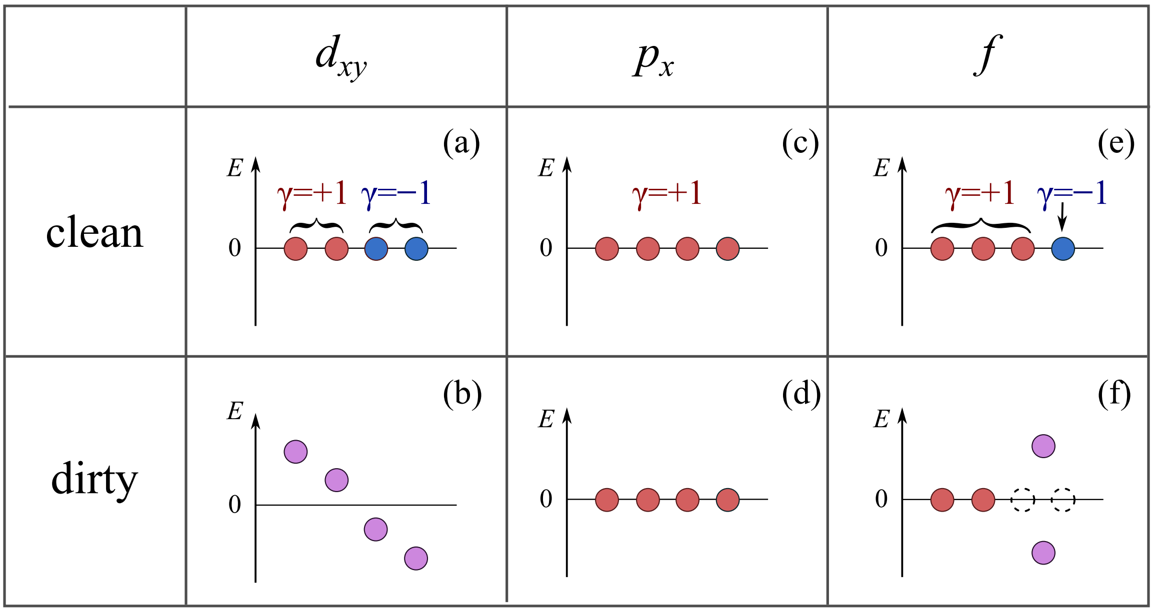


**Figure 3.3:** (Color online) (a)Fourfold degenerate zero-energy states (ZESs) at the clean NS junction with $d_{xy}$-wave pair potential. The number of positive chiral ZESs and that of negative chiral ZESs are the same( i.e., $N_+ = N_- = 2$). The fourfold degeneracy is protected by translational symmetry. (b)In the presence of potential disorders, a positive and a negative chiral ZES form a pair and departs from zero-energy. As a consequence, the potential disorder completely eliminate the degeneracy at zero energy. (c)Fourfold degenerate ZESs at the clean NS junction with $p_x$-wave pair potential. All ZESs belong to the positive chirality ( i.e., $N_+ = 4$, $N_- = 0$). (d)Even in the presence of potential disorders, the ZESs can retain their fourfold degeneracy because negative chiral ZESs is absent. (e)Fourfold degenerate ZESs at the clean NS junction with $f$-wave pair potential. Three of them belong to the positive chirality (i.e., $N_+ = 3$). One remaining ZES belongs to the negative chirality (i.e., $N_- = 1$). (f)In the presence of the disordered potential, the $N_-$ negative chiral ZES couples to $N_-$ positive chiral ZES. As a consequence, $2N_-$ ZESs depart from zero-energy. However, $N_+ - N_- = 2$ positive chiral ZESs remain at zero energy because their chiral partner is absent.

energy states whose number is $2N_-$. However, $|\mathcal{N}_{\mathrm{ZES}}| = N_+ - N_-$ positive chiral states can remain at zero energy even in the presence of potential disorder because their chiral partner is absent [See also Fig. 3.3(f)] . We note that the ZESs can be the eigenstates of $\hat{S}$ only when the Andreev reflection is perfect. Thus, the $|\mathcal{N}_{\mathrm{ZES}}|$-fold degenerate ZESs in dirty NS junction form the $|\mathcal{N}_{\mathrm{ZES}}|$ perfect transmission channels there. This explains the quantization of the conductance minimum at $(4e^2/h)\mathcal{N}_{\mathrm{ZES}}$, where $\mathcal{N}_{\mathrm{ZES}} < N_{\mathrm{C}}$.

## 3.6 Conclusion

In conclusion, we have discussed the zero-bias differential conductance in the normal-metal/superconductor junction, where the superconducting segment is characterized by unconventional pairing symmetries such as $d_{xy}$-, $p_x$- and $f$-wave pairing symmetry. The minimum value of $G_{\rm NS}$ in $p_x$- and $f$-wave NS junction is quantized at $(4e^2/h)|\mathcal{N}_{\rm ZES}|$. The integer number $\mathcal{N}_{\rm ZES}$ represents an Atiyah-Singer index which relates the topological property of an unconventional superconductor with the number of zero-energy states at its dirty surface. The analysis in terms of chiral symmetry of the Hamiltonian enables us to prove the existence of $|\mathcal{N}_{\rm ZES}|$ perfect transmission channels in the dirty NS junction. As a consequence, we provide the microscopic understanding of the minimal conductance quantization including the anomalous proximity effect of a $p_x$-wave superconductor.

# Chapter 4

# Degeneracy of Majorana bound states and fractional Josephson effect in a dirty SNS junction

## 4.1 Abstract

We theoretically study the stability of more than one Majorana Fermion appearing in a $p$-wave superconductor/dirty normal metal/$p$-wave superconductor junction in two-dimension by using chiral symmetry of Hamiltonian. At the phase difference across the junction $\varphi$ being $\pi$, we will show that all of the Majorana bound states in the normal metal belong to the same chirality. Due to this pure chiral feature, the Majorana bound states retain their high degree of degeneracy at the zero energy even in the presence of potential disorders. As a consequence, the resonant transmission of a Cooper pair via the degenerate Majorana bound states carries the Josephson current at $\varphi = \pi - 0^+$, which explains the fractional current-phase relationship discussed in a number of previous papers.

## 4.2 Introduction

Exotic properties of Majorana fermions (MFs) [53, 54] have been a hot issue in condensed matter physics. MFs emerge as the surface bound states of topologically nontrivial superconductors such as a $p$-wave superconductor [28, 55–57], a topological insulator/superconductor heterostructure [58], a spin-orbit coupled semiconductor/superconductor heterostructure [59–64] and a Shiba chain [68, 69]. Such the Majorana fermion bound states (MBSs) have attracted much attention from a view of the fault-tolerant topological quantum computation [89–91]. Thus, the realization of MBSs is a recent desired subject in experimental fields [66, 67, 70].

When two one-dimensional semi-infinite $p$-wave superconductors are joined in a superconductor/insulator/superconductor (SIS) junction, a pair of MFs staying at the two junction interfaces form the Andreev bound states. As a consequence, the Josephson current exhibits the fractional current-phase ($J$-$\varphi$) relationship of $J(\varphi) \propto \sin(\varphi/2)$ at the zero temperature [18, 56]. The fractional Josephson effect is especially important because the effect provides a way of read-out process in the fault-tolerant topological computation [91]. Here we note that $J$ is always $2\pi$ periodic in the direct-current Josephson effect. Thus the fractional current-phase relationship (CPR) means that the current jumps at $\varphi = \pm\pi$. It has been well known that a ballistic superconductor/normal metal/superconductor junction with the spin-singlet $s$-wave pairing symmetry [92–96] and a SIS junction with the spin-singlet $d_{xy}$-wave pairing symmetry [12, 13, 16, 17, 30] also indicate the fractional CPR. The unique feature to $p$-wave junctions is the persistence of the fractional CPR even in the presence of random impurity potentials [8]. In fact, a theoretical study [19, 20] reported the fractional Josephson effect in a two-dimensional $p_x$-wave superconductor/dirty normal-metal/$p_x$-wave superconductor (SNS) junction. In the two-dimensional junction, more than one MF retains their degeneracy at the zero energy in the dirty normal-metal and assist the resonant transmission of the Cooper pair at $\varphi = \pi - 0^+$. Generally speaking, the large degree of degeneracy in quantum states is a consequence of high symmetry of Hamiltonian. However it has been unclear what symmetry protects the degeneracy of the MBSs in a dirty normal metal. We address this issue in the present chapter.

Several previous studies have suggested that chiral symmetry of Hamiltonian is a key feature to explain the stability of more than one MF at a surface of topologically nontrivial superconductor [44–46]. On the basis of these novel insight, we will prove the robustness of the degenerate MBSs in dirty SNS junctions. In addition, we reconsider the meaning of a phenomenological theory of the fractional Josephson effect, where the tunneling Hamiltonian between the two edges at either sides of the insulator is described by $H_T = -it\cos(\varphi/2)\gamma_L\gamma_R$ [18, 56]. Here $t$ is the tunneling amplitude and $\gamma_L$ ($\gamma_R$) is the operator of a MF at the edge of the superconductor on the left (right)-hand side of the insulator. The Josephson current calculated from $J \propto \partial_\varphi \langle H_T \rangle$ exhibits the fractional CPR. However, this argument may be self-contradicted. The Josephson current flows at $\varphi = \pi - 0^+$ while the tunneling Hamiltonian vanishes. We also try to solve this puzzle in the present chapter.

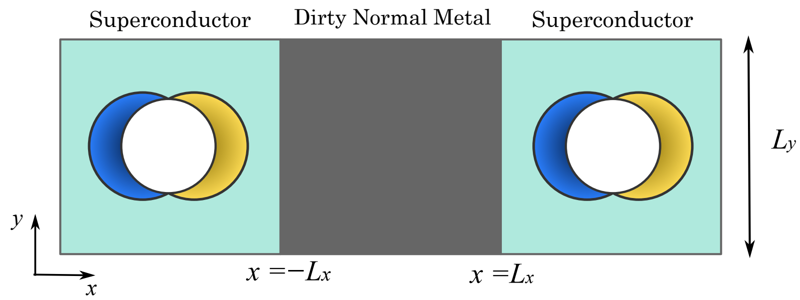


**Figure 4.1:** Schematic image of the $p_x$-wave superconductor/dirty normal metal/the $p_x$-wave superconductor junction.

## 4.3 chiral symmetry

Let us consider a two-dimensional SNS junction where two superconductors are characterized by an equal-spin-triplet $p_x$-wave symmetry as shown Fig. 4.1. The junction consists the three segments: a dirty normal metal ($-L_x \leq x \leq L_x$), and two superconductors ($L_x \leq j \leq \infty$ and $-\infty \leq j \leq -L_x$). The junction is described by the Bogoliubov-de Gennes Hamiltonian

$$\hat{H}(\varphi) = \hat{H}_L + \hat{H}_N + \hat{H}_R(\varphi), \tag{4.1}$$

$$\hat{H}_L = \begin{bmatrix} \xi(\boldsymbol{r}) & \frac{\Delta}{k_F}\partial_x \\ -\frac{\Delta}{k_F}\partial_x & -\xi(\boldsymbol{r}) \end{bmatrix}, \tag{4.2}$$

$$\hat{H}_R(\varphi) = \begin{bmatrix} \xi(\boldsymbol{r}) & \frac{\Delta e^{i\varphi}}{k_{\mathrm{F}}}\partial_x \\ -\frac{\Delta e^{-i\varphi}}{k_{\mathrm{F}}}\partial_x & -\xi(\boldsymbol{r}) \end{bmatrix}, \tag{4.3}$$

$$\hat{H}_N = \begin{bmatrix} \xi(\boldsymbol{r}) + v(\boldsymbol{r}) & 0 \\ 0 & -\xi(\boldsymbol{r}) - v(\boldsymbol{r}) \end{bmatrix}, \tag{4.4}$$

$$\xi(\boldsymbol{r}) = -\frac{\hbar^2}{2m}\nabla^2 - \mu, \qquad k_{\mathrm{F}} = \sqrt{2m\mu}/\hbar, \tag{4.5}$$

where $m$ denotes the effective mass of an electron, $\mu$ is the chemical potential, and $\Delta$ denotes the amplitude of the pair potential. In what follows, we consider $2 \times 2$ BdG Hamiltonian for one spin sector. The phase difference between the two superconductors is denoted by $\varphi$. The random impurity potential in the normal segment is represented by $v(\boldsymbol{r})$.

It is easy to confirm the following relations,

$$\hat{S}\hat{H}_L\hat{S}^{-1} = -\hat{H}_L, \tag{4.6}$$

$$(e^{i\varphi\hat{\tau}_3}\hat{S})\ \hat{H}_R\ (e^{i\varphi\hat{\tau}_3}\hat{S})^{-1} = -\hat{H}_R, \tag{4.7}$$

$$\hat{S}\hat{H}_N\hat{S}^{-1} = -\hat{H}_N, \tag{4.8}$$

$$(e^{i\varphi\hat{\tau}_3}\hat{S})\ \hat{H}_N\ (e^{i\varphi\hat{\tau}_3}\hat{S})^{-1} = -\hat{H}_N, \tag{4.9}$$

$$\hat{S} = \begin{bmatrix} 0 & 1 \\ 1 & 0 \end{bmatrix} = \hat{\tau}_1, \qquad \hat{\tau}_3 = \begin{bmatrix} 1 & 0 \\ 0 & -1 \end{bmatrix}, \tag{4.10}$$

Eq. (4.6) represents chiral symmetry of $\hat{H}_L$ with respect to $\hat{S}$. In the same way, Eq. (4.7) represents chiral symmetry of $\hat{H}_R$ with respect to $e^{i\varphi\hat{\tau}_3}\hat{S}$. The Hamiltonian in the normal part $\hat{H}_N$ preserves chiral symmetry for both $\hat{S}$ and $e^{i\varphi\hat{\tau}_3}\hat{S}$. When a Hamiltonian preserves chiral symmetry, the eigenstates of the Hamiltonian have two important features [9, 47]. In the case of Eq. (4.6), for instance, one can prove following properties of eigen states of $\hat{H}_L$.

(i) The eigenstates of the $\hat{H}_L$ at the zero energy are simultaneously the eigenstates of $\hat{S}$ with its eigenvalue (chirality) either $\gamma = +1$ or $-1$.

(ii) On the other hand, the nonzero-energy states of $\hat{H}_L$ are described by the linear combination of two different eigenstates of $\hat{S}$: one has $\gamma = +1$ and the other has $\gamma = -1$.

Below, we prove the stability of the highly degenerate zero energy states appearing in the SNS junction by taking these features into account. We note that the total Hamiltonian $\hat{H}$ preserves $\hat{S}\hat{H}\hat{S}^{-1} = -\hat{H}$ for $\varphi$ being either 0 or $\pm\pi$.

We first analyze the chiral property of the zero-energy states appealing at the surface of the two semi-infinite superconductors ($x \leq -L_x$ and $x \geq L_x$). To do this, we remove the normal segment ($-L_x \leq x \leq L_x$) and apply the hard-wall boundary condition at $x = -L_x$ and $x = L_x$. In the $y$ direction, the width of the superconductors is $L_y$ and the hard-wall boundary condition is applied. By solving the Bogoliubov-de Gennes equation, we obtain the wave function for the the zero-energy states as

$$\psi_{L,n}(\boldsymbol{r}) = \frac{1}{\sqrt{N_n}} \begin{bmatrix} 1 \\ 1 \end{bmatrix} X_{n,+}(x) Y_n(y), \tag{4.11}$$

$$\psi_{R,n}(\boldsymbol{r}) = \frac{1}{\sqrt{N_n}} \begin{bmatrix} e^{i\frac{\varphi}{2}} \\ -e^{-i\frac{\varphi}{2}} \end{bmatrix} X_{n,-}(x) Y_n(y), \tag{4.12}$$

$$X_{n,\pm}(x) = \sin[q_n(x \pm L_x)] e^{\pm x/\xi}, \tag{4.13}$$

$$Y_n(y) = \sqrt{\frac{2}{L_y}} \sin\left(\frac{n\pi}{L_y} y\right), \tag{4.14}$$

$$q_n = \sqrt{k_n^2 - \xi^{-2}}, \quad \xi = \hbar^2 k_{\mathrm{F}}/m\Delta, \tag{4.15}$$

$$k_n = \frac{\sqrt{2m\mu_n}}{\hbar}, \qquad \mu_n = \mu - \frac{\hbar^2}{2m}\left(\frac{n\pi}{L_y}\right)^2, \tag{4.16}$$

where $n$ indicates the propagating channels. The wave function $\psi_{L,n}$ ($\psi_{R,n}$) represents the $n$-th zero-energy state localized at the surface of the left (right) superconductor. The normalization coefficient is denoted by $N_n$. The degree of degeneracy at the zero energy is equal to the number of the propagating channels $N_c$ because a zero-energy state can be defined for each propagating channel. The derivations of the wave functions are shown in E. As indicated by the property (i), the zero-energy states in Eqs. (4.11) and (4.13) are the eigenstates of $\hat{S}$ and $e^{i\varphi\hat{\tau}_3}\hat{S}$, respectively.

The particle-hole symmetry of the total Hamiltonian is represented by

$$\hat{C}\, H\, \hat{C}^{-1} = -H, \quad \hat{C} = \hat{S}\, \mathcal{K}, \tag{4.17}$$

where $\mathcal{K}$ denotes the complex conjugation. Since

$$\hat{C}\psi_{L,n} = \psi_{L,n}, \tag{4.18}$$

$$\hat{C}\psi_{R,n} = -\psi_{R,n}, \tag{4.19}$$

all the zero-energy states are the Majorana bound states. Thus, at a surface of a $p_x$-wave superconductor, the degree of the degeneracy in MBSs is $N_c$.

## 4.4 zero-energy states in SNS junctions

To analyze the MBSs in a SNS junction, we insert a normal segment described by $H_N$ into the two superconductors. At $\varphi = 0$, the wave function $\psi_{L,n}$ and $\psi_{R,n}$ satisfies

$$\hat{S}\psi_{L,n} = \psi_{L,n} \tag{4.20}$$

$$\hat{S}\psi_{R,n} = -\psi_{R,n}, \tag{4.21}$$

for all $n$. Namely, all the MBSs in the left superconductor belong to $\gamma = +1$ while those in the right superconductor belong to $\gamma = -1$ as shown in Fig. 4.2 (a). The MBSs at the surface of the two different superconductors have the opposite chirality to each other. In a SNS junction, a normal metal connects the two superconductor. MBSs with $\gamma = +1$ (MBSs with $\gamma = -1$) penetrate into the normal metal from the left (right) superconductor. As a result, they form nonzero-energy states there. In this way, the penetration of MBSs into the normal metal lifts the high degeneracy at the zero-energy. In other wards, pairs of MFs couple back to conventional quasi-particles and the number of such pairs is $N_c$.

On the other hand at $\varphi = \pi$, one can find

$$\hat{S}\psi_{L,n} = \psi_{L,n} \tag{4.22}$$

$$\hat{S}\psi_{R,n} = \psi_{R,n}. \tag{4.23}$$

Both $\psi_{L,n}$ and $\psi_{R,n}$ belong to the same chirality $\gamma = +1$ as shown in Fig. 4.2 (b). The MBSs retain their high degree of degeneracy even in a SNS junction because the zero-energy states with $\gamma = -1$ are absent in the normal metal. According to the property (ii), the zero-energy states belonging the same chirality cannot form any nonzero-energy states.

To confirm the argument above, we calculate the wave function in a SNS junction. We first set the impurity potential $v(\boldsymbol{r}) = 0$ and solve the Bogoliubov-de Gennes equation at the zero energy for $\varphi = \pi$,

$$\hat{H}(\pi)\psi_0 = 0. \tag{4.24}$$

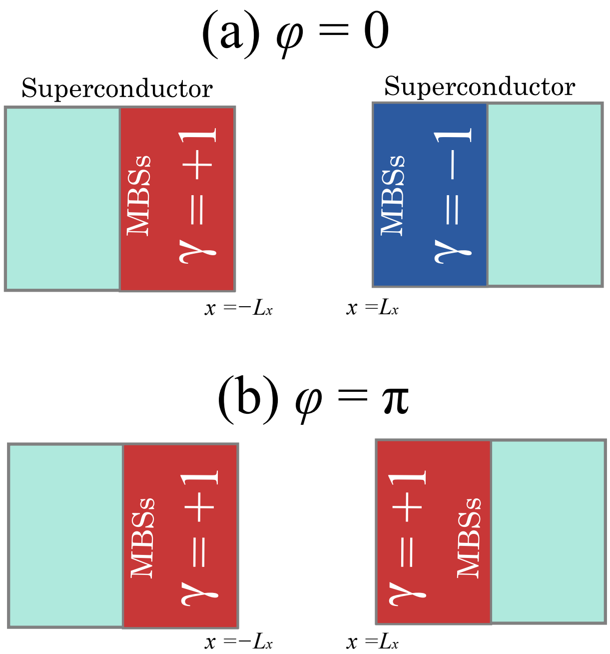


**Figure 4.2:** Schematic image for the chirality of the Majorana bound states. (a) At $\varphi = 0$, the left-side MBSs and the right-side MBSs have the opposite chirality each other. (b) On the other hand, at $\varphi = \pi$, both left-side and right-side MBSs have the chirality $\gamma = +1$.

A solution of Eq. (4.24) is given by [See also Appendix (E)]

$$\psi'_{L,n}(\boldsymbol{r}) = \begin{bmatrix} 1 \\ 1 \end{bmatrix} \left[a_L e^{iq_n x} + b_L e^{-iq_n x}\right] e^{x/\xi} Y_n(y), \tag{4.25}$$

$$\psi_{N,n}(\boldsymbol{r}) = \left[\begin{bmatrix} a_N \\ c_N \end{bmatrix} e^{ik_n x} + \begin{bmatrix} b_N \\ d_N \end{bmatrix} e^{-ik_n x}\right] Y_n(y), \tag{4.26}$$

$$\psi'_{R,n}(\boldsymbol{r}) = \begin{bmatrix} 1 \\ 1 \end{bmatrix} \left[a_R e^{iq_n x} + b_R e^{-iq_n x}\right] e^{-x/\xi} Y_n(y), \tag{4.27}$$

where $\psi'_{L,n}$, $\psi_{N,n}$, and $\psi'_{R,n}$ are the wave function at the $n$-th propagating channel in the left superconductor, the normal metal, and the right superconductor, respectively. By reflecting the chiral property of the MBSs in two superconductors, the vector structure of the wave functions in the superconducting segments takes the particular form of $\psi'_{L(R),n} \propto [1, 1]^{\mathrm{T}}$. By applying the boundary condition at the two interfaces, we obtain the two orthogonal zero-energy states for each propagating channel as

$$\psi_\pm = \frac{1}{\sqrt{N_\pm}} \begin{bmatrix} 1 \\ 1 \end{bmatrix} \phi_{n,\pm}(x) Y_n(y), \tag{4.28}$$

$$\phi_{n,+}(x) = \begin{cases} A_+(x) & \text{for} \quad x \leq -L_x \\ \sin(k_n x) & \text{for} \quad -L_x \leq x \leq L_x \\ B_+(x) & \text{for} \quad x \geq L_x, \end{cases} \tag{4.29}$$

$$\phi_{n,-}(x) = \begin{cases} A_-(x) & \text{for} \quad x \leq -L_x \\ \cos(k_n x) & \text{for} \quad -L_x \leq x \leq L_x \\ B_-(x) & \text{for} \quad x \geq L_x, \end{cases} \tag{4.30}$$

$$A_\pm(x) = c_\pm \sin\{q_n(x + L_x) \mp \theta_\pm\} e^{(x+L_x)/\xi}, \tag{4.31}$$

$$B_\pm(x) = c_\pm \sin\{q_n(x - L_x) \pm \theta_\pm\} e^{-(x-L_x)/\xi}, \tag{4.32}$$

$$c_\pm = \frac{\sqrt{k_n\{k_n \pm \xi^{-1} \sin(2k_n L_x)\}}}{q_n}, \tag{4.33}$$

$$\theta_+ = \arctan\left[\frac{q_n \sin(k_n L_x)}{k_n \cos(k_n L_x) + \xi^{-1} \sin(k_n L_x)}\right], \tag{4.34}$$

$$\theta_- = \arctan\left[\frac{q_n \cos(k_n L_x)}{k_n \sin(k_n L_x) - \xi^{-1} \cos(k_n L_x)}\right], \tag{4.35}$$

where $N_\pm$ is a normalization coefficient. Since we obtain the two zero-energy states for each propagating channel, the degeneracy of the zero-energy bound states becomes twice the number of the propagating channel $N_c$. More importantly, Eq. (4.28) suggests that all the zero-energy states in SNS junction are the eigenstates of $\hat{S}$ belonging to $\gamma = +1$.

Next we introduce the impurity potential $v(\boldsymbol{r})$ into the normal segment. The random potential modifies the wave function in Eq. (4.28). Actually we cannot analytically describe how the wave function depends on $\boldsymbol{r}$ anymore. But the vector part of the wave function $[1, 1]^{\mathrm{T}}$ remains unchanged even in the presence of impurity potentials because $v(\boldsymbol{r})$ preserves the chiral symmetry. Therefore all the zero-energy states keep their chirality at $\gamma = +1$ even in the presence of $v(\boldsymbol{r})$. According to the property (ii), such chirality aligned zero-energy states keep their high degeneracy because they cannot construct nonzero-energy states in the absence of their chiral partner belonging to $\gamma = -1$. As a result, the degenerate MBSs form the resonant transmission channels in the normal metal. The Josephson current at $\varphi = \pi - 0^+$ flows through such highly degenerate resonant states. Our analysis provides a mathematical background for understanding the fractional Josephson effect in a dirty SNS junction which was numerically shown in the previous papers [19, 20].

## 4.5 Phenomenological theory

The fractional Josephson effect in one-dimensional SIS can be phenomenologically explained in terms of the effective hopping Hamiltonian between the two Majorana bound states. At the edge of isolated semi-infinite $p$-wave superconductor, the electron operators at the edges are described by

$$\Psi_L = \gamma_L, \tag{4.36}$$
$$\Psi_R = ie^{i\varphi/2}\gamma_R, \tag{4.37}$$

where $\gamma_L$ ($\gamma_R$) is the operator of a Majorana fermion at the edge of left (right) superconductor. The tunneling Hamiltonian between the two edges becomes

$$\begin{aligned} H_T &= -t\left[\Psi_L^\dagger\Psi_R + \Psi_R^\dagger\Psi_L\right] && (4.38)\\ &= -2it\cos(\varphi/2)\,\gamma_L\,\gamma_R. && (4.39)\end{aligned}$$

The expectation value of the tunneling Hamiltonian could be

$$\langle H_T\rangle = -2tC_0\cos(\varphi/2), \tag{4.40}$$

where we assume that $\langle i\gamma_L\,\gamma_R\rangle = C_0$ is a constant. The Josephson current calculated as

$$J = \frac{e}{\hbar}\partial_\varphi\langle H_T\rangle = \frac{e2tC_0}{\hbar}\sin(\varphi/2), \tag{4.41}$$

describes the fractional current-phase relationship. At $\varphi = \pi - 0^+$, we obtain

$$\langle H_T\rangle = -tC_0\,0^+, \tag{4.42}$$
$$J = \frac{e2tC_0}{\hbar}\left(1 - \frac{(0^+)^2}{8}\right). \tag{4.43}$$

The Josephson current takes its maximum, whereas the amplitude of the tunneling Hamiltonian is proportional to $0^+$. The Josephson current at $\varphi = \pi - 0^+$ flows as a result of the resonant transmission through the junction. Therefore the amplitude of the current is not proportional to the amplitude of the tunneling Hamiltonian. This argument is valid as far as $\varphi = \pi - 0^+$. At $\varphi = \pi$, the tunneling Hamiltonian vanishes exactly, which leads to the absence of the Josephson current. In this way, the phenomenological argument using Eq. (4.38) is consistent with the microscopic theory of the fractional Josephson effect.

## 4.6 Conclusion

We have studied the stability of more than one Majorana Fermion appearing in a two-dimensional superconductor/normal-metal/superconductor (SNS) junction in terms of chiral symmetry of Hamiltonian, where the two superconductors are characterized by spin-triplet $p_x$-wave symmetry. When the phase difference across the junction $\varphi$ is either 0 or $\pi$, the Hamiltonian of the SNS junction preserves chiral symmetry. At $\varphi = \pi$, the Majorana bound states (MBSs) in the normal metal can retain their high degree of degeneracy at the zero energy even in the presence of the impurity scatterings because all of the MBSs belong to the same chirality. As a consequence, the resonant transmission of a Cooper pair via such highly degenerate MBSs carries the Josephson current at $\varphi = \pi - 0^+$. The physical picture obtained in this chapter well explains the persistence of the fractional current-phase relationship in a dirty SNS junction, which was numerically shown in previous papers. We have also discussed a way of understanding the fractional current-phase relationship derived from a phenomenological tunneling Hamiltonian of a Majorana Fermion.

# Chapter 5

# Anomalous proximity effect in a superconductor/semiconductor hybrid system

## 5.1 Abstract

We theoretically study the transport properties of a superconducting thin film with the Dresselhaus[110] spin-orbit coupling under an in-plane Zeeman field. In the topologically nontrivial phase, the Dresselhaus superconductor preserves an additional chiral symmetry and traps more than one Majorana bound state at is edges. All the Majorana baound states at an edge belong to the same chirality due to the effective $p$-wave pairing symmetry. When we attach a normal metal to the superconductor, such Majorana bound states penetrate into the dirty normal segment while retaining their high degree of degeneracy at the Fermi level. As a result, we find that the Dresselhaus superconductor shows the perfect conductance quantization in a dirty normal-metal/superconductor junction and the fractional Josephson effect in a superconductor/dirty normal-metal/superconductor junction.

## 5.2 Introduction

The proximity effect has been an important issue in the physics of superconductivity. In a normal metal attached to a spin-singlet $s$-wave superconductor, penetrating Cooper pairs form the gap structure in the quasi-particle density of states (DOS) at the Fermi level (zero energy) and modify low energy properties there [96–99]. In spin-triplet $p_x$-wave superconductor junctions, however, the penetrating Cooper pairs form a zero energy peak in the DOS [19, 100, 101]. This induces various anomalous electromagnetic properties in the normal metal [14, 15, 102]. This effect is called the anomalous proximity effect. For instance, a perfect Andreev reflection from a $p_x$-wave superconductor into a dirty normal metal causes anomalous low-energy transport in the $x$ direction such as a zero-bias conductance quantization in normal-metal/superconductor (NS) junctions [14] and a fractional current-phase relationship in superconductor/normal-metal/ superconductor (SNS) junctions [19].

Recently, these characteristic transport phenomena have been investigated in the context of Majorana physics [53, 54] based on the topological classification of materials [4]. In fact, as a consequence of the topologically nontrivial property of the wave function, the spin-triplet $p_x$-wave superconductor hosts more than one Majorana fermion at its edges [9]. The energy dispersion of the topological edge states is flat as a function of the wave vector in the transverse direction (say $k_y$ ), which represents the high degree of the degeneracy in the zero-energy states (ZESs). All the ZESs of a $p_x$-wave superconductor belong to the same chiral eigenvalue of the chiral symmetry operator. Such the pure chiral nature of the $p_x$-wave pairing symmetry is responsible for the robustness of highly degenerate ZESs in the presence of potential disorders [47]. The anomalous proximity effect stems from the penetration of ZESs into the dirty normal-metal while retaining their degeneracy [19, 48, 49, 100].

However, it has been difficult to fabricate spin-triplet superconducting junctions using existing materials. Nevertheless, the rapid progress in the Majorana physics of artificial superconductors [59–64] and in spintronics for controlling the spin-orbit interaction [74–77] has diffused the situation. A set of three potentials is needed to realize topologically nontrivial superconductors artificially, namely the spin-orbit coupling, the Zeeman field, and the pair potential. Among them, the spin-orbit interaction mainly affects the energy spectra of the edge states. In InSb or GaAs, for example, the Dresselhaus spin-orbit interactions are large in films growing along the [110] crystal direction [103]. Theoretical studies [36, 37] have shown that such artificial superconductors host more than one ZES similar to those of the $p_x$-wave superconductor.

In this chapter, we theoretically study the transport properties of the Dresselhaus superconductors in large magnetic fields by using the lattice Green function method on the two-dimensional tight-binding lattice. As a result, we find that the Dresselhaus superconductor shows the perfect conductance quantization in a dirty NS junction and the fractional Josephson effect in a dirty SNS junction. To explain these numerical results, we analytically demonstrate that the effective Hamiltonian of the Dresselhaus superconductor in the topologically nontrivial phase is unitary equivalent to the Bogoliubov-de Gennes Hamiltoanian of the spin-triplet $p_x$-wave superconductor [50].

## 5.3 Numerical Result

### 5.3.1 Conductance quantization

First, we numerically demonstrate the anomalous proximity effect of a Dresselhaus superconductor. Let us consider a semiconductor thin film with the strong Dresselhaus[110] spin-orbit coupling fabricated on an insulator/metallic superconductor junction as shown in Fig. 5.1. A segment on the superconductor is in the superconducting state due to the proximity-induced $s$-wave pair potential. We describe the present junction on the two-dimensional tight-binding model with the lattice constant $a_0$. A lattice site is indicated by a vector $\boldsymbol{r} = j\boldsymbol{x}+m\boldsymbol{y}$, where $\boldsymbol{x}$ ($\boldsymbol{y}$) is the vector in the $x$ ($y$) direction with $|\boldsymbol{x}| = |\boldsymbol{y}| = a_0$. The present junction consists three segments: an ideal lead wire ($\infty \leq j \leq 0$), a normal disordered segment ($1 \leq j \leq L/a_0$) and a superconducting segment ($L + 1/a_0 \leq j \leq \infty$). The Hamiltonian reads

$$H_{\mathrm{BdG}} = H_{\mathrm{kin}} + H_{\mathrm{D}} + H_{\mathrm{Z}} + H_{\Delta} + H_{\mathrm{imp}}, \tag{5.1}$$

$$\begin{aligned} H_{\mathrm{kin}} =& -t \sum_{\sigma=\uparrow,\downarrow} \sum_{j=-\infty}^{\infty} \sum_{m=1}^{M/a_0} \left( c^{\dagger}_{\boldsymbol{r}+\boldsymbol{x},\sigma} c_{\boldsymbol{r},\sigma} + c^{\dagger}_{\boldsymbol{r},\sigma} c_{\boldsymbol{r}+\boldsymbol{x},\sigma} \right) \\ & -t \sum_{\sigma=\uparrow,\downarrow} \sum_{j=-\infty}^{\infty} \sum_{m=1}^{M/a_0-1} \left( c^{\dagger}_{\boldsymbol{r}+\boldsymbol{y},\sigma} c_{\boldsymbol{r},\sigma} + c^{\dagger}_{\boldsymbol{r},\sigma} c_{\boldsymbol{r}+\boldsymbol{y},\sigma} \right) \\ & + \sum_{\sigma=\uparrow,\downarrow} \sum_{j=-\infty}^{\infty} \sum_{m=1}^{M/a_0} (4t - \mu) c^{\dagger}_{\boldsymbol{r},\sigma} c_{\boldsymbol{r},\sigma} \end{aligned} \tag{5.2}$$

$$H_{\mathrm{D}} = -i\frac{\lambda_{\mathrm{D}}}{2a_0} \sum_{\alpha,\beta} \sum_{j=-\infty}^{\infty} \sum_{m=1}^{M/a_0} (\sigma_3)_{\alpha,\beta} \left( c^{\dagger}_{\boldsymbol{r}+\boldsymbol{x},\alpha} c_{\boldsymbol{r},\beta} - c^{\dagger}_{\boldsymbol{r},\alpha} c_{\boldsymbol{r}+\boldsymbol{x},\beta} \right), \tag{5.3}$$

$$H_{\mathrm{Z}} = -\sum_{\alpha,\beta} \sum_{j=-\infty}^{\infty} \sum_{m=1}^{M/a_0} V_{ex} (\sigma_1)_{\alpha,\beta} c^{\dagger}_{\boldsymbol{r},\alpha} c_{\boldsymbol{r},\beta}, \tag{5.4}$$

$$H_{\Delta} = \sum_{j>L/a_0}^{\infty} \sum_{m=1}^{M/a_0} \Delta_0 \left( c^{\dagger}_{\boldsymbol{r},\uparrow} c^{\dagger}_{\boldsymbol{r},\downarrow} + H.c. \right), \tag{5.5}$$

$$H_{\mathrm{imp}} = \sum_{\sigma=\uparrow,\downarrow} \sum_{j=1}^{L/a_0} \sum_{m=1}^{M/a_0} V_{\mathrm{imp}}(\boldsymbol{r}) \psi^{\dagger}_{\boldsymbol{r},\sigma} \psi_{\boldsymbol{r},\sigma} \tag{5.6}$$

where $c^{\dagger}_{\boldsymbol{r},\sigma}(c_{\boldsymbol{r},\sigma})$ is the creation(annihilation) operator of an electron at the site $\boldsymbol{r}$ with spin $\sigma = (\uparrow \text{ or } \downarrow)$, $t = \hbar^2/(2ma_0^2)$ denotes the hopping integral between the nearest neighbor hopping, $m$ is the effective mass of an electron, $\mu$ is the chemical potential, $\lambda_D$ represents the strength of the Dresselhaus [110] spin-orbit interaction, $\Delta_0$ is the proximity-induced $s$-wave pair potential at the zero temperature. By tuning the magnetic field $B$ in the $x$ direction as shown in Fig. 5.1, it is possible to introduce the external Zeeman potential $V_{ex}$. The parameters $t$, $\mu$, $\lambda_{\mathrm{D}}$ and $V_{ex}$ are common to the superconductor and the normal metal. In the $y$ direction, the number of the lattice sites is $M/a_0$ and the hard-wall boundary condition is applied. The Pauli's matrices in spin space are represented by $\hat{\sigma}_j$ for $j=1$-3 and the unit matrix in spin space is $\hat{\sigma}_0$. We introduce the impurity potential given randomly in the range of $-W/2 \leq V_{\mathrm{imp}}(\boldsymbol{r}) \leq W/2$ in the normal segment ($1 \leq j \leq L/a_0$).

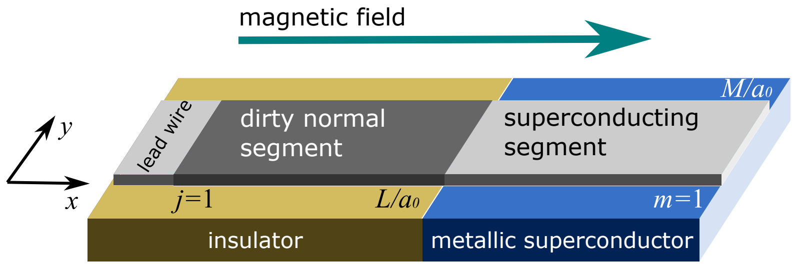


**Figure 5.1:** (Color online) Schematic image of the NS junction of a Dresselhaus superconductor. The superconductor proximitizes the InSb thin film, which is grown along the [110] crystal direction.

We calculate the differential conductance $G_{\mathrm{NS}}$ of the NS junctions based on the Blonder-Tinkham-Klapwijk formula [83]

$$G_{\mathrm{NS}}(eV) = \frac{e^2}{h} \sum_{\zeta,\eta} \left[ \delta_{\zeta,\eta} - \left| r^{ee}_{\zeta,\eta} \right|^2 + \left| r^{he}_{\zeta,\eta} \right|^2 \right]_{eV=E}, \tag{5.7}$$

where $r^{ee}_{\zeta,\eta}$ and $r^{he}_{\zeta,\eta}$ denote the normal and Andreev reflection coefficients at the energy $E$, respectively. The index $\zeta$ and $\eta$ label the outgoing channel and the incoming one, respectively. These reflection coefficients are calculated by using the lattice Green's function method [84, 85, 88]. With this method, it is possible to calculate the transport coefficients exactly even in the presence of random impurity potentials. In Fig. 5.2, we present the differential conductance of the Dresselhaus superconductor as a function of the bias voltage for several choices of the lengths of the disordered segments $L$, where we choose the parameters of $\mu = 1.0t$, $\lambda_{\mathrm{D}} = 0.2ta_0$, $W = 2.0t$, $M = 10a_0$, and $\Delta_0 = 0.1t$. The results are normalized to $G_Q = 2e^2/h$. In Fig. 5.2(a), We chose $V_{ex} = 1.2t$, which leads to the propagating channel number $N_{\mathrm{c}} = 5$. The differential conductance decreases with increasing $L$ for finite bias voltages. However, the zero-bias conductance is quantized at $G_Q N_{\mathrm{c}}$ irrespective of $L$. The results suggest that there are $N_{\mathrm{c}}$ perfect transmission channels in a disordered normal segment. [48, 100] The conductance quantization at zero bias is an aspect of the anomalous proximity effect of a $p_x$-wave superconductor. Such anomalous behaviors can be seen when the Zeeman field exceeds a critical value $V_{ex} > V_{\rm c} = \sqrt{\mu_0^2 + \Delta_0^2}$ with $\mu_0 = \mu - [1 - \cos\{\pi/(M/a_0 + 1)\}]$. With the present parameter choice, we obtain $V_{\rm c} = 0.92t$. On the other hand for $V_{ex} < V_{\rm c}$, the conductance quantization is absent as shown in Fig. 5.2(b), where we choose $V_{ex} = 0.5t < V_{\rm c}$. The zero-bias conductance quantization at $G_Q N_{\rm c}$ is a robust phenomenon in the topologically nontrivial phase described by $V_{ex} > V_{\rm c}$ and $\lambda_{\rm D} \neq 0$, and is independent of such parameters as $M$, $W$, and $\mu$. In the experiment [66,67], for instance, the condition $V_{ex} > V_{\rm c}$ may be satisfied under a magnetic field of less than 1T in InSb nanowires owing to its large $g$ factor and small Fermi energy. Inversion symmetry in the $z$ direction is broken in the junction shown in Fig. 5.1. In such case, Rashba spin-orbit interaction $\lambda_{\rm R}(k_y\hat{\sigma}_1 - k_x\hat{\sigma}_2)$ is not negligible. Unfortunately, the Rashba term easily destroys the conductance quantization at zero bias because it breaks chiral symmetry discussed below. To delete the Rashba term, we need to recover inversion symmetry by attaching an appropriate insulator or the same superconductor on top of the InSb thin film.

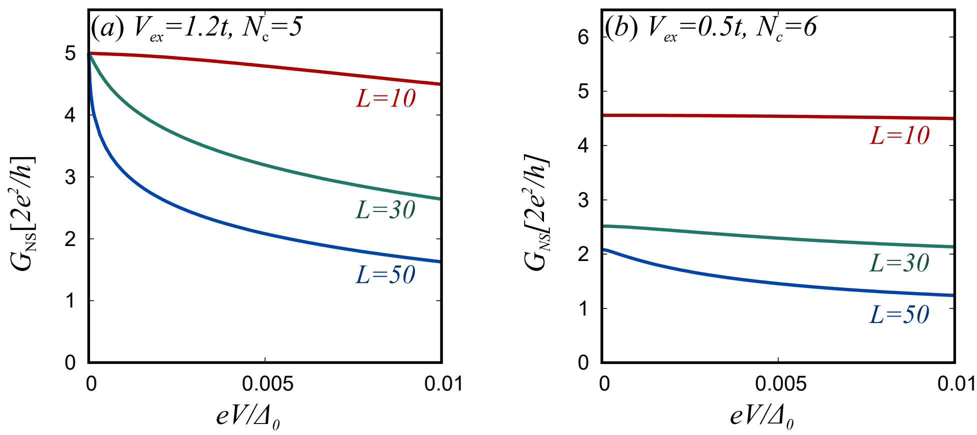


**Figure 5.2:** (Color online) The differential conductance is plotted as a function of the bias voltage for several lengths of disordered segment $L$ in units of $a_0$. In (a), the Zeeman potential $V_{ex} = 1.2t$ is chosen that is larger than a critical value of $V_{\rm c} = 0.92t$. The number of propagating channels $N$c is 5. In (b), we choose $V_{ex} = 0.5t < V_{\rm c}$ leading to $N_{\rm c} = 6$.

### 5.3.2 Fractional Josephson effect

Second, we study the Josephson effect in the junction shown in Fig. 5.3. The junction consists three segment: a disordered normal segment ($1 \leq j \leq L$) and two Dresselhaus superconducting nanowires ($\infty \leq j \leq 0$ and $L+1 \leq j \leq \infty$). The pair potential for the

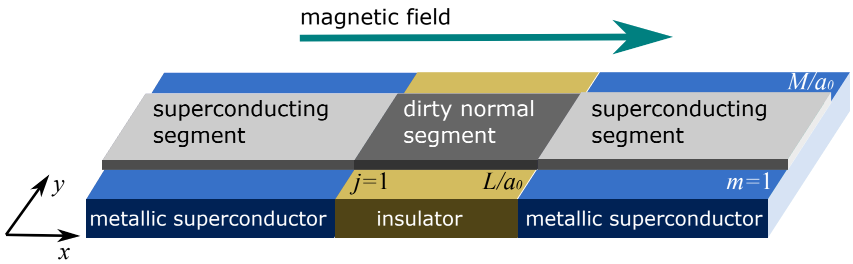


**Figure 5.3:** (Color online) Schematic image of the SNS junction of a Dresselhaus superconductor.

left superconductor is described by

$$H_{\Delta}^{L}=\sum_{j\leq 0}\sum_{m=1}^{M/a_0}\left(\Delta_0 e^{i\varphi}c^{\dagger}_{\boldsymbol{r},\uparrow}c^{\dagger}_{\boldsymbol{r},\downarrow}+H.c.\right), \tag{5.8}$$

where $\varphi$ corresponds to the phase difference of the pair potential between two superconductors. The Josephson current is calculated by using the Green's function method [88]. In Fig. 5.4, we plot the Josephson current at $T = 0.001T_c$ as a function of the phase difference for several choices of $W$ such as $1.0t$, $2.0t$ and $3.0t$, where $M = 10$, $L = 30$, and $V_{ex} = 1.5t > V_c$. For comparison, we also plot the result for the conventional $s$-wave superconductor junction (i.e., $V_{ex} = 0$ and $\lambda_D = 0$) with a dashed line. The current-phase relationship for the conventional junction slightly deviate the sinusoidal function. The results suggest the small contribution of the higher harmonics such as $\sin(2\varphi)$ and $\sin(3\varphi)$ to the Josephson current. This is the well know behavior of the Josephson current in diffusive SNS junction of the metallic superconductor [95]. On the other hand, the Josephson current in the Dresselhaus nanowires indicates the large contribution of the higher harmonics to the Josephson current at a low temperature. As a consequence, the results are close to the fractional current-phase relationship of $J \propto \sin(\varphi/2)$ irrespective of $W$. Such fractional relationship also indicates the perfect transmission through the disordered normal segment [8, 19, 20].

## 5.4 Effective $p_x$-wave pairing symmetry

In this section, we explain why the Dresselhaus superconductor shows the anomalous proximity effect which is unique to the $p_x$-wave spin-triplet superconductor. In what follows, we consider the Dresselhaus superconductor in the continuous space for simplicity.

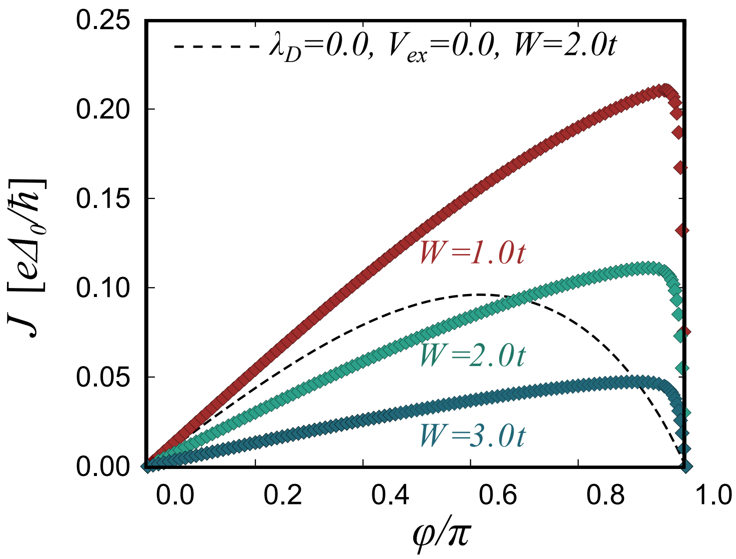


**Figure 5.4:** (Color online) The Josephson current at $T = 0.001T_c$ is plotted as a function of the phase difference, where $L = 30$, $M = 10$, and $V_{ex} = 1.5t$. We plot the result for several choices of $W$ such as $1.0t$, $2.0t$ and $3.0t$. We also plot the results for the conventional $s$-wave superconductor (i.e. , $V_{ex} = 0$ and $\lambda_D = 0$) at $W = 2.0t$ with a dashed line. The number of samples used for the random ensemble average is 500 for all the plots.

The Hamiltonian is represented by

$$\check{H}_0 = \begin{bmatrix} \hat{h} & i\Delta_0\hat{\sigma}_2 \\ -i\Delta_0\hat{\sigma}_2 & -\hat{h}^* \end{bmatrix}, \tag{5.9}$$

$$\hat{h} = \xi\hat{\sigma}_0 - V_{ex}\hat{\sigma}_1 + i\lambda_D\partial_x\hat{\sigma}_3, \qquad \xi = \frac{-\hbar^2}{2m}\boldsymbol{\nabla}^2 - \mu. \tag{5.10}$$

By using the unitary matrix

$$\check{R} = \begin{bmatrix} \hat{r} & 0 \\ 0 & \hat{r}^* \end{bmatrix}, \ \hat{r} = \frac{1}{\sqrt{2}}\begin{bmatrix} e^{-i\pi/4} & -e^{-i\pi/4} \\ e^{i\pi/4} & e^{i\pi/4} \end{bmatrix}, \tag{5.11}$$

the BdG Hamiltonian $\check{H}_0$ is first transformed to

$$\check{H}' = \check{R}\check{H}_0\check{R}^\dagger = \begin{bmatrix} \hat{h}' & i\Delta_0\hat{\sigma}_2 \\ -i\Delta_0\hat{\sigma}_0 & -\hat{h}' \end{bmatrix}, \tag{5.12}$$

$$\hat{h}' = \xi\hat{\sigma}_0 + V_{ex}\hat{\sigma}_3 + i\lambda_D\partial_x\hat{\sigma}_2. \tag{5.13}$$

The Hamiltonian in this basis is represented only by real numbers. Next we apply a transformation which is similar to the Foldy-Wouthysen transformation [104] to the BdG

Hamiltonian in Eq. (5.12). Using a unitary matrix

$$\check{U} = \begin{bmatrix} \hat{u} & 0 \\ 0 & \hat{u} \end{bmatrix}, \quad \hat{u} = \exp[i\hat{S}], \quad \hat{S} = \frac{\lambda_D}{2\hbar V_{ex}} p_x \hat{\sigma}_1, \tag{5.14}$$

with $p_x = -i\hbar\partial_x$, we transform $H'$ into

$$\check{U}\check{H}'\check{U}^\dagger = \begin{bmatrix} e^{i\hat{S}}\hat{h}' e^{-i\hat{S}} & e^{i\hat{S}}(i\Delta_0\hat{\sigma}_2)e^{-i\hat{S}} \\ -e^{i\hat{S}}(i\Delta_0\hat{\sigma}_2)e^{-i\hat{S}} & -e^{i\hat{S}}\hat{h}' e^{-i\hat{S}} \end{bmatrix}. \tag{5.15}$$

The diagonal term of Eq. (5.12) can be expanded as

$$e^{i\hat{S}}\hat{h}' e^{i\hat{S}} = \hat{h}' + i[\hat{S}, \hat{h}'] + \frac{i^2}{2!}[\hat{S}, [\hat{S}, \hat{h}']] + \cdots, \tag{5.16}$$

with using the Baker-Housdorff formula. We assume large enough Zeeman potential so that $\lambda_D k_F \ll V_{ex}$ is satisfied where $k_F = \sqrt{2m\mu}/\hbar$ denotes Fermi wave number. From this assumption, we obtain

$$e^{i\hat{S}}\hat{h} e^{i\hat{S}} = \xi\hat{\sigma}_0 + V_{ex}\hat{\sigma}_3 + O\left[\left(\frac{\lambda_D k_F}{V_{ex}}\right)^2\right], \tag{5.17}$$

within the first order of $\lambda_D k_F/V_{ex}$. The off-diagonal term corresponding to the pair potential is transformed to

$$\begin{aligned} e^{i\hat{S}}(i\Delta_0\hat{\sigma}_2)e^{-i\hat{S}} &= i\Delta_0\hat{\sigma}_2 + i[\hat{S}, i\Delta_0\hat{\sigma}_2] + \cdots \\ &= i\Delta_0\hat{\sigma}_2 - i\frac{\lambda_D\Delta_0}{\hbar V_{ex}} p_x\hat{\sigma}_3 + O\left(\frac{(\lambda_D k_F)^2}{V_{ex}^2}\right), \end{aligned} \tag{5.18}$$

where we assume the uniform pair potential (i.e., $[p_x, \Delta_0] = 0$). As the result, the BdG Hamiltonian can be written as

$$\begin{aligned} \check{U}\check{H}'\check{U}^\dagger = &\begin{bmatrix} \xi + V_{ex} & 0 & -i\frac{\lambda_D\Delta_0}{\hbar V_{ex}}p_x & \Delta_0 \\ 0 & \xi - V_{ex} & -\Delta_0 & i\frac{\lambda_D\Delta_0}{\hbar V_{ex}}p_x \\ i\frac{\lambda_D\Delta_0}{\hbar V_{ex}}p_x & -\Delta_0 & -\xi - V_{ex} & 0 \\ \Delta_0 & -i\frac{\lambda_D\Delta_0}{\hbar V_{ex}}p_x & 0 & -\xi + V \end{bmatrix} \\ &+ O\left(\frac{(\lambda_D k_F)^2}{V_{ex}^2}\right). \end{aligned} \tag{5.19}$$

By interchanging the second column and the third one, and by interchanging the second row and the third one, the Hamiltonian can be deformed as

$$\check{H}_{\mathrm{eff}} = \check{H}_{p_x} + \check{V}_{\Delta}, \tag{5.20}$$

$$\check{H}_{p_x} = \begin{bmatrix} \hat{h}_{p_x,\uparrow} & 0 \\ 0 & \hat{h}_{p_x,\downarrow} \end{bmatrix}, \tag{5.21}$$

$$\hat{h}_{p_x,\sigma} = \begin{bmatrix} \xi + s_s V_{ex} & -s_s i \frac{\lambda_D \Delta_0}{\hbar V_{ex}} p_x \\ s_s i \frac{\lambda_D \Delta_0}{\hbar V_{ex}} p_x & -\xi - s_s V_{ex} \end{bmatrix}, \tag{5.22}$$

$$\check{V}_{\Delta} = \begin{bmatrix} 0 & i\Delta_0 \hat{\sigma}_2 \\ -i\Delta_0 \hat{\sigma}_2 & 0 \end{bmatrix}, \tag{5.23}$$

$$s_s = \begin{cases} 1 & \text{for } \sigma = \uparrow \\ -1 & \text{for } \sigma = \downarrow . \end{cases}, \tag{5.24}$$

where the diagonal components $\hat{h}_{p_x,\sigma}$ are equivalent to the Hamiltonian of the spin-triplet $p_x$-wave superconductor. Therefore, Eq. (5.20) corresponds to the BdG Hamiltonian of the spin-full $p_x$-wave superconductor $\check{H}_{p_x}$ with the spin-mixing term $\check{V}_{\Delta}$. In the topologically nontrivial phase $V_{ex} > V_{\mathrm{c}} = \sqrt{\mu_0^2 + \Delta_0^2}$ with $\mu_0 = \mu - [1 - \cos\{\pi/(M/a_0 + 1)\}]$, all the spin-$\uparrow$ states pinch off from the Fermi level and only the spin-$\downarrow$ states remain at the Fermi level. Therefore the spin-mixing term $\check{V}_{\Delta}$ does not affect the remaining spin-$\downarrow$ states at all. In this way, we can shrink the $4 \times 4$ Hamiltonian $\check{H}_0$ of the Dresselhaus superconductor to the $2 \times 2$ Hamiltonian $\hat{h}_{p_x,\downarrow}$ of the $p_x$-wave superconductor. Therefore, in the topologically nontrivial phase, physics in the Dresselhaus superconductor is the same as that of a $p_x$-wave superconductor. We assumed the two conditions $\lambda_{\mathrm{D}} k_{\mathrm{F}} \ll V_{ex}$ and $V_{ex} > V_{\mathrm{c}}$ independently. To realize the $p_x$-wave superconductor, they can be unified into one condition $\lambda_{\mathrm{D}} k_{\mathrm{F}} \ll V_c$, which is accessible in the experiment [66, 67]. We also confirm that such effective $p_x$-wave superconductors are realized also in a superconducting spin-helix thin film [74, 75] with appropriate tuning of the Zeeman field as shown in Appendix (F).

Finally, we discuss the effect of higher order terms of $(\lambda_{\mathrm{D}} k_{\mathrm{F}}/V_{ex})$ which is ignored in the effective Hamiltonian $\hat{h}_{p_x,\downarrow}$. The effective Hamiltonian $\hat{h}_{p_x,\downarrow}$ preserves chiral symmetry as

$$\hat{\tau}_1 \, \hat{h}_{p_x,\downarrow} \, \hat{\tau}_1 = -\hat{h}_{p_x,\downarrow}, \quad \hat{\tau}_1 = \begin{bmatrix} 0 & 1 \\ 1 & 0 \end{bmatrix}. \tag{5.25}$$

As shown in Ref. [47], all the zero-energy states at the surface of a $p_x$-wave superconductor have the same chirality for the chiral symmetry operator $\hat{\tau}_1$. Such pure chiral state never lift their high degree of degeneracy as long as chiral symmetry is preserved. We note that chiral symmetry in the original basis represented by

$$\check{\Gamma}_0 \, \check{H}_0 \, \check{\Gamma}_0^{-1} = -\check{H}_0, \quad \Gamma_0 = \left[ \begin{array}{cc} 0 & -i\hat{\sigma}_1 \\ i\hat{\sigma}_1 & 0 \end{array} \right], \tag{5.26}$$

where $\check{H}_0$ is the original Hamiltonian in Eq. (5.9). This fact implies that the zero-energy states are robust under perturbations preserving chiral symmetry even if we take the higher order terms of $(\lambda_{\mathrm{D}} k_{\mathrm{F}}/V_{ex})$ into account.

## 5.5 Conclusion

We have studied transport properties in junctions consisting of a superconducting thin film with strong Dresselhaus[110] spin-orbit coupling. The Dresselhaus superconductor under a large in-plane magnetic field hosts more than one ZES at its edges. These ZESs have the pure chiral property due to the effective $p_x$-wave pair potential. As a consequence, the Dresselhaus superconductor shows the perfect zero-bias conductance quantization in a dirty NS junction and the fractional Josephson effect in a dirty SNS junction.

# Chapter 6

# Conclusion

Exotic properties of topologically nontrivial superconductors have been a central issue in both physics of superconductivity and that of topological phase of matter. In a fully gapped topological superconductor, the topological surface bound states have the linear dispersion. On the other hands, a nodal superconductor hosts the flat-band zero-energy states(ZESs) which have the high degree of degeneracy at the Fermi level. It has been widely accepted that such degenerate ZESs of a nodal superconductor cause drastic anomalies in low-energy electromagnetic phenomena. Therefore, a nodal superconductor would be a promising testing ground for physics of topologically nontrivial superconductivity. However, these statements are true as far as the surface or the junction interface of the superconductor is clean enough.

Quantum mechanics tells us that high degree of degeneracy in quantum states is a consequence from high symmetry of the Hamiltonian. To characterize a nodal superconductor topologically, we need to assume translational symmetry. This fact implies that the high degree of degeneracy in the surface bound states of a nodal superconductor is a consequence from the translational symmetry. In experiments, however, potential disorders breaking translational symmetry is inevitable in the vicinity of the surface or the junction interface. Therefore, in a real nodal superconductor, potential disorders may lift the degeneracy of the ZESs and may wash out the characteristic electromagnetic properties. In this situation, a theoretical method that measures the robustness of the flat-band ZESs is desired.

In this thesis, we have established an index theorem that relates the topological property of a nodal superconductor with the number of the ZESs at its dirty surface. By focusing on the chiral symmetry of the Bogoliubov-de Gennes Hamiltonian, we find that the index $\mathcal{N}_{\rm ZES}$ well characterizes the number of the ZESs at a dirty surface. The index $\mathcal{N}_{\rm ZES}$ is an invariant in terms of the chiral eigenvalues of the ZESs. Simultaneously, $\mathcal{N}_{\rm ZES}$ is a topological invariant in terms of the wave functions of the superconducting states.

We conclude that the index $\mathcal{N}_{\rm ZES}$ defined in the clean limit exactly predicts the degree of degeneracy in the ZESs at the dirty surface of a nodal superconductor.

We have also discussed the zero-bias differential conductance $G_{\rm NS}$ of a normal-metal / superconductor junction with nodal unconventional pairing symmetries such as $d_{xy}$-, $p_x$-, and $f$-wave pairing symmetry. By using the lattice Green function technique, we demonstrated that $G_{\rm NS}$ is quantized at $(4e^2/h)|\mathcal{N}_{\rm ZES}|$ in the limit of strong impurity scattering in the normal segment. The analysis in terms of chiral symmetry enables us to prove the existence of $|\mathcal{N}_{\rm ZES}|$-fold degenerate resonant states in the dirty normal metal and provide a microscopic understanding of the quantization in the conductance minimum.

The index theorem of $\mathcal{N}_{\rm ZES}$ involves another important aspect. The surface bound states of a $p_x$-wave superconductor are consist of Majorana particles. In the phenomenological physics of superconductivity, it has been already known that the $p_x$-wave superconductor shows the anomalous proximity effect which causes the perfect conductance quantization in a normal-metal/superconductor junction and the fractional Josephson effect in a superconductor/normal-metal/superconductor junction. The anomalous proximity effect stems from the penetration of the Majorana bound states into the attached dirty normal metal. However, it had been unclear why the degenerate Majorana bound states can retain their high degree of degeneracy even in the presence of potential disorders. Our theory based on the index $\mathcal{N}_{\rm ZES}$ also explains the robustness of more than one Majorana particle against potential disorders and provide the microscopic understanding of the anomalous proximity effect of a $p_x$-wave superconductor.

Finally, we have studied the transport properties of an artificial nodal superconducting state which is realized in a semiconductor thin film with strong Dresselhaus[110] spin-orbit coupling fabricated on a metallic superconductor under large in-plane Zeeman field. To our knowledge, $\mathcal{N}_{\rm ZES}$ becomes nonzero in several nodal superconductors characterized by spin-triplet $p$- and $f$-wave pairing symmetries. However, it has been difficult to fabricate spin-triplet superconducting junctions using existing materials. The previous theoretical studies have shown that the Dresselhaus superconductor host the flat ZESs similar to those of the $p_x$-wave superconductor. In this thesis, we numerically demonstrate that the Dresselhaus superconductor shows the zero-bias conductance quantization and the fractional Josephson effect even in the presence of potential disorders. We also demonstrate that the anomalous proximity effect of the Dresselhaus superconductor is originated from the effective $p_x$-wave pairing symmetry.

In this thesis, we have established a comprehensive theory regarding with the stability of the flat-band zero-energy states of a nodal superconductor in the presence of potential disorders. Specifically, we have provided the bulk-boundary correspondence of a nodal superconductor with the dirty surface. In addition, we have investigated the drastic transport phenomena which indicate the way of observing the nontrivial topological nature of a nodal superconductor in experiments.

# Appendix A

# Zero energy states under chiral symmetry

Here, we briefly summarize the argument in Ref. [9] which shows the important properties of zero-energy states under a chiral symmetry. We consider the BdG Hamiltonian $\mathcal{H}$ which preserves the chiral symmetry

$$\mathcal{S}\mathcal{H}\mathcal{S}^{-1} = -\mathcal{H}, \quad \mathcal{S}^2 = 1. \tag{A.1}$$

The relation is equivalent to

$$[\mathcal{H}^2, \mathcal{S}] = 0. \tag{A.2}$$

The BdG equation is given by

$$\mathcal{H}\varphi_E(\boldsymbol{r}) = E\varphi_E(\boldsymbol{r}). \tag{A.3}$$

When we consider the eigen equation of $\mathcal{H}^2$,

$$\mathcal{H}^2\chi_{E^2}(\boldsymbol{r}) = E^2\chi_{E^2}(\boldsymbol{r}), \tag{A.4}$$

Eq. (A.2) suggests that the eigen state $\chi_{E^2}(\boldsymbol{r})$ is also the eigen state of $\mathcal{S}$ at the same time. Since $\mathcal{S}^2 = 1$, we find that the eigen value of $\mathcal{S}$ is $+1$ or $-1$. Namely the eigen equation

$$\mathcal{S}\chi_{E^2\gamma}(\boldsymbol{r}) = \gamma\chi_{E^2\gamma}(\boldsymbol{r}), \tag{A.5}$$

holds for $\gamma = \pm 1$. By multiplying $\mathcal{H}$ to Eq. (A.5) from the left side and by using Eq. (A.1), we obtain the equation

$$\mathcal{S}\mathcal{H}\chi_{E^2\gamma}(\boldsymbol{r}) = -\gamma\mathcal{H}\chi_{E^2\gamma}(\boldsymbol{r}). \tag{A.6}$$

We find that $\mathcal{H}\chi_{E^2\gamma}(\boldsymbol{r})$ is the eigen state of $\mathcal{S}$ belonging to $-\gamma$. Thus we can connect $\chi_{E^2+}(\boldsymbol{r})$ and $\chi_{E^2-}(\boldsymbol{r})$ as

$$\mathcal{H}\chi_{E^2\gamma}(\boldsymbol{r}) = c_{E^2\gamma}\chi_{E^2-\gamma}(\boldsymbol{r}), \tag{A.7}$$

where $c_{E^2\gamma}$ is a constant.

The one-to-one correspondence exists between $\varphi_E(\boldsymbol{r})$ and $\chi_{E^2}(\boldsymbol{r})$. At first, we consider zero-energy states $\chi_{0\gamma}(\boldsymbol{r})$ which satisfies

$$\mathcal{H}^2\chi_{0\gamma}(\boldsymbol{r}) = 0, \tag{A.8}$$

in Eq. (A.4). The integration of $\boldsymbol{r}$ after multiplying $\chi^\dagger_{0\gamma}(\boldsymbol{r})$ from the left results in

$$\int d\boldsymbol{r}\, |\mathcal{H}\chi_{0\gamma}(\boldsymbol{r})|^2 = 0. \tag{A.9}$$

This means that the norm of $\mathcal{H}\chi_{0\gamma}(\boldsymbol{r})$ is zero. Therefore we conclude that

$$\mathcal{H}\chi_{0\gamma}(\boldsymbol{r}) = 0. \tag{A.10}$$

As a result, we find the relation

$$\varphi_{0\gamma}(\boldsymbol{r}) = \chi_{0\gamma}(\boldsymbol{r}). \tag{A.11}$$

When a zero energy state is described by $\varphi_{0+}(\boldsymbol{r}) = \chi_{0+}(\boldsymbol{r})$, the relations in Eqs. (A.7) and (A.10) suggest that $\chi_{0-}(\boldsymbol{r}) = 0$. Therefore the zero-energy states are always the eigen states of $\mathcal{S}$.

For $E \neq 0$, it is possible to represent $\varphi_E(\boldsymbol{r})$ by $\chi_{E^2\pm}(\boldsymbol{r})$. By calculating the norm of $\mathcal{H}\chi_{E^2\gamma}(\boldsymbol{r})$, we obtain

$$E^2 = |c_{E^2\gamma}|^2. \tag{A.12}$$

Multiplying $\mathcal{H}$ to Eq. (A.7) from the left alternatively gives a relation

$$c_{E^2\gamma}c_{E^2-\gamma} = 1. \tag{A.13}$$

Therefore, we find the relation

$$\mathcal{H}\chi_{E^2\gamma}(\boldsymbol{r}) = Ee^{i\gamma\theta_{E^2}}\chi_{E^2-\gamma}(\boldsymbol{r}). \tag{A.14}$$

Although we cannot fix the phase factor $\theta_{E^2}$, it is possible to express the states $\varphi_E(\boldsymbol{r})$ for $E \neq 0$ as

$$\varphi_E(\boldsymbol{r}) = \frac{1}{\sqrt{2}}\left(e^{-i\theta_{E^2}/2}\chi_{E^2+}(\boldsymbol{r}) + s_E e^{i\theta_{E^2}/2}\chi_{E^2-}(\boldsymbol{r})\right), \tag{A.15}$$

$$s_E = \begin{cases} 1 & \text{for } E > 0 \\ -1 & \text{for } E < 0. \end{cases} \tag{A.16}$$

The nonzero-energy states are constructed by a pair of eigen states of $\mathcal{S}$: one belongs to $\gamma = 1$ and the other belongs $\gamma = -1$. Therefore, the states with $E \neq 0$ are not the eigen states of $\mathcal{S}$.

# Appendix B

# Bogoliubov-de Gennes Hamiltonian on the tight-binding model

We present the BdG Hamiltonian on a two-dimensional tight-binding lattice. The eigenvalues in Sec. (2.4) are by diagonalizing the tight-binding Hamiltonian. The kinetic energy part and the impurity potential are common for all the superconductors and are given by

$$
\begin{aligned}
H_{\rm kin} =& \sum_{m=1}^{l_y} \sum_{\alpha=\uparrow,\downarrow} \left[ -t \sum_{j=1}^{l_x-1} \left( \psi^{\dagger}_{\boldsymbol{r}+\hat{\boldsymbol{x}},\alpha} \psi_{\boldsymbol{r},\alpha} + \psi^{\dagger}_{\boldsymbol{r},\alpha} \psi_{\boldsymbol{r}+\hat{\boldsymbol{x}},\alpha} \right) - t \sum_{j=1}^{l_x} \left( \psi^{\dagger}_{\boldsymbol{r}+\hat{\boldsymbol{y}},\alpha} \psi_{\boldsymbol{r},\alpha} + \psi^{\dagger}_{\boldsymbol{r},\alpha} \psi_{\boldsymbol{r}+\hat{\boldsymbol{y}},\alpha} \right) \right] \\
&+ \sum_{m=1}^{l_y} \sum_{\alpha=\uparrow,\downarrow} \sum_{j=1}^{l_x} (4t - \mu) \, \psi^{\dagger}_{\boldsymbol{r},\alpha} \psi_{\boldsymbol{r},\alpha}, \qquad \text{(B.1)}
\end{aligned}
$$

$$
H_{\rm imp} = \left( \sum_{j=1}^{l_d} + \sum_{j=l_x-l_d+1}^{l_x} \right) \sum_{m=1}^{l_y} \sum_{\alpha=\uparrow,\downarrow} v\left(\boldsymbol{r}\right) \psi^{\dagger}_{\boldsymbol{r},\alpha} \psi_{\boldsymbol{r},\alpha}, \qquad \text{(B.2)}
$$

where $\psi_{\boldsymbol{r},\alpha}$ ($\psi^{\dagger}_{\boldsymbol{r},\alpha}$) is the annihilation (creation) operator of a electron at $\boldsymbol{r} = j a_0 \boldsymbol{x} + m a_0 \boldsymbol{y}$ with spin $\alpha$, $t$ is the hopping integral, and $\mu$ is the chemical potential. The unit lattice vector in the $x$ and $y$ directions are defined by $\hat{\boldsymbol{x}}$ and $\hat{\boldsymbol{y}}$, respectively. The number of the lattice site in the $x$ ($y$) direction is represented by $l_x = L_x/a_0$ ($l_y = L_y/a_0$). We introduce the impurity potential $v\left(\boldsymbol{r}\right)$ in the outermost $l_d = L_d/a_0$ layers in the $x$-direction. The non-magnetic impurity potential is described by $v\left(\boldsymbol{r}\right)$ which is given randomly in the range of $-W/2 \leq v\left(\boldsymbol{r}\right) \leq W/2$.

## B.1 Unconventional superconductors

The total Hamiltonian of the unconventional superconductors is represented as $H = H_{\text{kin}} + H_\mu + H_{\text{imp}}$, where $H_\mu$ for $\mu = p$, $d$ and $f$ depends on the pairing symmetry as

$$H_p = \sum_{j=1}^{l_x-1}\sum_{m=1}^{l_y}\sum_{\alpha} \frac{i\Delta_0}{2}\left(\psi^\dagger_{\boldsymbol{r}+\hat{\boldsymbol{x}},\alpha}\psi^\dagger_{\boldsymbol{r},\bar{\alpha}} - \psi^\dagger_{\boldsymbol{r},\alpha}\psi^\dagger_{\boldsymbol{r}+\hat{\boldsymbol{x}},\bar{\alpha}}\right) + \text{H.c.}, \tag{B.3}$$

$$\begin{aligned} H_d =& \sum_{j=1}^{l_x-1}\sum_{m=1}^{l_y}\sum_{\alpha} \frac{s_\alpha\Delta_0}{4}\left(\psi^\dagger_{\boldsymbol{r}+\hat{\boldsymbol{x}}+\hat{\boldsymbol{y}},\alpha}\psi^\dagger_{\boldsymbol{r},\bar{\alpha}} + \psi^\dagger_{\boldsymbol{r},\alpha}\psi^\dagger_{\boldsymbol{r}+\hat{\boldsymbol{x}}+\hat{\boldsymbol{y}},\bar{\alpha}}\right) \\ &- \sum_{j=1}^{l_x-1}\sum_{m=1}^{l_y}\sum_{\alpha} \frac{s_\alpha\Delta_0}{4}\left(\psi^\dagger_{\boldsymbol{r}+\hat{\boldsymbol{x}}-\hat{\boldsymbol{y}},\alpha}\psi^\dagger_{\boldsymbol{r},\bar{\alpha}} + \psi^\dagger_{\boldsymbol{r},\alpha}\psi^\dagger_{\boldsymbol{r}+\hat{\boldsymbol{x}}-\hat{\boldsymbol{y}},\bar{\alpha}}\right) + \text{H.c.}, \end{aligned} \tag{B.4}$$

$$\begin{aligned} H_f =& \sum_{j=1}^{l_x-1}\sum_{m=1}^{l_y}\sum_{\alpha} \frac{i\Delta_0}{4}\left(\psi^\dagger_{\boldsymbol{r}+\hat{\boldsymbol{x}}+2\hat{\boldsymbol{y}},\alpha}\psi^\dagger_{\boldsymbol{r},\bar{\alpha}} + \psi^\dagger_{\boldsymbol{r}+\hat{\boldsymbol{x}}-2\hat{\boldsymbol{y}},\alpha}\psi^\dagger_{\boldsymbol{r},\bar{\alpha}}\right) \\ &- \sum_{j=1}^{l_x-1}\sum_{m=1}^{l_y}\sum_{\alpha} \frac{i\Delta_0}{4}\left(\psi^\dagger_{\boldsymbol{r},\alpha}\psi^\dagger_{\boldsymbol{r}+\hat{\boldsymbol{x}}+2\hat{\boldsymbol{y}},\bar{\alpha}} - \psi^\dagger_{\boldsymbol{r},\alpha}\psi^\dagger_{\boldsymbol{r}+\hat{\boldsymbol{x}}-2\hat{\boldsymbol{y}},\bar{\alpha}}\right) + \text{H.c.}, \end{aligned} \tag{B.5}$$

where $\bar{\alpha}$ is the opposite spin of $\alpha$ and $\Delta_0$ is the pair potential at zero temperature. The factor$s_\alpha$ is $+1$ for $\alpha =\uparrow$ and is $-1$ for $\alpha =\downarrow$. For spin-triplet case, we assume a Cooper pair consists of two electrons with the opposite spin directions. In Sec. 2.4.1, we diagonalize the reduced BdG Hamiltonian into $2 \times 2$ Nambu space.

## B.2 $(d_{xy} + p)$-wave superconductor

The Hamiltonian of the $(d_{xy}+p)$-wave superconductor discussed in Sec. (2.4.2) is described by adding the Rashba spin orbit interaction $H_{\text{R}}$ and the pair potential $H_{d_{xy}+p}$ to $H_{\text{kin}} + H_{\text{imp}}$. The spin-orbit coupling term is represented by

$$\begin{aligned} H_{\text{R}} =& -i\frac{\lambda_{\text{R}}}{2}\sum_{\alpha,\beta}\sum_{m=1}^{l_y}\sum_{j=1}^{l_x-1}(\sigma_y)_{\alpha,\beta}\left(\psi^\dagger_{\boldsymbol{r}+\hat{\boldsymbol{x}},\alpha}\psi_{\boldsymbol{r},\beta} - \psi^\dagger_{\boldsymbol{r},\alpha}\psi_{\boldsymbol{r}+\hat{\boldsymbol{x}},\beta}\right) \\ &+i\frac{\lambda_{\text{R}}}{2}\sum_{\alpha,\beta}\sum_{m=1}^{l_y}\sum_{j=1}^{l_x}(\sigma_x)_{\alpha,\beta}\left(\psi^\dagger_{\boldsymbol{r}+\hat{\boldsymbol{y}},\alpha}\psi_{\boldsymbol{r},\beta} - \psi^\dagger_{\boldsymbol{r},\alpha}\psi_{\boldsymbol{r}+\hat{\boldsymbol{y}},\beta}\right). \end{aligned} \tag{B.6}$$

The pair potential consists of five parts: $H_{d_{xy}+p} = H_{\Delta 1} + H_{\Delta 1} + H_{\Delta 2} + H_{\Delta 4} + H_{\Delta 5}$. The each parts are represented by

$$\begin{aligned} H_{\Delta 1} =& i\frac{\Delta_s}{4}\sum_{\alpha,\beta}\sum_{j=1}^{l_x-1}\sum_{m=1}^{l_y}(\sigma_y)_{\alpha,\beta}\left(\psi^\dagger_{\boldsymbol{r}+\hat{\boldsymbol{x}}+\hat{\boldsymbol{y}},\alpha}\psi^\dagger_{\boldsymbol{r},\beta} + \psi^\dagger_{\boldsymbol{r},\alpha}\psi^\dagger_{\boldsymbol{r}+\hat{\boldsymbol{x}}+\hat{\boldsymbol{y}},\beta}\right) \\ &- i\frac{\Delta_s}{4}\sum_{\alpha,\beta}\sum_{j=1}^{l_x-1}\sum_{m=1}^{l_y}(\sigma_y)_{\alpha,\beta}\left(\psi^\dagger_{\boldsymbol{r}+\hat{\boldsymbol{x}}-\hat{\boldsymbol{y}},\alpha}\psi^\dagger_{\boldsymbol{r},\beta} + \psi^\dagger_{\boldsymbol{r},\alpha}\psi^\dagger_{\boldsymbol{r}+\hat{\boldsymbol{x}}-\hat{\boldsymbol{y}},\beta}\right) + \text{H.c.}, \end{aligned} \tag{B.7}$$

$$H_{\Delta 2} = -i\frac{\Delta_t}{4}\sum_{\alpha,\beta}\sum_{j=1}^{l_x-1}\sum_{m=1}^{l_y}(\sigma_z)_{\alpha,\beta}\left[\psi^\dagger_{\boldsymbol{r}+\hat{\boldsymbol{x}},\alpha}\psi^\dagger_{\boldsymbol{r},\beta} - \psi^\dagger_{\boldsymbol{r},\alpha}\psi^\dagger_{\boldsymbol{r}+\hat{\boldsymbol{x}},\beta}\right] + \text{H.c.}, \tag{B.8}$$

$$H_{\Delta 3} = \frac{\Delta_t}{4}\sum_{\alpha}\sum_{j=1}^{l_x}\sum_{m=1}^{l_y}\left[\psi^\dagger_{\boldsymbol{r}+\hat{\boldsymbol{y}},\alpha}\psi^\dagger_{\boldsymbol{r},\alpha} - \psi^\dagger_{\boldsymbol{r},\alpha}\psi^\dagger_{\boldsymbol{r}+\hat{\boldsymbol{y}},\alpha}\right] + \text{H.c.}, \tag{B.9}$$

$$\begin{aligned} H_{\Delta 4} =& i\frac{\Delta_t}{8}\sum_{\alpha,\beta}\sum_{j=1}^{l_x-1}\sum_{m=1}^{l_y}(\sigma_z)_{\alpha,\beta}\left(\psi^\dagger_{\boldsymbol{r}+\hat{\boldsymbol{x}}+2\hat{\boldsymbol{y}},\alpha}\psi^\dagger_{\boldsymbol{r},\beta} + \psi^\dagger_{\boldsymbol{r}+\hat{\boldsymbol{x}}-2\hat{\boldsymbol{y}},\alpha}\psi^\dagger_{\boldsymbol{r},\beta}\right) \\ &- i\frac{\Delta_t}{8}\sum_{\alpha,\beta}\sum_{j=1}^{l_x-1}\sum_{m=1}^{l_y}(\sigma_z)_{\alpha,\beta}\left(\psi^\dagger_{\boldsymbol{r},\alpha}\psi^\dagger_{\boldsymbol{r}+\hat{\boldsymbol{x}}+2\hat{\boldsymbol{y}},\beta} + \psi^\dagger_{\boldsymbol{r},\alpha}\psi^\dagger_{\boldsymbol{r}+\hat{\boldsymbol{x}}-2\hat{\boldsymbol{y}},\beta}\right) + \text{H.c.}, \end{aligned} \tag{B.10}$$

$$\begin{aligned} H_{\Delta 5} =& -\frac{\Delta_t}{8}\sum_{\alpha}\sum_{j=1}^{l_x-2}\sum_{m=1}^{l_y}\left(\psi^\dagger_{\boldsymbol{r}+2\hat{\boldsymbol{x}}+\hat{\boldsymbol{y}},\alpha}\psi^\dagger_{\boldsymbol{r},\alpha} + \psi^\dagger_{\boldsymbol{r}-2\hat{\boldsymbol{x}}+\hat{\boldsymbol{y}},\alpha}\psi^\dagger_{\boldsymbol{r},\alpha}\right) \\ &+ \frac{\Delta_t}{8}\sum_{\alpha}\sum_{j=1}^{l_x-2}\sum_{m=1}^{l_y}\left(\psi^\dagger_{\boldsymbol{r},\alpha}\psi^\dagger_{\boldsymbol{r}+2\hat{\boldsymbol{x}}+\hat{\boldsymbol{y}},\alpha}\psi^\dagger_{\boldsymbol{r},\alpha}\psi^\dagger_{\boldsymbol{r}-2\hat{\boldsymbol{x}}+\hat{\boldsymbol{y}},\alpha}\right) + \text{H.c.} \end{aligned} \tag{B.11}$$

The amplitude of the pair potential for the spin-singlet (-triplet) component is represented by $\Delta_s$ ($\Delta_t$). The Pauli matrices in spin space are represented by $\sigma_\nu$ ($\nu = x, y, z$).

## B.3 Noncentrosymmetric superconductor with the persistent helix states

The BdG Hamiltonian for a NCS with the persistent spin-helix states discussed in Sec. 2.4.3 is described by $H = H_{\text{kin}} + H_{\text{D}}^{110} + H_{\Delta_p} + H_{\text{imp}}$. The spin-orbit coupling and the pair potential are given by

$$H_{\mathrm{D}}^{110} = i\frac{\lambda_D}{2}\sum_{\alpha,\beta}\sum_{j=1}^{l_x-1}\sum_{m=1}^{l_y}(\sigma_z)_{\alpha,\beta}\left(\psi^\dagger_{\boldsymbol{r}+\hat{\boldsymbol{x}},\alpha}\psi_{\boldsymbol{r},\beta} - \psi^\dagger_{\boldsymbol{r},\alpha}\psi_{\boldsymbol{r}+\hat{\boldsymbol{x}},\beta}\right), \tag{B.12}$$

$$\begin{aligned} H_{\Delta_p} =& \sum_{\alpha,\beta}\sum_{m=1}^{l_y}\sum_{j=1}^{l_x} i\Delta_s(\sigma_y)_{\alpha,\beta}\psi^\dagger_{\boldsymbol{r},\alpha}\psi^\dagger_{\boldsymbol{r},\beta} \\ &+ \sum_{\alpha,\beta}\sum_{m=1}^{l_y}\sum_{j=1}^{l_x-1} i\frac{\Delta_t}{2}(\sigma_x)_{\alpha,\beta}\left(\psi^\dagger_{\boldsymbol{r}+\hat{\boldsymbol{x}},\alpha}\psi^\dagger_{\boldsymbol{r},\beta} - \psi^\dagger_{\boldsymbol{r},\alpha}\psi^\dagger_{\boldsymbol{r}+\hat{\boldsymbol{x}},\beta}\right) + \mathrm{H.c.}, \end{aligned} \tag{B.13}$$

where $\lambda_{\mathrm{D}}$ denotes the strength of the Dresselhaus[110] spin-orbit coupling.

# Appendix C

# Unitary transformation for the $(d_{xy} + p)$-wave superconductor

The BdG Hamiltonian of a $(d_{xy} + p)$ superconductor in Sec. (2.4.2) is represented by

$$H_{\boldsymbol{k}} = \begin{bmatrix} \hat{h}_{\boldsymbol{k}} & \hat{\Delta}_{\boldsymbol{k}} \\ -\hat{\Delta}^*_{-\boldsymbol{k}} & -\hat{h}^*_{-\boldsymbol{k}} \end{bmatrix}, \tag{C.1}$$

$$\hat{h}_{\boldsymbol{k}} = \xi(\boldsymbol{k})\hat{\sigma}_0 + \boldsymbol{g}_{\mathrm{r}}(\boldsymbol{k}) \cdot \hat{\boldsymbol{\sigma}}, \tag{C.2}$$

$$\hat{\Delta}_{\boldsymbol{k}} = if(\boldsymbol{k})[\Delta_s + \Delta_t \frac{\Delta_t}{\alpha k}\boldsymbol{g}_{\mathrm{r}}(\boldsymbol{k}) \cdot \hat{\boldsymbol{\sigma}}]\hat{\sigma}_2, \tag{C.3}$$

where $\boldsymbol{g}_{\mathrm{r}}(\boldsymbol{k}) = \alpha(k_y\boldsymbol{x} - k_x\boldsymbol{y})$, $f(\boldsymbol{k}) = (k_xk_y/k^2)$ and $k = \sqrt{k_x^2 + k_y^2}$. We first apply a unitary transformation to $U^\dagger_{\boldsymbol{k}} H_{\boldsymbol{k}} U_{\boldsymbol{k}} = H'_{\boldsymbol{k}}$ with

$$U_{\boldsymbol{k}} = \begin{bmatrix} \hat{u}_{\boldsymbol{k}} & 0 \\ 0 & \hat{u}^*_{-\boldsymbol{k}} \end{bmatrix}, \quad \hat{u}_{\boldsymbol{k}} = \frac{1}{\sqrt{2}} \begin{bmatrix} 1 & ie^{-i\theta_{\boldsymbol{k}}} \\ -ie^{i\theta_{\boldsymbol{k}}} & -1 \end{bmatrix}, \quad \theta_{\boldsymbol{k}} = \arctan\left[\frac{k_y}{k_x}\right]. \tag{C.4}$$

The second unitary transformation

$$H_\gamma(\boldsymbol{k}) = U_0^\dagger H'_{\boldsymbol{k}} U_0, \quad U_0 = \begin{bmatrix} 1 & 0 & 0 & 0 \\ 0 & 0 & 1 & 0 \\ 0 & 0 & 0 & 1 \\ 0 & 1 & 0 & 0 \end{bmatrix}, \tag{C.5}$$

results in

$$H_\gamma(\boldsymbol{k}) = \begin{bmatrix} \hat{H}_+(\boldsymbol{k}) & 0 \\ 0 & \hat{H}_-(\boldsymbol{k}) \end{bmatrix}, \tag{C.6}$$

$$\hat{H}_\pm(\boldsymbol{k}) = \begin{bmatrix} E_\pm(\boldsymbol{k}) & -\Delta_\pm(\boldsymbol{k}) \\ -\Delta_\pm(\boldsymbol{k}) & -E_\pm(\boldsymbol{k}) \end{bmatrix}, \tag{C.7}$$

$$E_\pm(\boldsymbol{k}) = \xi(\boldsymbol{k}) \pm \mid \boldsymbol{g}_{\mathrm{R}}(\boldsymbol{k}) \mid, \quad \Delta_\pm(\boldsymbol{k}) = f(\boldsymbol{k})[\Delta_t \pm \Delta_s]. \tag{C.8}$$

# Appendix D

# Persistent spin-helix states with coexistence of Rashba and Dresselhaus[100] spin-orbit coupling

We shown an alternative way to realize the persistent spin-helix states [74, 75]. Let us consider the thin film growing along the [001] crystal direction. In such the two dimensional eletron system, the Rashba type SOC $\boldsymbol{g}_{\mathrm{r}}(\boldsymbol{k}) = \alpha(k_y\boldsymbol{x} - k_x\boldsymbol{y})$ and the Dresselhaus [001] type SOC $\boldsymbol{g}'_{\mathrm{d}}(\boldsymbol{k}) = \beta'(k_x\boldsymbol{x} - k_y\boldsymbol{y})$ coexist. The Hamiltonian is described as

$$\hat{h}_{\mathrm{RD}}(\boldsymbol{k}) = \xi(\boldsymbol{k})\hat{\sigma}_0 + \hat{h}_{\mathrm{R}}(\boldsymbol{k}) + \hat{h}_{\mathrm{D}}^{100}(\boldsymbol{k}), \tag{D.1}$$

$$\hat{h}_R = \alpha\left(k_y\hat{\sigma}_x - k_x\hat{\sigma}_y\right), \tag{D.2}$$

$$\hat{h}_D^{100} = \beta'\left(k_x\hat{\sigma}_x - k_y\hat{\sigma}_y\right). \tag{D.3}$$

When we define

$$k_\pm = \frac{1}{\sqrt{2}}\left(k_x \pm k_y\right), \tag{D.4}$$

the Hamiltonian is rewritten as

$$\hat{h}_{\mathrm{RD}}(\boldsymbol{k}) = \xi'(\boldsymbol{k})\hat{\sigma}_0 + \hat{h}_+ + \hat{h}_-, \tag{D.5}$$

where

$$\xi'(\boldsymbol{k}) = \frac{\hbar^2}{2m}\left(k_+^2 + k_-^2\right) - \mu_{\mathrm{F}}, \tag{D.6}$$

$$\hat{h}_\pm = \lambda_\pm k_\pm \hat{\sigma}_\pm, \quad \lambda_\pm = \frac{1}{\hbar}\left(\beta \pm \alpha\right), \quad \hat{\sigma}_\pm = \frac{1}{\sqrt{2}}\left(\hat{\sigma}_x \mp \hat{\sigma}_y\right). \tag{D.7}$$

The strength of the Rashba SOC is tunable by an externally applied electric field. When we consider a special case of $\alpha = \beta'$, which can be experimentally accessible [76, 77], the Hamiltonian is deformed as

$$\hat{h}(\boldsymbol{k}) = \left[\frac{\hbar^2}{2m}(k_+^2 + k_-^2) - \mu_{\mathrm{F}}\right]\hat{\sigma}_0 + \beta' p_+ \hat{\sigma}_+. \tag{D.8}$$

The Hamiltonian in Eq. (D.8) is unitary equivalent to that in Eq. (2.40). Therefore the persistent spin-helix states can also obtained in the thin film growing along the [001] crystal direction. Moreover, as discussed in Sec. (2.4.3), we can expect the flat ZESs at a dirty surface of a superconducting thin film with coexistence of Rashba and Dresselhaus[001] spin-orbit coupling.

# Appendix E

# Wave functions of zero energy states

We derive the wave functions of the zero-energy states appearing in the two semi-infinite $p_x$-wave superconductors illustrated in Fig. 4.2. In the $y$ direction, the width is denoted by $L_y$ and the hard-wall boundary condition is applied. The Bogoliubov-de Gennes equation is given by

$$\hat{H}_\alpha \varphi_{\alpha,E} = E\varphi_{\alpha,E}, \quad \hat{H}_\alpha = \begin{bmatrix} \xi(\boldsymbol{r}) & \frac{\Delta e^{i\varphi_\alpha}}{k_\mathrm{F}}\partial_x \\ -\frac{\Delta e^{-i\varphi_\alpha}}{k_\mathrm{F}}\partial_x & -\xi(\boldsymbol{r}) \end{bmatrix}, \tag{E.1}$$

where the index $\alpha = L,R$ labels the left superconductor ($x \leq -L_x$) and the right superconductor ($x \geq L_x$), respectively. The superconducting phase is given as

$$\varphi_L = 0, \tag{E.2}$$

$$\varphi_R = \varphi. \tag{E.3}$$

The Hamiltonian $\hat{H}_\alpha$ preserves chiral symmetry as

$$(e^{i\varphi_\alpha\hat{\tau}_3}\hat{S})\ \hat{H}_\alpha\ (e^{i\varphi_\alpha\hat{\tau}_3}\hat{S})^{-1} = -\hat{H}_\alpha, \tag{E.4}$$

$$\hat{S} = \begin{bmatrix} 0 & 1 \\ 1 & 0 \end{bmatrix} = \hat{\tau}_1, \quad \hat{\tau}_3 = \begin{bmatrix} 1 & 0 \\ 0 & -1 \end{bmatrix}. \tag{E.5}$$

By solving Eq. (E.1), we obtain the wave function belonging to an energy $E$ as

$$\psi_{\alpha,E} = \phi_n(x)Y_n(y) \tag{E.6}$$

$$\phi_n(x) = c_1 \begin{bmatrix} E+\Omega_+ \\ -i\Delta e^{-i\varphi_\alpha}(k_+/k_{\mathrm{F}}) \end{bmatrix} e^{ik_+x} + c_2 \begin{bmatrix} i\Delta e^{i\varphi_\alpha}(k_-/k_{\mathrm{F}}) \\ E+\Omega_- \end{bmatrix} e^{ik_-x}$$
$$+ c_3 \begin{bmatrix} -i\Delta e^{i\varphi_\alpha}(k_-/k_{\mathrm{F}}) \\ E+\Omega_- \end{bmatrix} e^{-ik_-x} + c_4 \begin{bmatrix} E+\Omega_+ \\ i\Delta e^{-i\varphi_\alpha}(k_+/k_{\mathrm{F}}) \end{bmatrix} e^{-ik_+x}, \tag{E.7}$$

$$Y_n(y) = \sqrt{\frac{2}{L_y}} \sin\left(\frac{n\pi}{L_y} y\right), \tag{E.8}$$
$$\Omega_\pm = \sqrt{E^2 - \frac{\Delta^2}{\mu}\left(\mu_n - \frac{\Delta^2}{4\mu}\right)} \mp \frac{\Delta^2}{2\mu}, \tag{E.9}$$
$$k_\pm = k_n\sqrt{1 \pm \frac{\Omega_\pm}{\mu_n}}, \qquad k_n = \frac{\sqrt{2m\mu_n}}{\hbar}, \tag{E.10}$$
$$\mu_n = \mu - \frac{\hbar^2}{2m}\left(\frac{n\pi}{W}\right)^2, \tag{E.11}$$

where $c_i$ ($i$ = 1-4) are numerical coefficients. At $E = 0$, the wave function is deformed as

$$\psi_{\alpha,0}(x,y) = \left[\phi_{\alpha,n,1}(x) + \phi_{\alpha,n,2}(x)\right] Y_n(y), \tag{E.12}$$
$$\phi_{\alpha,n,1}(x) = \begin{bmatrix} e^{i\frac{\varphi_\alpha}{2}} \\ -e^{-i\frac{\varphi_\alpha}{2}} \end{bmatrix} \left[c_1' e^{iq_nx} + c_3' e^{-iq_nx}\right] e^{-x/\xi}, \tag{E.13}$$
$$\phi_{\alpha,n,2}(x) = \begin{bmatrix} e^{i\frac{\varphi_\alpha}{2}} \\ e^{-i\frac{\varphi_\alpha}{2}} \end{bmatrix} \left[c_2' e^{iq_nx} + c_4' e^{-iq_nx}\right] e^{x/\xi}, \tag{E.14}$$
$$q_n = \sqrt{k_n^2 - \xi^{-2}}, \qquad \xi = \hbar^2 k_{\mathrm{F}}/m\Delta. \tag{E.15}$$

We note that the components of $\phi_{\alpha,n,1}$ and $\phi_{\alpha,n,2}$ are the eigenstates of the chiral symmetry operator as

$$(e^{i\varphi_\alpha\hat{\tau}_3}\hat{S})\phi_{\alpha,n,1}(x) = -\phi_{\alpha,n,1}(x), \tag{E.16}$$
$$(e^{i\varphi_\alpha\hat{\tau}_3}\hat{S})\phi_{\alpha,n,2}(x) = \phi_{\alpha,n,2}(x). \tag{E.17}$$

First, we calculate the wave function of the zero-energy states in the left superconductor. We apply the boundary condition in the $x$ direction as

$$\psi_{L,0}(-\infty, y) = \psi_{L,0}(-L_x, y) = 0. \tag{E.18}$$

As a result, we obtain the two zero-energy states for each propagating channel as

$$\psi_L = \frac{1}{\sqrt{N_n}} \begin{bmatrix} 1 \\ 1 \end{bmatrix} \sin[q_n(x + L_x)] e^{x/\xi} Y_n(y), \tag{E.19}$$

where the normalization coefficient is denoted by $N_n$. In is easy to show that the zero energy states of left superconductor are simultaneously the eigenstates of chiral symmetry operator $\hat{S}$ with the eigenvalue $\gamma = +1$. Next, we consider the right superconductor. By applying the boundary condition in the $x$ direction as

$$\psi_{R,0}(L_x, y) = \psi_{R,0}(\infty, y) = 0, \tag{E.20}$$

we find the wave function for the zero-energy states as

$$\psi_R = \frac{1}{\sqrt{N_n}} \begin{bmatrix} e^{i\frac{\varphi}{2}} \\ -e^{-i\frac{\varphi}{2}} \end{bmatrix} \sin[q_n(x - L_x)] e^{-x/\xi} Y_n(y). \tag{E.21}$$

The zero-energy states of the right superconductor $\psi_R$ hold $\gamma = -1$ for the chiral symmetry operator $e^{i\varphi\hat{\tau}_3}\hat{S}$.

# Appendix F

# Effective $p_x$-wave superconductor with coexistence of Rashba and Dresselhaus[100] spin-orbit coupling

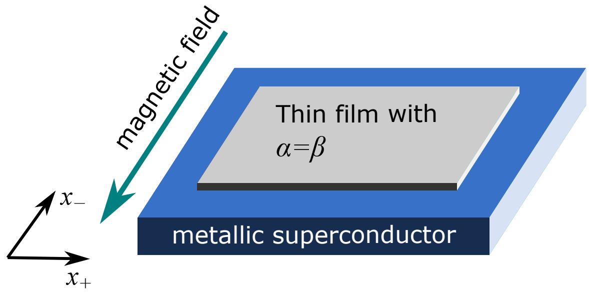


**Figure F.1:** (Color online) Schematic picture of the effective $p_x$-wave superconductor with the coexistence of the Rahba and Dresselhaus [100] spin-orbit coupling.

We propose an alternative artificial superconductor whose Hamiltonian is unitary equivalent to Eq. (5.9). Let us consider the two dimensional electron system where the Rashba spin-orbit coupling and the Dresselhaus[100] one coexist. The Hamiltonian is represented by

$$\hat{h}_{RD} = \hat{h}_{\rm kin} + \hat{h}_R + \hat{h}_D^{100} + \hat{h}_V, \tag{F.1}$$

$$\hat{h}_{\rm kin} = \frac{1}{2m}\left(p_x^2 + p_y^2\right) - \mu, \tag{F.2}$$

$$\hat{h}_R = \frac{\alpha}{\hbar}\left(p_y\hat{\sigma}_1 - p_x\hat{\sigma}_2\right), \tag{F.3}$$

$$\hat{h}_D^{100} = \frac{\beta}{\hbar}\left(p_x\hat{\sigma}_1 - p_y\hat{\sigma}_2\right), \tag{F.4}$$

$$\hat{h}_V = -\boldsymbol{V}\cdot\hat{\boldsymbol{\sigma}}, \quad \boldsymbol{V} = V_x\boldsymbol{e}_1 + V_y\boldsymbol{e}_2, \tag{F.5}$$

where $m$, $\mu$, $\alpha$ and $\beta$ denotes the effective mass of an electron, the chemical potential, the strength of the Rashba spin-orbit coupling and the strength of the Dresselhaus[100] spin-orbit coupling, respectively. The unit vectors in spin space is denoted by $\boldsymbol{e}_j$ with $j$ = 1-3. The part of the Hamiltonian $\hat{h}_V$ denotes the Zeeman potential induced by the in-plane external magnetic field. When we define

$$p_\pm = \frac{1}{\sqrt{2}}\left(p_x \pm p_y\right), \quad x_\pm = \frac{1}{\sqrt{2}}\left(x \pm y\right), \tag{F.6}$$

the commutation relations among $p_\pm$ and $x_\pm$ become

$$[x_\nu, p_\nu] = i\hbar\delta_{\nu,\nu}, \tag{F.7}$$

$$[x_\nu, x_\nu] = [p_\nu, p_\nu] = 0. \tag{F.8}$$

In this basis, the Hamiltonian is represented as

$$\hat{h}_{RD} = \hat{h}'_{\rm kin} + \hat{h}_+ + \hat{h}_- + \hat{h}_V, \tag{F.9}$$

where

$$\hat{h}'_{\rm kin} = \frac{1}{2m}\left(p_+^2 + p_-^2\right) - \mu, \tag{F.10}$$

$$\hat{h}_\pm = \lambda_\pm p_\pm \hat{\sigma}_\pm, \tag{F.11}$$

$$\lambda_\pm = \frac{1}{\hbar}\left(\alpha \pm \beta\right), \quad \hat{\sigma}_\pm = \frac{1}{\sqrt{2}}\left(\hat{\sigma}_2 \pm \hat{\sigma}_1\right). \tag{F.12}$$

The direction $\boldsymbol{e}_+ = (\boldsymbol{e}_1 + \boldsymbol{e}_2)/\sqrt{2}$ and $\boldsymbol{e}_- = (\boldsymbol{e}_1 - \boldsymbol{e}_2)/\sqrt{2}$ are orthogonal to each other in spin space. When the strength of the Rashba spin-orbit coupling $\alpha$ and the strength of the Dresslhaus spin-orbit coupling $\beta$ are equal to each other (i.e., $\alpha = \beta$), $\lambda_-$ becomes zero. Such electron systems have been studied in spintronics because they show unusual spin property so called spin-helix [74, 75]. In addition, we tune the Zeeman potential as $V_x = -V_y = V/\sqrt{2}$. The Hamiltonian is constructed by the two orthogonal components in the spin space as

$$\hat{h}_{RD} = \hat{h}'_{\text{kin}} + \lambda_+ p_+ \hat{\sigma}_+ + V\hat{\sigma}_-. \tag{F.13}$$

By multiplying a unitary matrix,

$$\hat{d} = \frac{1}{\sqrt{2}} \begin{bmatrix} e^{-i\pi/8} & ie^{i\pi/8} \\ ie^{-i\pi/8} & e^{i\pi/8} \end{bmatrix}, \tag{F.14}$$

the Hamiltonian is transformed into

$$\begin{aligned} \hat{h}'_{RD} &= \hat{d}\, \hat{h}_{RD}\, \hat{d}^\dagger \\ &= \hat{h}'_{\text{kin}} - \lambda_+ p_+ \hat{\sigma}_3 - V\hat{\sigma}_1. \end{aligned} \tag{F.15}$$

The Hamiltonian $\hat{h}'_{RD}$ is equivalent to the Hamiltonian with the Dresselhaus [110] spin-orbit coupling and with the in-plane magnetic field.

Next, we introduce the proximity-induced $s$-wave pair potential. The BdG Hamiltonian for the original basis in Eq. (F.5) is given by

$$\check{H}_{RD} = \begin{bmatrix} \hat{h}_{RD} & i\Delta_0\hat{\sigma}_2 \\ -i\Delta_0\hat{\sigma}_0 & -\hat{h}^*_{RD} \end{bmatrix}. \tag{F.16}$$

When $\alpha = \beta$ and $V_x = -V_y = V/\sqrt{2}$, the BdG Hamiltonian is transformed into

$$\check{H}'_{RD} = \hat{D}\hat{H}_{RD}\hat{D}^\dagger = \begin{bmatrix} \hat{h}'_{RD} & i\Delta_0\hat{\sigma}_2 \\ -i\Delta_0\hat{\sigma}_0 & -\hat{h}'^*_{RD} \end{bmatrix}, \tag{F.17}$$

$$\check{D} = \begin{bmatrix} \hat{d} & 0 \\ 0 & \hat{d}^* \end{bmatrix}. \tag{F.18}$$

The BdG Hamiltonian $\check{H}'_{RD}$ is unitary equivalent to the BdG Hamiltonian in Eq. (5.9). Therefore, by applying the unitary transformations introduced in Sec. (5.4), we can obtain the BdG Hamiltonian of the effective $p_x$-wave super conductor in Eq. (5.22). As shown in Fig. F.1, we have to apply the magnetic field in the $x_-$ direction. More generally, by applying the appropriate unitary transformation, we also obtain the Hamiltonian $\check{H}'_{RD}$

with

$$\boldsymbol{V} = V\left[\frac{\sin\phi}{\sqrt{2}}\boldsymbol{e}_1 - \frac{\sin\phi}{\sqrt{2}}\boldsymbol{e}_2 + \cos\phi\boldsymbol{e}_3\right], \tag{F.19}$$

where $\phi$ is the arbitrary angle of the magnetic field. Alternatively, it is possible to reach BdG Hamiltonian in Eq. (5.9) when we prepare the nanowire along the $x_-$ direction with $\alpha = -\beta$ and

$$\boldsymbol{V} = V\left[\frac{\sin\phi}{\sqrt{2}}\boldsymbol{e}_1 + \frac{\sin\phi}{\sqrt{2}}\boldsymbol{e}_2 + \cos\phi\boldsymbol{e}_3\right]. \tag{F.20}$$

# Bibliography


[1] M. Z. Hasan and C. L. Kane, Rev. Mod. Phys. **82**, 3045 (2010).

[2] X -L. Qi and S. C Zhang, Phys, Mod. Phys. **83**, 1058 (2011).

[3] M. Sato and Y. Ando, Rep. Prog. Phys. **80**, 076501 (2017).

[4] A. P. Schnyder, S. Ryu, A. Furusaki, A. W. W. Ludwig, Phys. Rev. B **78**, 195125 (2008).

[5] Y. Hatsugai, Phys. Rev. Lett. **71**, 3697 (1993).

[6] Y. Hatsugai, Phys. Rev. B **48**, 11851 (1993).

[7] Y. Tanaka, Yu. V. Nazarov, and S. Kashiwaya, Phys. Rev. Lett. **90**, 167003 (2003).

[8] Y. Asano and Y. Tanaka, Phys. Rev. B **87**, 104513 (2013).

[9] M. Sato, Y. Tanaka, K. Yada, and T. Yokoyama, Phys. Rev. B **83**, 224511 (2011).

[10] S. Matsuura, P.-Y. Chang, A. P. Schnyder, and S. Ryu, New J. Phys. **15**, 065001 (2013)

[11] A. P. Schnyder and P. M. R. Brydon, J. Phys.: Condens. Matter **27**, 243201 (2015).

[12] Y. Tanaka and S. Kashiwaya, Phys. Rev. Lett. **74**, 3451 (1995).

[13] Y. Asano, Y. Tanaka, and S. Kashiwaya, Phys. Rev. B **69**, 134501 (2004).

[14] Y. Tanaka and S. Kashiwaya, Phys. Rev. B **70**, 012507 (2004).

[15] Y. Asano, Y. Tanaka, A. A. Golubov, and S. Kashiwaya, Phys. Rev. Lett. **99**, 067005 (2007).

[16] Y. Tanaka and S. Kashiwaya, Phys. Rev. B **53**, 11957(R) (1996).

[17] Y. S. Barash, H. Burkhardt and D. Rainer, Phys. Rev. Lett. **77**, 4070 (1996).

[18] H. -J. Kwon, K. Sengupta, and V. M. Yakovenko, Eur. Phys. J. B **37**, 349−361(2004).

[19] Y. Asano, Y. Tanaka, and S. Kashiwaya, Phys. Rev. Lett. **96**, 097007 (2006).

[20] Y. Asano, Y. Tanaka, T. Yokoyama and S. Kashiwaya, Phys. Rev. B **74**, 064507 (2006).

[21] S. Higashitani, J. Phys. Soc. Jpn., **66**, 2556 (1997).

[22] H. Walter, W. Prusseit, R. Semerad, H. Kinder, W. Assmann, H. Huber, H. Burkhardt, D. Rainer, and J. A. Sauls, Phys. Rev. Lett. **80**, 3598 (1998).

[23] A. B. Vorontsov, Phys. Rev. Lett. **102**, 177001 (2009).

[24] S.-I. Suzuki and Y. Asano, Phys. Rev. B **89**, 184508 (2014).

[25] S.-I. Suzuki and Y. Asano, Phys. Rev. B **91**, 214510 (2015).

[26] M. Hakansson, T. Lofwander and M. Fogelstrom, Nat. Phys. **11**, 755 (2015).

[27] S. Valentini, R. Fazio, V. Giovannetti, and F. Taddei, Phys. Rev. B **91**, 045430 (2015).

[28] L. J. Buchholtz and G. Zwicknagl, Phys. Rev. B **23**, 5788 (1981).

[29] J. Hara and K. Nagai, Prog. Theor. Phys. **74**,1237 (1986).

[30] C. R. Hu, Phys. Rev. Lett. **72**, 1526 (1994).

[31] Y. Tanaka, Y. Mizuno, T. Yokoyama, K. Yada, and M. Sato, Phys. Rev. Lett. **105**, 097002 (2010).

[32] K. Yada, M. Sato, Y. Tanaka, and T. Yokoyama, Phys. Rev. B **83**, 064505 (2011).

[33] P. M. R. Brydon, A. P. Schnyder, and C. Timm, Phys. Rev. B **84**, 020501(R) (2011).

[34] A. P. Schnyder and S. Ryu, Phys. Rev. B **84**, 060504(R) (2011).

[35] A. P. Schnyder, P. M. R. Brydon and C. Timm, Phys. Rev. B **85**, 024522 (2012).

[36] J. Alicea, Phys. Rev. B **81**, 125318 (2010).

[37] J. You, C. H. Oh, and V. Vedral, Phys. Rev. B **87**, 054501 (2013).

[38] N. F. Q. Yuan, Y. Lu, J. J. He, and K. T. Law, Phys. Rev. B **95**, 195102 (2017).

[39] T. Mizushima, M. Sato, and K. Machida, Phys. Rev. Lett. **109**, 165301(2012).

[40] C. L. M. Wong, J. Liu, K. T. Law, P. A. Lee, Phys. Rev. B **88**, 060504(R) (2013).

[41] S. Deng, G. Ortiz, A. Poudel, and L. Viola, Phys. Rev. B **89**, 140507(R) (2014).

[42] A. Chen and M. Franz, Phys. Rev. B **93**, 201105(R) (2016).

[43] R. Queiroz an A. P. Schnyder, Phys. Rev. B **89**, 054501 (2014).

[44] S. Tewari and J. D. Sau, Phys. Rev. Lett. **109**, 150408 (2012).

[45] Y. Niu, S. -B. Chung, C. -H. Hsu, I. Mandal, S. Raghu, and S. Chakravarty, Phys. Rev. B **85**, 035110 (2012).

[46] M. Diez, J. P. Dahlhaus, M. Wimmer, and C. W. J. Beenakker , Phys. Rev. B **86**, 094501 (2012).

[47] S. Ikegaya and Y. Asano, Phys. Rev. B **95**, 214503 (2017).

[48] S. Ikegaya, S.-I. Suzuki, Y. Tanaka, and Y. Asano, Phys. Rev. B **94**, 054512 (2016).

[49] S. Ikegaya and Y. Asano, J. Phys.: Condens. Matter **28**, 375702 (2016).

[50] S. Ikegaya, Y. Asano, and Y. Tanaka, Phys. Rev. B **91**, 174511 (2015).

[51] C. L. Kane and E. J. Mele, Phys. Rev. Lett. **95**, 226801 (2005).

[52] C. L. Kane and E. J. Mele, Phys. Rev. Lett. **95**, 146802 (2005).

[53] E. Majorana, Nuovo Cimento, **14**, 171 (1937).

[54] F.Wilczek, Nat. Phys. **5**, 614 (2009).

[55] N. Read and D. Green, Phys. Rev. B **61**, 15 (2000).

[56] A. Y. Kitaev, Phys. Usp. **44**, 131 (2001).

[57] A. Furusaki, M. Matsumoto, and M. Sigrist, Phys. Rev. B **64**, 054514 (2001).

[58] L. Fu and C. L. Kane, Phys. Rev. Lett. **100**, 096407 (2008).

[59] M. Sato, Y. Takahashi, and S. Fujimoto, Phys. Rev. Lett. **103**, 020401 (2009).

[60] M. Sato, Y. Takahashi, and S. Fujimoto, Phys. Rev. B **82**, 134521 (2010).

[61] J. D. Sau, R. M. Lutchyn, S. Tewari, and S. D. Sarma, Phys. Rev. Lett. **104**, 040502 (2010).

[62] R. M. Lutchyn, J. D. Sau, and S. D. Sarma, Phys. Rev. Lett. **105**, 077001 (2010).

[63] Y. Oreg, G. Refael, and F. von Oppen, Phys. Rev. Lett. **105**, 177002 (2010).

[64] T. D. Stanescu, R. M. Lutchyn, and S. D. Sarma, Phys. Rev. B **84**, 144522 (2011).

[65] M. Sato and S. Fujimoto, Phys. Rev. B **79**, 094594 (2009).

[66] V. Mourik, K. Zuo, S. M. Frolov, S. R. Plissard, E. P. A. M. Bakkers, L. P. Kouwenhoven, Science **336**, 1003 (2012).

[67] M. T. Deng, C. L. Yu, G. Y. Huang, M. Larsson, P. Caroff, and H. Q. Xu, Nano Lett. **12**, 6414 (2012).

[68] T.-P. Choy, J. M. Edge, A. R. Akhmerov, and C. W. J. Beenakker, Phys. Rev. B **84**, 195442(2011).

[69] S. Nadj-Perge, I. K. Drozdov, B. A. Bernevig, and A. Yazdani, Phys. Rev. B **88**, 020407(R)(2013).

[70] S. Nadj-Perge, I. K. Drozdov, J. Li, H. Chen, S. Jeon, J. Seo, A. H. MacDonald, B. A. Bernevig, and A. Yazdani, Science **346**, 6209(2014).

[71] P. A. Frigeri, D. F. Agterberg, A. Koga, and M. Sigrist, Phys. Rev. Lett. **92**, 097001 (2004).

[72] S. Fujimoto, J. Phys. Soc. Jpn. **76**, 051008 (2007).

[73] K. Yada, S. Onari, Y. Tanaka, and J. -I. Inoue, Phys. Rev. B **80**, 140509(R) (2009).

[74] B. A. Bernevig, J. Orenstein, and S. C. Zhang, Phys. Rev. Lett. **97**, 236601 (2006).

[75] M.-H. Liu, K.-W. Chen, S.-H. Chen, and C.-R. Chang, Phys. Rev. B 74, 235322 (2006).

[76] M. Kohda, V. Lechner, Y. Kunihashi, T. Dollinger, P. Olbrich, C. Schonhuber, I. Caspers, V. V. Bel ’ kov, L. E. Golub, D. Weiss, K. Richter, J. Nitta, and S. D. Ganichev, Phys. Rev. B **86**, 081306(R) (2012).

[77] M. P. Walser, C. Reichl, W. Wegscheider, and G. Salis, Nat. Phys. **8**, 757-762 (2012).

[78] K. v. Klitzing, G. Dorda, and M. Pepper, Phys. Rev. Lett. **45**, 494 (1980).

[79] D. J. Thouless, M. Kohmoto, M. P. Nightingale, and M. d. Nijs, Phys. Rev. Lett. **49**, 405 (1982).

[80] A. R. Akhmerov, J. P. Dahlhaus, F. Hassler, M. Wimmer, and C. W. J. Beenakker, Phys. Rev. Lett. **106**, 057001(2011).

[81] I. C. Fulga, F. Hassler, A. R. Akhmerov, and C. W. J. Beenakker, Phys. Rev. B **83**, 155492(2011).

[82] M. Diez, J. P. Dahlhaus, M. Wimmer, and C. W. J. Beenakker, Phys. Rev. B **86**, 094501(2012).

[83] G. E. Blonder, M. Tinkham, and T. M. Klapwijk, Phys .Rev. B **25**, 4515 (1982).

[84] P. A. Lee and D. S. Fisher, Phys. Rev. Lett. **47**, 882-885 (1981).

[85] T. Ando, Phys. Rev. B **44**, 8817-8027 (1991).

[86] Y. Asano, Phys. Rev. B **63**, 052512 (2001).

[87] Y. Asano, Phys. Rev. B **64**, 224515 (2001).

[88] Y. Asano, Phys. Rev. B **63**, 014511 (2001).

[89] D. A. Ivanov, Phys. Rev. Lett. **86**, 268 (2001).

[90] C. Nayak, S. H. Simon, A. Stem, M. Freedman, and S. D. Sarma, Rev. Mod. Phys. **80**, 1083(2008).

[91] J. D. Sau, D. J. Clarke, and S. Tewari, Phys. Rev B **84**, 094505 (2011).

[92] C. Ishii, Prog. Theor. Phys. **44**, 1525(1970).

[93] C. Ishii, Prog. Theor. Phys. **47**, 1646(1972).

[94] I. O. Kulik and A. N. Omel'yanchuk, Sov. J. Low. Temp. Phys. **3**, 459 (1977) [Fiz. Nizk. Temp. **3**, 945 (1977)].

[95] K. K. Likharev, Rev. Mod. Phys. **51**, 101(1979 ).

[96] A. A. Golubov, M. Y. Kupriyanov and E. Il'ichev Rev. Mod. Phys. **76**, 411(2004 ).

[97] W. L. McMillan, Phys. Rev. Lett. **175**, 537 (1968).

[98] B. Pannetier ans H. Courtois, J. Low Temp. Phys. **118**, 599 (2000).

[99] T. M. Kpalwijk, J. Supercond. **17**, 593 (2004).

[100] Y. Tanaka, Y. Asano, A. A. Golubov, and S. Kashiwaya, Phys. Rev. B **72**, 140503(R) (2005).

[101] Y. Tanaka and A. A. Golubov, Phys. Rev. Lett. **98**, 037003 (2007).

[102] Y. Asano, A. A. Golubov, Ya. V. Fominov, and Y. Tanaka, Phys. Rev. Lett. **107**, 087001 (2011).

[103] G. Dresselhaus, Phys. Rev. **100**, 580 (1955).

[104] L. L. Foldy and S. S. Wouthuysen, Phys. Rev. **78**, 29-36 (1950).